THE UNIVERSITY
of EDINBURGH

Multi-modal retinal scanning for diagnostic and therapeutic biomarker discovery in neurodegenerative disease

Thomas Pearson

Doctor of Philosophy

University of Edinburgh

2018

Declaration

I hereby declare that this thesis submission comprises work which is entirely my own, with the understanding that where reference is made to the published work of others it is explicitly cited. All research, data collection and statistical analysis was carried out by the author of this thesis. This work is original and as such has not been submitted, in full or in part, to contribute to any other degree or personal/professional qualification.

Thomas Pearson

Abstract

Purpose

Investigate changes in retinal structure and function caused by multiple sclerosis (MS) using established and novel modes of image acquisition and analysis, in order to identify candidate biomarkers of disease. Use longitudinal analysis to determine the rate at which changes to the retinal anatomy occur and whether this rate-of-change alters throughout the MS disease course.

Method

Within the Anne Rowling Regenerative Neurology Clinic (Royal Infirmary of Edinburgh), 72 MS participants (53 female, 19 male, age range 20-79, median age 44) and 80 healthy volunteers (HV) (61 female, 19 male, age range 23–73, median age 38) received spectral domain optical coherence tomography (SD-OCT) and ultra-wide field scanning laser ophthalmoscope (UWF-SLO) scans at baseline. Within the MS group, 16 (9 right eyes and 10 left eyes) had at least one clinically diagnosed episode of optic neuritis (ON). Follow up scans were taken at approximately 3, 6 and 12-month intervals over the course of two years. Visual acuity (VA) as an indicator of retinal function was also measured at each visit using Sloan letter charts at 100% and 2.5% illumination.

Through proprietary software, automatic segmentation of SD-OCT images quantified changes to retinal nerve fibre layer (RNFL) thickness and macular volume. Novel image processing algorithms specifically adapted to semi-automatically segment the vasculature in UWF-SLO images (using multi-scale filtering and supervised classification) allowed for measurement of vessel diameter. Data from the 3 participant groups (MS (no ON), MS (ON) and HV) was first tested statistically for significant differences. Linear regression modelling with the inclusion

of *disease*, *sex*, *length-of-disease* and *age* as predictors was then used to estimate the true effects of disease on the retinal anatomy without confounders.

Results

Baseline data showed that individuals with MS (no ON) have a reduced RNFL thickness in all peripapillary regions and a reduced macular volume when compared with HVs. The reduction in RNFL thickness was seen globally in both eyes (OS: -10μm, OD: -11μm, $p<0.001$) but was greatest in the inferior temporal region (OS: -15μm, OD: -13μm, $p<0.01$). In the MS (ON) group the reduction in RNFL thickness was even greater, again being largest in the inferior temporal region (OS: -29μm, OD: -24μm). Linear regression models confirmed the effect of disease on RNFL thickness and macular volume with significant coefficients in all regions but the inferior nasal. Follow-up analysis showed that the MS (no ON) group had a larger annual rate-of-thinning of the RNFL than HVs in the majority of regions, the largest difference being in the inferior nasal (OS: -1.32μm/year, OD: -1.06μm/year, $p<0.05$) and superior nasal (OS: -1.11μm/year, OD: -1.13μm/year, $p<0.05$) regions.

Retinal arteries were shown to have a significantly reduced diameter in only the inferior nasal quadrant, where the greatest reduction in vessel width was found (OS: -0.005mm, OD: -0.007mm, $p<0.05$). For mean venous width, the inferior nasal quadrant of the right eye also showed a statistically significant difference between the two groups (OS: -0.005mm, OD: -0.005mm). Linear regression models were more frequently significant for arterial rather than venous data, despite both vessel types having significant disease coefficients in the inferior nasal quadrant. Follow-up data was inconclusive on the effect that disease has on the annual rate-of-change of vessel thinning.

Median baseline high contrast VA (OS: -6, OD: -3, $p< 0.05$) and low contrast VA (OS: -6, OD: -6, $p<0.01$) scores were significantly reduced in the MS (no ON) group when compared to HVs. In this study, MS seemed responsible for a 1 line drop in both high contrast and low

contrast VA scores in the MS (no ON) group. A significant difference between the HV group and MS (ON) group was only found in the median low contrast VA score of the left eye (OS: -21, OD: -4, $p< 0.05$). As with vessel analysis, follow-up data showed no significant rates-of-change in VA score.

Conclusions

At baseline, the RNFL and blood vessels of the retina were significantly thinner in the MS (no ON) group when compared to HVs in particular regions. Consistent with previous reports in the literature, both RNFL and macular volume showed a significant decrease in individuals with MS (no ON). However, this is the first study to show that both arteries and veins in the retinal periphery also have a reduced width in the inferior nasal quadrant. Such changes in the retinal anatomy correlate with a drop in visual function as measured by VA.

An increased annual rate of RNFL thinning was also seen in participants with MS (no ON) indicating that anatomical changes occur over time rather than acutely, however this rate-of-change is largest early in the disease course. A similar pattern was observed with the rate at which macular volume decreases in individuals with MS (no ON). Whether changes to the retinal blood vessels occur over time was not determinable within this study, due to the effect size being too small for the number of participants recruited. Future studies should focus on replicating findings pertaining to retinal blood vessels and determining when in the MS disease course these changes occur.

Lay Summary

My research looks at whether images of the back of the eye could be used to identify the early signs of multiple sclerosis (MS) and better understand its initial stages. MS is a chronic illness most commonly diagnosed in people between the ages of 20 and 50, which causes an individual to become progressively more disabled as the disease advances. It is characterised by a gradual decrease in one's ability to control movement as the nerves, which form a network transmitting signals from the brain and spinal cord to muscles throughout the body, are damaged over time. MS affects more than 2.3 million people worldwide, reducing average life expectancy by 7 years and potentially ending with paralysis. An individual's symptoms can vary widely making both diagnosis and prognosis potentially difficult. This is problematic as for an individual to derive the greatest benefit from a treatment, it is important they are diagnosed as early as possible. Even with an early diagnosis, there is no known cure and there are some types of the disease for which there are no successful treatments. The causes of MS are not yet known but it is thought that a breakdown of the protective lining of the brain (the blood-brain barrier), which filters out cells from within the blood and prevents them from entering the brain, could partially be to blame. A more complete understanding of the disease could help make better use of existing drugs, aid the development of new treatments and offer early detection methods for patients before the onset of any severe symptoms. Specifically, the question as to whether blood vessels or nerves are the first to be affected is important in understanding the initial stages of MS.

Retinal scanning offers researchers an inexpensive and patient-friendly method of measuring the thickness of blood vessels and nerves in the back of the eye (the retina) much more precisely than other imaging methods such as magnetic resonance imaging (MRI). The retina is linked directly to the brain via the optic nerve and as such, it is considered an extension of the body's network of nerves (known as the central nervous system) and shares structural similarities with the brain; much as the brain is affected by MS, so are the nerves within the

retina. By measuring the thickness of these nerves with the help of computer software, previous studies have shown how the retina can be used to reveal the damage done by MS. However, studies looking at changes in retinal blood vessels in patients with MS are scarce, despite the retina having a blood-tissue barrier similar to that of the brain- which is thought to be breached early in the disease course. Over a two-year time period, I investigated changes to the retina in MS by imaging people with the disease and comparing these scans with those taken from healthy volunteers within the Anne Rowling Regenerative Neurology Clinic, Edinburgh. Using two different retinal scanning devices and specialised image analysis techniques, I was able to measure the width of retinal nerves and blood vessels at the back of the eye and track any changes over time. I also used a series of letter charts to measure each participant's visual function and determine how changes to nerves and blood vessels can affect an individual's ability to clearly view fine details (known as visual acuity).

My results support previous findings that the retina's nerve layer is thinner, and therefore more damaged, in people with MS. This difference in thickness acts as an indication of disease activity. I also found that changes to the retinal nerves occur gradually over the MS disease course, with the largest changes happening early-on and slowing down over time. Furthermore, this study has shown for the first time ever that within specific regions of the retina, both arteries and veins have a reduced width in individuals with MS. Although, whether these changes to the blood vessels occur gradually over time or only happen early in the disease course could not be adequately concluded. These findings are relevant to an individual's everyday life, for with these changes there comes a fall in retinal function (i.e. ability to resolve fine details) as measured by letter charts throughout the study.

My results contribute knowledge relating to the effects of MS on the retinal blood vessels and as such, should encourage future studies to further investigate these changes. Future work should focus on confirming when retinal changes occur in the disease course of MS and

whether retinal scanning can help identify those patients who are most at risk of developing debilitating symptoms.

Acknowledgements

I am extremely grateful for all the support I have received throughout this degree, without which I would have struggled immeasurably. Firstly, my principle supervisor Dr Tom MacGillivray has suffered through all my terrible ideas, misunderstandings and intellectual dead ends with class and grace. He has never failed to be encouraging, patient, good humoured and helpful; I've felt endlessly lucky to be able to draw from his experience and guidance.

Prof Baljean Dhillon has also gone above and beyond in his supervisory role. Not only do I appreciate his approachable nature, optimistic outlook and invaluable clinical expertise, but he has also supported me through the development of my future career aspirations, for which I shall always be thankful.

Dr Jano van Hemert has my gratitude for educating me on the more professional/commercial applications of research, helping with any technical details or software issues. I also thank him as a member of the original interview panel alongside Dr Tom MacGillivray and Prof Baljean Dhillon for giving me the opportunity to partake in this degree to begin with. In the same vein, both Optos and the MRC funded my research and in doing so, invested in my professional development. I will never be able to repay that debt and so will forever be appreciative.

Without the trust of Prof Siddharthan Chandran, who believed in me enough to place me in a clinical environment to interact with patients, I would not have derived such enjoyment from this degree, nor would I have stumbled upon my aspirations to pursue clinical interests. Despite his busy schedule, he still found time to impart a fraction of his understanding of MS to me, which I found invaluable when writing this thesis.

For acting like a fourth supervisor to me and being somewhat of a guru when it comes to retinal imaging, Dr James Cameron deserves huge thanks. His expert training on retinal imaging devices made collecting data much easier than it might've been, and no doubt I'll keep using some of his choice lines in any future presentations or patient interactions.

All staff from the Anne Rowling Regenerative Neurology Clinic, CCBS and QMRI were extremely accommodating and without them, none of this research would be possible. Special thanks go to Matt Justin, Nicola MacLeod, Dr Katy Murray, Dr Belinda Weller and Prof Anna Williams for convincing so many people to participate in the study. I also thank Shuna Colville, Pamela Macdonald, Liz Adams, Carol Ostrowski, Anne Heron, Dawn Lyle, Claire Young and Moira Henderson for every bit of help I received from them, whether that be scheduling appointments, trawling through patient histories or helping with administrative tasks. I would also like to thank Dr Scott Semple and Prof Jackie Price for their roles on my thesis committee.

Dr Gavin Robertson and Dr Enrico Pellegrini both showed generosity and patience when teaching me how to get the most out of their software, without which analysing hundreds of images would've been impossible within the time frame of the project. Dr Sarah McGrory showed similar patience when faced with my all-too-basic stats questions, and as such she greatly increased my understanding of how to handle the data.

On a personal note, without a strong network of friends and family to keep me sane when times were difficult and grounded when things were going well, I doubt this work would ever have been finished. My mother and step-father have always fully supported me and fuelled my ambition, regardless of how daunting the task ahead may have seemed. Meanwhile, I know I can always rely on my father and step-mother no matter how tough things get, which makes pursuits such as these much less intimidating. Victoria, my sister, was always available when I needed a quick escape to Liverpool for some family comfort.

Edinburgh could sometimes seem like a long way from home, which made the friends I had all the more important during my time there. My thanks to Lindsay and Stu for all whiskies past and future, to Carlos for keeping me company despite occasionally being a cantankerous flatmate, to Nevin for "the craic" and to Eimear for the adventures and for always believing in me.

Finally, I would like to thank all those who very generously lent me their time and participated in the study- I hope I've made good use of your contributions.

Contents

List of abbreviations

A-scan	axial scan
ARRNC	Anne Rowling Regenerative Neurology Clinic
ART	automatic real time
B-scan	2D image created from A-scans
BBB	blood-brain barrier
BRB	blood-retina barrier
CI	confidence interval
CNS	central nervous system
CSF	cerebrospinal fluid
DIS	dissemination in space
DIT	dissemination in time
EDSS	enhanced disability status score
ETDRS	Early Treatment Diabetic Retinopathy Study
FOV	field of view
FS	functional symptom
G	global
HCVA	high contrast visual acuity
HV	healthy volunteer
ICC	intraclass correlation coefficient
IQR	interquartile range
LCVA	low contrast visual acuity
MRI	magnetic resonance imaging
MS	multiple sclerosis
MSFC	multiple sclerosis functional composite
MS (no ON)	multiple sclerosis without clinical history of optic neuritis

MS (ON)	multiple sclerosis with a clinical history of optic neuritis
N	nasal
NI	nasal inferior
NS	nasal superior
OCT	optical coherence tomography
OD	right eye
ON	optic neuritis
OS	left eye
PMB	papillomacular bundle
PPMS	primary progressive multiple sclerosis
PRMS	progressive relapsing multiple sclerosis
RGC	retinal ganglion cell
RNFL	retinal nerve fibre layer
ROI	region of interest
RPE	retinal pigment epithelium
RRMS	relapse remitting multiple sclerosis
SD	spectral domain
SD-OCT	spectral domain optical coherence tomography
SE	standard error
SLO	scanning laser ophthalmoscope
SNR	signal-to-noise ratio
SPMS	secondary progressive multiple sclerosis
T	temporal
TD-OCT	time domain optical coherence tomography
TI	temporal inferior
TS	temporal superior
UWF-SLO	ultra-wide field scanning laser ophthalmoscope
VA	visual acuity

Chapter 1

Introduction

1.1 Motivation

The use of retinal imaging to identify anatomical changes caused by multiple sclerosis (MS) has shown evidence to support its use as a tool to track disease activity. Previous studies have largely focused on analysing data from optical coherence tomography (OCT) images, which quantifies changes to the central nervous system that may act as surrogates for similar changes in the brain. Studies that analyse changes to the retinal vasculature are scarce in comparison, and as such the understanding of how MS affects the retinal vasculature is under investigated. MS patients may stand to benefit from studies which focus on changes to blood vessels in the retina, as they could develop our understanding of the initial disease mechanisms and aid in the development of screening tools which can identify the signs of MS prior to the onset of symptoms.

1.2 Hypotheses

A longitudinal cohort study was planned to address the following three hypotheses:

1. An individual diagnosed with MS will have quantifiable differences to their retinal vasculature at baseline imaging compared to healthy controls
2. An individual diagnosed with MS will have quantifiable differences to their RNFL thickness and macular volume as measured by OCT
3. An individual diagnosed with MS will have quantifiable changes to their retinal vasculature which occur longitudinally and correlate with disease progression and worsening severity

1.3 Thesis outline

In chapter 2, I will describe the relevant pathology and epidemiology of MS, highlighting the importance of early diagnosis and the current difficulties with diagnosis and accurate prognosis. The anatomy of the retina is then considered alongside a summary of findings from previous studies which provide evidence for how the retina is affected by MS. Chapter 3 continues by describing the imaging techniques which are used during this study (OCT, ultra-widefield scanning laser ophthalmoscope (UWF-SLO)) with the technical details of each device, alongside information on visual acuity (VA) and its use in measuring retinal functionality. How each of these methods were used to answer the hypotheses set out in chapter 1.2 are described in detail in chapter 4 as I lay out the methodology behind patient recruitment, image analysis and acquisition and the statistical methods used. Analysis of the data will be divided into two distinct chapters: baseline (chapter 5) and longitudinal (chapter 6). Both chapters will follow the same pattern of analysis as participant groups are first compared through Student's t-test or Mann-Whitney U test, and then compared through the use of linear regression models. Finally, the discussion in chapter 7 will detail the limitations of the data collected, interpret the results, place them in the context of previous studies and recommend the appropriate future research to complete based on the findings of this study.

Chapter 2

Multiple Sclerosis and the Retina

2.1 Introduction

MS is a chronic neurodegenerative disease; with over 2.3 million sufferers worldwide (1), it is the most common cause of non-traumatic neurological disability in young adults (2). A quick diagnosis of MS is essential for patient care, however many of the symptoms are not specific only to MS (3). The diagnostic procedure may be prolonged as it frequently relies on expensive magnetic resonance imaging (MRI) procedures to view the central nervous system (CNS) as well as clinical assessments, such as blood tests and assessments of cognitive and motor function. The advent of a novel technique which could help diagnose and prognose MS at an early stage would help improve current clinical practice and benefit patients who could receive disease-modifying treatments earlier.

2.2 Multiple sclerosis

2.2.1 Pathology

Fundamentally the CNS is a collection of neurons (see Figure 2.1): specialized nerve cells that relay electrical potentials from sensory receptors to effector organs. Neurons comprise a cell body containing a nucleus, around which are typically several dendrites that receive signals from surrounding neurons. A single axon stretches out from the cell body and is responsible for relaying impulses to adjacent neurons. To increase the speed of this process, the axon is surrounded by a myelin sheath. This fatty layer insulates the axon enabling an action potential to travel from one node to another at a higher velocity than would otherwise be possible (conduction velocity in myelinated fibres 5-120 m/s compared to unmyelinated fibres 0.5-2.5 m/s) (4).

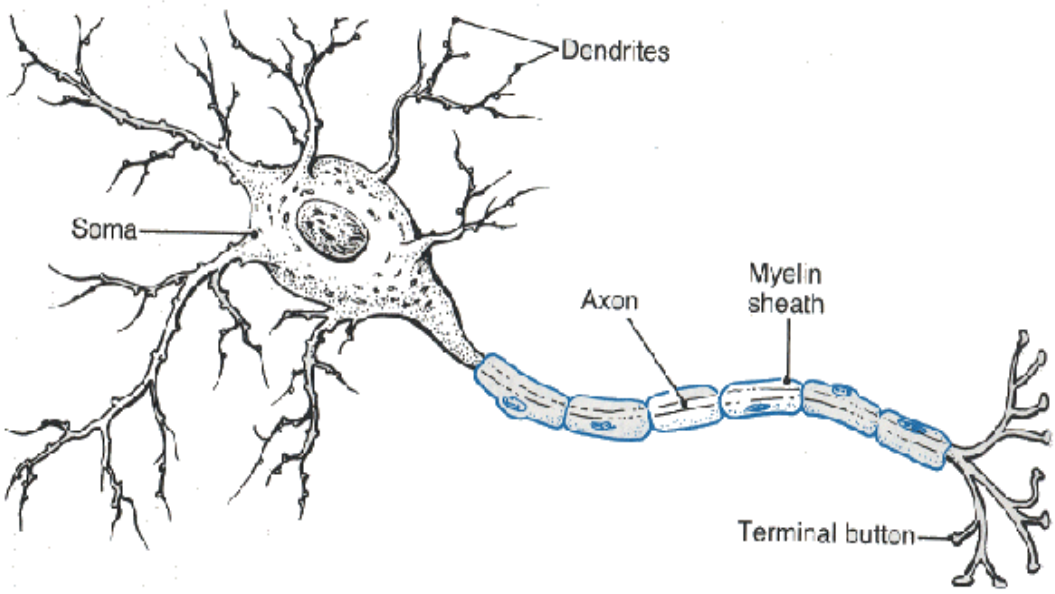

Figure 2.1: Diagram of a neuron, showing the axon surrounded by a myelin sheath (101)

MS is characterised by demyelination of the axon and its eventual degeneration. A comprehensive understanding of the disease's cause has yet to be attained, but it is thought that both genetics and environmental factors contribute to onset (3). Pathogenetically, the disease develops due to immunopathological responses within the CNS; one of the earliest manifestations of MS is a migration of autoreactive lymphocytes through the blood-brain barrier (BBB) (5) (6) (7).

Though increased permeability of the BBB is not unique to MS, it may be responsible for the initial inflammation which in turn causes the formation of sclerotic plaques after demyelination (6). The subsequent plaques impede rapid electrical conduction through individual axons- the drivers of motor functions. Spontaneous remyelination does occur to a limited extent within the CNS leading to periods of remission, but its success differs between individuals and can be short-lived (8). The question as to whether inflammation is indeed a precursor to neurodegeneration has yet to be definitively answered- it is possible that inflammation is a secondary response to neurodegeneration (6).

2.2.2 Epidemiology

Environment undoubtedly plays an important role in the cause of MS but the extent to which is yet unclear (9). A decrease in mortality rates in the UK has seen a statistical increase in the prevalence of MS, however a study on incidence between 1990 and 2010 showed a downward trend in new cases of MS being diagnosed in the UK. This may be due to better diagnosis resulting in fewer false positives (10). The typical age of onset is between 20 and 50 years (9). MS disproportionally affects women, with a mean female-to-male ratio of 2.4 (10). Studies on the distribution of MS rates worldwide show a general increase in prevalence with a greater distance from the equator, with the highest rates being in Orkney and the Shetland Isles (11). As such, it is thought that vitamin D deficiency may be a contributing factor in higher rates of MS.

Genetics also contributes to the incidence of MS (9). Individuals with close family members who suffer from MS show an increased incidence, denoting a positive correlation between genetic sharing and lifetime risk of developing the disease (6).

2.2.3 Diagnosis and prognosis

Though 95% of patients with MS show white matter abnormalities on MRI of the brain and spinal cord, this is not adequate for a diagnosis; diagnosis is not determined by a single test (e.g., cerebrospinal fluid (CSF) analysis) or clinical feature, but through clinical assessment (6) (12) (3). The 2010 McDonald criteria (see table 2.1) for diagnosis of MS requires "objective clinical evidence of 2 lesions or objective clinical evidence of 1 lesion with reasonable historical evidence of prior attack" for a diagnosis without need of any additional information (12) (13). As such, correct diagnosis can be a long and frustrating ordeal for the patient as successive symptoms may have large periods of time between them.

Once diagnosed, patients are grouped into one of four disease subtypes through patient history and examination: primary progressive (PPMS), secondary progressive (SPMS), relapse and remitting (RRMS) and progressive relapsing (PRMS). Each of these subtypes progress in a

different manner, as is displayed in Figure 2.2. The frequency and severity of attacks within the initial stages of the disease are considered fair indicators of how quickly the disease will progress in the future (3). In 85-90% of cases, a patient will first experience RRMS characterised by cycles of acute attack and recovery. Difficulties can occur in disease categorisation as patients will often make the transition from RRMS to more progressive forms (65% within 25 years) (3). Several disease-modifying treatments are available for non-progressive sufferers, which for the most part aim to reduce inflammation (14). Clinical trials have shown both first and second line therapies to be effective against placebo at reducing disability progression in patients with RRMS (14). Treatments are not without their side-effects, one example being fingolimod which is associated with an increased risk of macular oedema (15).

Quick intervention has been shown to be more effective for the prevention of disease progression, suggesting long-term damage to axons is reduced when the time spent subjected to early inflammatory responses is reduced (16). Additionally, there is also suggestion that patients who receive treatment at disease presentation derived greater benefit from later treatments than those who waited a period of two years before intervention (17). Uncertain prognosis becomes troublesome when deciding which treatment, therapy and potency is best suited to a patient. Currently, no disease-modifying treatments have proven effective on progressive disease onset.

Clinically, SPMS would be diagnosed after a "period of sustained deterioration in neurological function without remission" of roughly six months, as then the likelihood of reversibility of symptoms becomes small (3). As displayed in Figure 2.2, independent of previous disease course the progression of symptoms appears to occur at a steady rate in patients with SPMS, rather than in periods of relapse. Such a diagnosis may only be possible after retrospectively observing the increased rate of decline over time (3).

Clinical Presentation	Additional Data Needed for MS Diagnosis
≥2 attacks; objective clinical evidence of ≥ 2 lesions or objective clinical evidence of 1 lesion with regional historical evidence of a prior attack	None
≥2 attacks; objective clinical evidence of 1 lesion	Dissemination in space (DIS), demonstrated by: ≥1 T2 lesion in at least 2 of 4 MS-typical regions of the CNS (periventricular, juxtacortical, infratentorial or spinal cord); or await a further clinical attack implicating a different CNS site
1 attack; objective clinical evidence of ≥ 2 lesions	Dissemination in time (DIT), demonstrated by: Simultaneous presence of asymptomatic gadolinium-enhancing and nonenhancing lesions at any time; or a new T2 and/or gadolinium-enhancing lesion(s) on follow-up MRI, irrespective of its timing with reference to a baseline scan; or await a second clinical attack
1 attack; objective clinical evidence of 1 lesion (clinically isolated syndrome)	Dissemination in space and time, demonstrated by: For DIS: ≥1 T2 lesion in at least 2 of 4 MS-typical regions of the CNS (periventricular, juxtacortical, infratentorial or spinal cord); and For DIT: Simultaneous presence of asymptomatic gadolinium-enhancing. A new T2 and/or gadolinium-enhancing lesion(s) on follow-up MRI, await second clinical attack
Insidious neurological progression suggestive of MS (PPMS)	1 year of disease progression (retrospectively or prospectively determined) plus 2 of 3 of the following criteria; 1. Evidence for DIS in the brain based on ≥1 T2 lesions in the MS-characteristic (periventricular, juxtacortical or infratentorial) regions 2. Evidence for DIS in the spinal cord based on ≥2 T2 lesions in the cord 3. Positive CSF (isoelectric focusing evidence of oligoclonal bands and/or elevated IgG index)

Table 2.1: 2010 Macdonald criteria for diagnosis of MS, showing the additional clinical data required for a diagnosis given each clinical presentation (12)

Both progressive forms of MS can manifest themselves through spinal cord dysfunction-evidence for which can be presented as lesions on the spinal cord as shown with MRI and associated symptoms e.g., lower limb dysfunction. PPMS diagnosis differs from SPMS as the time from disease onset to advanced disability has been shown to be shorter (3). However, progression of the disease is similar to that of SPMS.

Although the disease is not fatal, the increased prevalence of infection and illnesses related to immobility reduces life expectancy by a mean of seven years; from time-of-diagnosis the median time to death is thirty years and in 2/3 of cases MS is the attributable cause of death (6). Despite categorising an individual's MS into one of four subtypes, progression of the disease is widely variable between individuals (3). Though some patients with MS will have relatively benign cases, quality of life is invariably affected as symptoms include cognitive impairment, pain, fatigue, bladder dysfunction, loss of vision and poor balance. Furthermore, individuals with MS are three times more likely to suffer from depression when compared with the general population, though it is unclear whether this is driven by psychological or mechanistic factors (18).

The Expanded Disability Status Score (EDSS) is an attempt to quantify how severely disabled a patient is due to MS. Measurements are made of impairment in eight functional symptoms, including bowel and bladder function and weakness in limbs (19). For each of these, a score is given, with an additional score for impairment of the ability to walk. A score of zero represents no disability, whereas scores of six or above indicate severe disability. Despite being the most widely used tool by neurologists to stratify patients during clinical assessment, the EDSS lacks sensitivity to change (20). As such, competing tools e.g., Multiple Sclerosis Functional Composite (MSFC) have been increasingly used in clinical trials to offer a multidimensional metric with which to assess clinical status (20). Such tools may include a

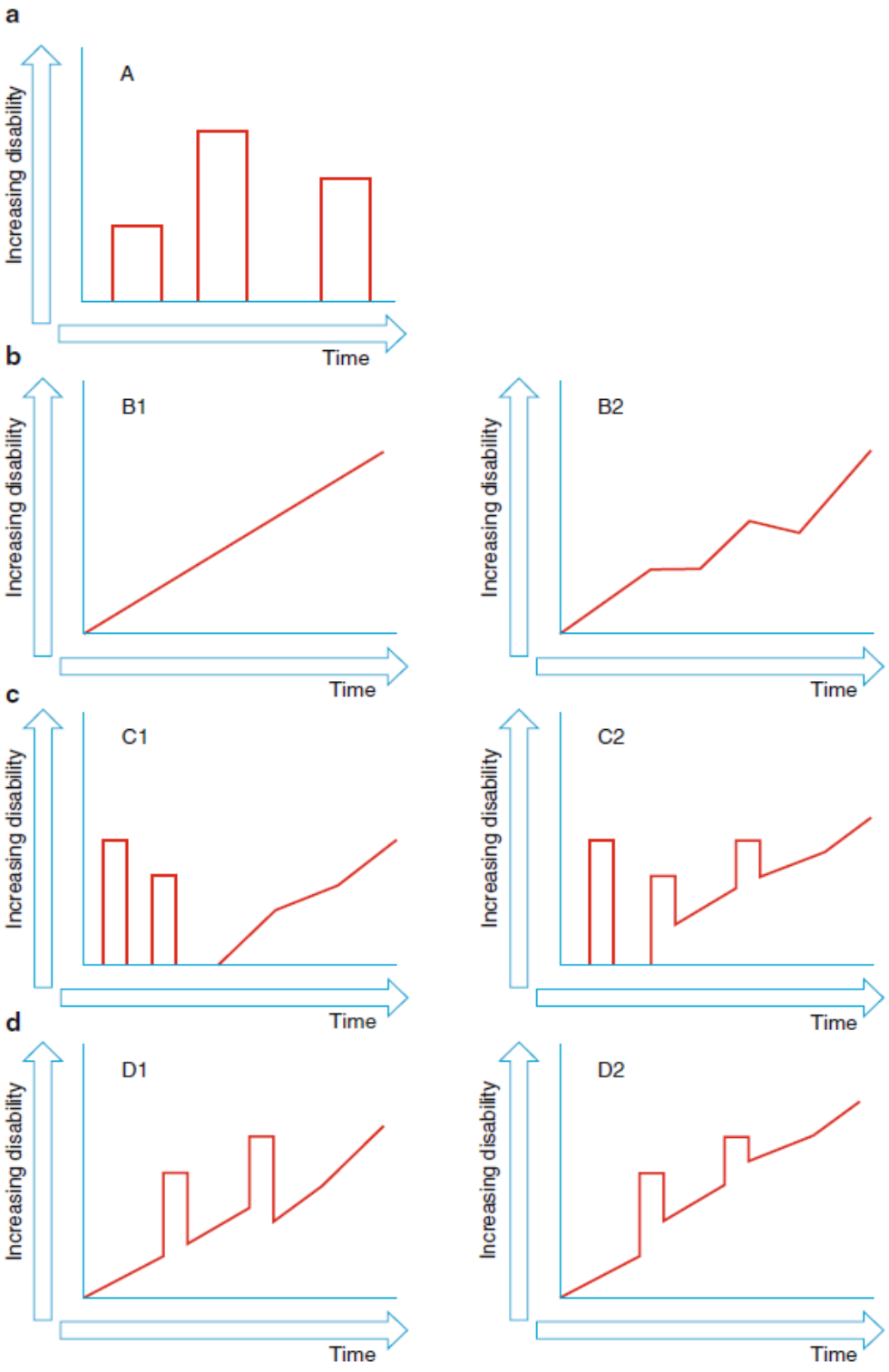

Figure 2.2: Disease progression in MS: a) RRMS, where we see the cycles of attack and full recovery b) PPMS shows a constant increase in disease severity in B1, and a steady increase in B2 but with periods of improvement c) SPMS where RRMS is followed by a progression of disease with periods of acute attack in C2 and without in C1 d) PRMS with acute attacks but with periods of slight recovery in D1 and without in D2 (3)

Score	Description
1	No disability, minimal signs in one FS.
1.5	No disability, minimal signs in more than one FS.
2	Minimal disability in one FS.
2.5	Mild disability in one FS or minimal disability in two FS.
3	Moderate disability in one FS, or mild disability in three or four FS. No impairment to walking.
3.5	Moderate disability in one FS and more than minimal disability in several others. No impairment to walking.
4	Significant disability but self-sufficient and up and about some 12 hours a day. Able to walk without aid or rest for 500m.
4.5	Significant disability but up and about much of the day, able to work full day, may otherwise have some limitation of full activity or require minimal assistance. Able to walk without aid or rest for 300m.
5	Disability severe to impair full daily activities and ability to work a full day without special provisions. Able to walk without aid or rest for 200m.
5.5	Disability severe enough to preclude full daily activities. Able to walk without aid or rest for 100m.
6	Requires a walking aid – cane, crutch, etc. – to walk about 100m with or without resting.
6.5	Requires two walking aids- pair of canes, crutches, etc. – to walk about 20m without resting.
7	Unable to walk beyond approximately 5m even with aid. Essentially restricted to wheelchair; though wheels self in standard wheelchair and transfers alone. Up and about in wheelchair some 12 hours a day
7.5	Unable to take more than a few steps. Restricted to wheelchair and may need aid in transferring. Can wheel self but cannot carry on in standard wheelchair for a full day and may require a motorised wheelchair.
8	Essentially restricted to bed or chair or pushed in wheelchair. May be out of bed itself much of the day. Retains many self-care functions. Generally has effective use of arms
8.5	Essentially restricted to bed much of the day. Has some effective use of arms and retains some self-care functions.
9	Confined to bed. Can still communicate and eat.
9.5	Confined to bed and totally dependent. Unable to communicate effectively or eat/swallow.
10	Death due to MS.

Table 2.2: EDSS definitions. Functional symptoms (FS) are distinguished as: pyramidal, cerebellar, brainstem, sensory, bowel and bladder function, visual function, cerebral functions and other (100)

2.3 The Retina

The retina comprises the inner most layers of the eye. Not only does the retina directly link to the brain via the optic nerve, but it is considered an extension of the CNS (21). In embryonic development, the retina develops in tandem with the optic nerve as an extension of the diencephalon and as such they share a great deal in common with respect to anatomy, pathology and physiology (4). It is therefore argued that changes to the retina may act as valuable surrogates for changes which also occur within the brain (22).

2.3.1 Anatomy of the Retina

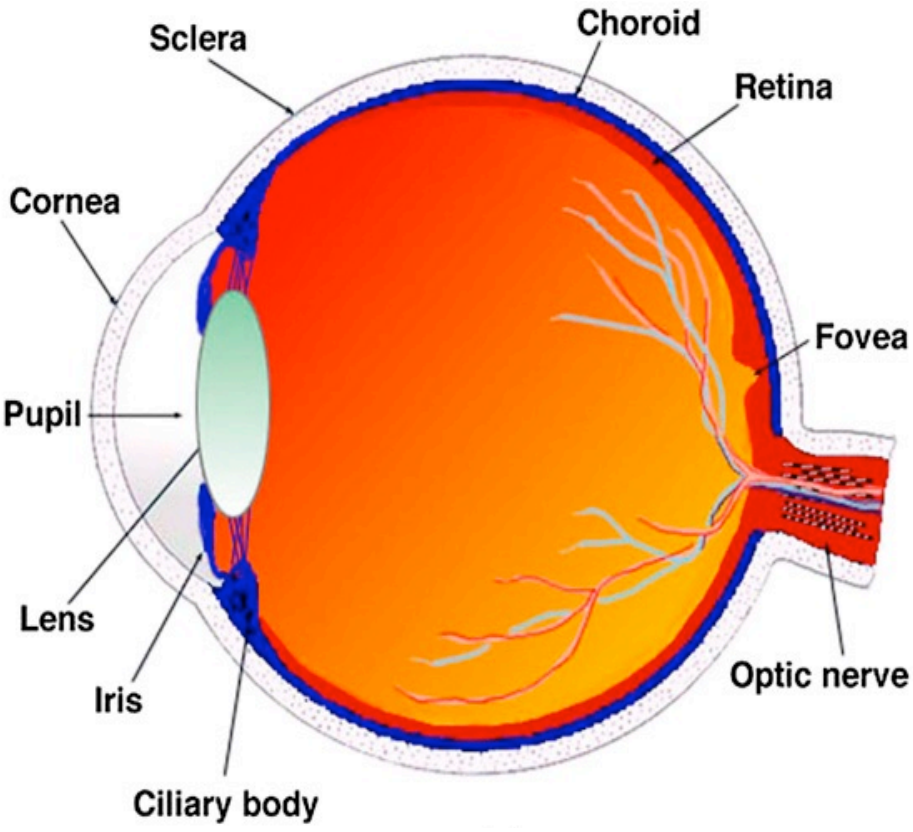

Figure 2.3: A diagram of the human eye, showing the internal structures and their location. At the rear of the eye, we see the retina and its supply of blood vessels, both of which converge at the optic nerve (24)

The eye's inner surface, or retina, is responsible for turning images acquired from external stimuli into neural impulses to be processed in the brain. It comprises an axonal layer above multiple different cell layers (see Figure 2.4). As light enters the pupil, it is refracted by the lens and converges on the fovea- an area on the retina which is densely populated with cone cells (one of two types of photoreceptors).

A process of visual phototransduction then occurs, where the incident light signal is converted to a neural impulse and sent via bipolar cells to the retinal ganglion cells (RGCs)- neurons formed to create the innermost cellular layer) (4). The axons of these cells bundle together to from a layer of unmyelinated tissue known as the retinal nerve fibre layer (RNFL). This layer gradually gets thicker with proximity to the optical disk, the bridge between the eye and the optical nerve.

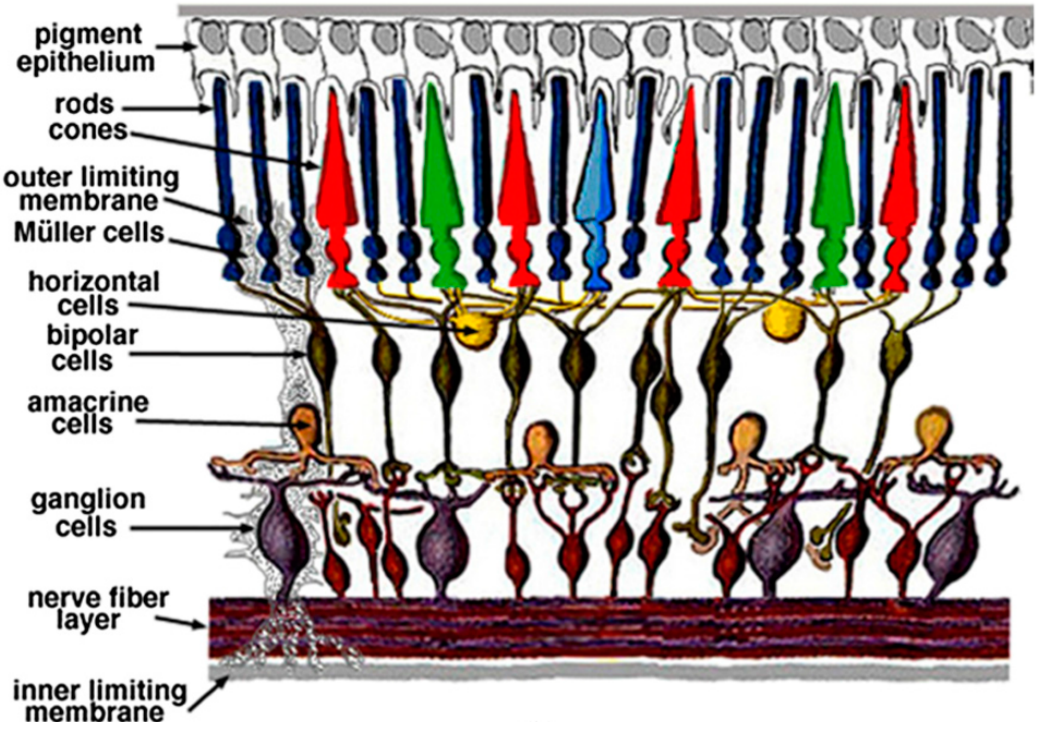

Figure 2.4: A diagram of the retinal cell layers, the RNFL being closest to the surface of the retina (24)

The optic disk can be identified as the bright circular spot in an image of the retina (see Figure 2.5). It is the location to which nerve fibres converge and form the optic nerve that passes through the sclera at the rear of the eyeball (23). The optic nerve acts as the information highway, channelling electrical charge between the lateral geniculate body and the eye (4). Whereas the neurons found in the retina resemble that of grey matter within the brain, the optic nerve itself is composed of white matter. As such, it is not a peripheral nerve but rather part of the CNS (4) (24).

Figure 2.5: Fundus camera image of the retina in a left eye. As described, the bright circular spot is the optic disk, from which the blood vessels spread out to the periphery of the retina. The dark spot to the right of the optic disk is the macular, at the centre of which lies the foveal dip.

Another structural similarity to the brain is the blood-retina barrier (BRB). Acting as a regulator for the passage of immune cells and pathogens within the retinal pigment epithelium (RPE), it protects neurons within the retina much as the BBB does in the brain (21) (23). Blood flow to the retina occurs via two sources: the choroid oxygenates the photoreceptors and outer layers of the retina, whereas the inner layers are supplied by blood vessels which emanate outwards from the optic disk all the way into the periphery of the retina (see Figure 2.5) (4).

2.3.2 How MS affects the retina

Ophthalmological problems are very commonplace in MS: in 20% of cases optic neuritis (ON) is the presenting symptom (25). ON is an inflammatory demyelinating disease of the optic nerve and is reported in 75% of MS patients at some point during their life (21). The disease strips myelin from the optic nerve- causing poor conduction and subsequent damage to the axons of the optic nerve and RNFL. Patients with ON complain of a painful temporary loss or impairment of vision in one eye (26). The footprints of ON remain even once visual function is restored: during ON, oedema causes the RNFL to swell in thickness which leads to a significant thinning of the RNFL (as measured via OCT- see chapter 3). In a meta-analysis of 2,063 eyes a mean RNFL thickness reduction of 20μm was measured using time domain OCT (TD-OCT) in patients with a history of ON, corresponding to a 20% reduction in thickness (27).

MS patients without history of a clinical episode of ON also show a loss in RNFL thickness over time (again measured with TD-OCT, 3.4mm circumferentially around the centre of the optic disc), though it is smaller than that expected after an episode of ON (28) (27). Another meta-analysis, this time of 3,100 eyes, found a mean RNFL reduction of 7μm was found in MS patients who had never reported a clinical episode of ON, whilst a large multi-centre study using spectral domain OCT (SD-OCT) on 414 MS patients measured a global reduction of 10μm (29). Macular volume has also been shown to decrease in patients with MS; a study of 530 participants found a 2.9% reduction in total macular volume (the sum of the volumes of the neural retina in the central 6mm of the macula) when comparing MS patients to healthy controls in both eyes using TD-OCT (30). When relating macular volume to RNFL thickness, the same study found that a 10μm reduction in RNFL thickness corresponded with a 0.2mm^3 reduction in macular volume (30). Patients in this study had their pupils dilated using tropicamide, 1%, when necessary (<5mm) as well as a patch placed over their non-tested eye.

When considering the peripapillary quadrants individually, the most significant changes occur

in the temporal region. RNFL changes are greater temporally to the extent that studies have differentiated between SPMS and PPMS patients using temporal RNFL thickness reductions alone (31). Moreover, focal defects are exclusively located in the temporal region of the retina (32). As such, it seems that the temporal retina is more severely affected by MS than other regions. Furthermore, thinning of the RNFL and macular appears to occur gradually as the disease progresses. A study of 135 patients with MS (median disease duration of 16.4 years, 68% of which were diagnosed as having RRMS) were imaged over a period of two years and had a global RNFL thinning of 1.1μm over this period of time as measured with SD-OCT (33). The same study also included 16 healthy volunteers (HVs) who showed a thinning in the RNFL of -0.5μm over a two-year period, indicating that RNFL thinning occurs at a greater pace than in patients with MS than in HVs (33).

Similarly, a study of 299 patients with MS scanned at regular 6-month intervals showed a global RNFL thinning of 2.9μm in 2 to 3 years and a 6.1μm loss in 3 to 4.5 years using TD-OCT (34). This study again used a protocol of pupil dilation when necessary (pupils <5mm) and a patch placed over the non-tested eye. Finally, a study which imaged 34 MS patients (16 PPMS, 18 SPMS) over a median time of 575 days showed no significant changes using TD-OCT, but nevertheless a global reduction of 0.99μm annually (35). The study also saw a $0.038mm^3$ ($p = 0.013$, 95% CI -0.067, -0.008) reduction in macular volume per year in MS patients, although it compared with a $0.031mm^3$ ($p = 0.005$, 95% CI -0.052, -0.009)) reduction seen in 18 HVs most likely as a consequence of aging. Significant age-related declines in macular volume and RNFL thickness have been reported in multiple studies, using both SD-OCT and dissection of HV eyes (36) (37). The effect of age on macular volume is thought to be more observable than in RNFL thickness- some studies inferring that this is due to macular volume measures proportionately containing a greater amount of ganglion cells which are more at risk of degeneration as a function of age (35). However, this theory is not consistent across all histological studies on the subject (36). Despite this, longitudinal imaging of 70 eyes over a 30-month period found an approximate -0.52μm/year thinning of the RNFL, largely

concentrated in the superior and inferior quadrants (36).

The rate that the RNFL thins may not be uniform, as was also reported by Balk et al (33). In this study, the predictor *length-of-disease* was categorised it into 6 bins e.g., <5 years, 5-9.9 years etc. The subsequent modelling showed that neurodegeneration was more pronounced early in the disease course whereby every additional year an individual lived with MS resulted in a 0.05μm reduction in the thinning of the RNFL over a two-year period.

Retinal symptoms are not exclusive to the CNS; 10% of patients with MS suffer from retinal periphlebitis (RP), a vasculitis of the peripheral retinal vasculature (38). A classic way in which this disease presents itself is in perivascular sheathing where blood vessels may appear cuffed in a white plaque as inflammatory cells surround affected blood vessels (39). Symptoms can include blurred vision, floaters and pain. Research suggests that individuals with higher EDSS scores are more likely to suffer from RP, supporting its use as a biomarker of disease progression (38). Also, regarding the retinal vasculature: a study of 71 subjects which used peripapillary OCT scans (see chapter 3) to measure vessel width at a radius of 3.4mm from the optic disk found that vessels were significantly thinner in participants with MS (40). No attempt was made to classify the vessels as artery or vein or to separate the blood vessels into their respective quadrants, and no association between blood vessel diameter and a history of ON was found in this cohort.

Finally, a reduction in the retinal functionality of patients with MS has also been reported, as measured by low-contrast visual acuity (LCVA) which itself has been found to correlate with axonal and neuronal loss as measured with OCT and changes in EDSS score (41). Talman et al.'s study of 299 patients with MS scanned with a minimum of 6 months between baseline and follow-up showed 12% of participants with a drop in high contrast visual acuity (HCVA) score of ≥5 letters and 13% of participants with a ≥7 letter fall in LCVA score. Results for individuals with a history of ON were the same for HCVA score but only 12% had a clinically significant drop in their LCVA score (42). This study also showed that eyes with the greatest

degree of visual loss also showed the thinnest RNFL. However, a study of RRMS patients, which imaged 61 participants at baseline and at 6 years follow-up determined that MS individuals had a visual acuity score which remained constant, but individuals with a history of ON showed a significant drop off in their score (43).

2.4 Summary

The difficulty in rapid diagnosis and prognosis of MS presents an obstacle to patients benefitting from disease-modifying treatments early in their disease course. The ability to view the vasculature and CNS non-invasively through the pupil offers great potential. With its structural similarities to the brain, the retina is a versatile site that could enable a greater understanding of the pathological and anatomical changes occurring in MS. Changes should not be considered in isolation but may prove to be surrogates for similar changes occurring within the brain; reduction in RNFL and macular volume are associated with global brain atrophy as quantified with MRI (44). Detecting such changes early could offer a more comprehensive understanding of the initial mechanisms of the disease (i.e. inflammation and neurodegeneration), thus aiding the creation of new targeted treatments and therapies. The next chapter will introduce several modalities for imaging and studying the retina.

Chapter 3

Retinal Imaging

3.1 Introduction

The eye offers an inexpensive, quick and non-invasive method of capturing images of the CNS and microvasculature at high resolution via the anterior visual pathways. Images are obtained in a matter of seconds and with semi-automatic image analysis algorithms, anatomical information can be extracted in vivo without the need for an invasive biopsy. Operators can be trained in a short period of time and patients suffer none of the anxiety which may come with MRI such as claustrophobia (45). As such, retinal imaging has the potential to play a pivotal role in the diagnosis and tracking of neurodegenerative diseases.

3.2 Optical Coherence Tomography

Since it was first shown possible to image and segment the retina's cellular layers and measure their thicknesses by Huang et al., OCT has become a hugely popular technique in the field of retinal imaging; its high resolution (typically 7μm axially) delivers the ability to make precise axonal measurements (46). OCT has helped expand on not only the general understanding of how eye diseases develop, but also the role that neurodegenerative diseases play in affecting the retina and CNS; studies show a thinning of the RNFL in patients of MS, Parkinson's and Alzheimer's disease (17) (47) (48) (27).

OCT is analogous to ultrasound (49). In ultrasound, high frequency 'pulse' sound waves are transmitted through body tissue (such as the womb of an expectant mother) and an image is constructed using measurements of the time taken for these sound waves to echo and return to a detector (50). Rather than sound, OCT uses infrared light for a similar purpose. It is when detecting the reflected signal that OCT diverges from ultrasound. To observe directly the time

taken for light to travel to the retina and back, measurements would have to be made on a femtosecond (10^{-15}) scale (51). As this is not currently possible, techniques that rely on interferometry are used instead.

Interferometry exploits the wave nature of light, measuring distances in a sample through the coherence of a detected signal with a reference signal (51). A schematic of the process is displayed in Figure 3.1. Utilising infrared light (which is more penetrative of the retinal cell layers than light of visible wavelengths (52)), the light incident on the beam splitter, E_i, is directed fifty-fifty towards a reference mirror and a tissue sample e.g., the retina. For the purposes of explanation, it is useful to use a model with discrete surfaces though in reality the sample would be better represented by a continuous function (51). The wave reflected from the sample, E_S, is a combination of all the waves which have been reflected at the different surface boundaries within the sample (51). The reflected wave then interferes with the wave E_R from the reference mirror, at which point the resulting incidence ray I_D propagates towards the photodetector (53).

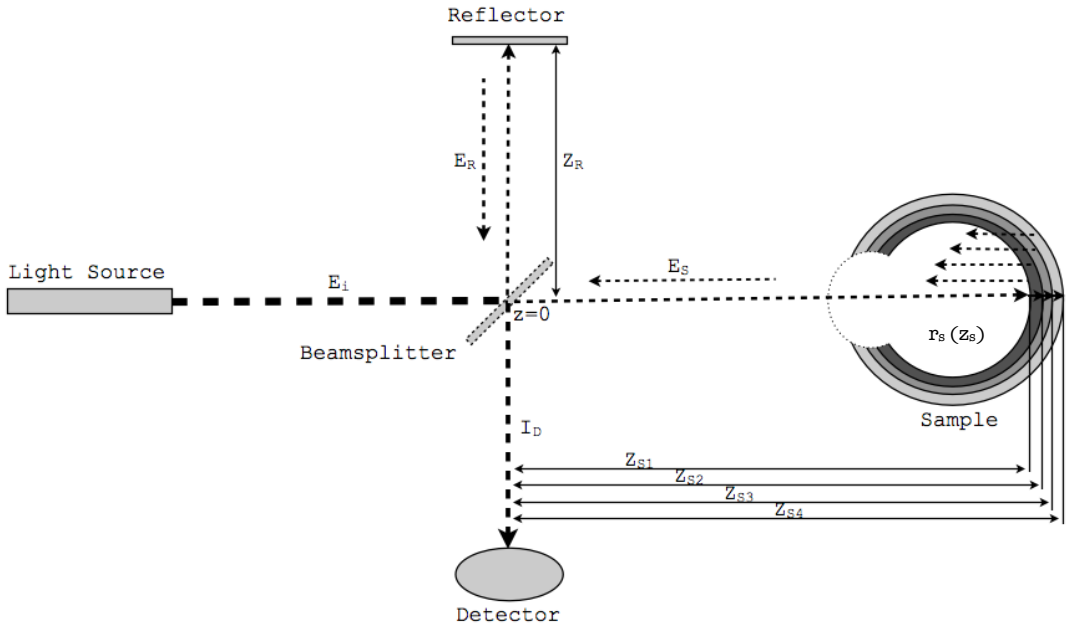

Figure 3.1: The theory of TD-OCT to image the retinal cell layers. E_i is the incident light beam which is split 50:50 to the reference mirror, Z_R, and the sample (the retina), Z_S. E_S comprises all the waves reflected from retinal cell layer boundaries, E_R is the beam reflected from the reference mirror. I_D is the beam constructed from both E_S and E_R.

Early time domain (TD) systems used mechanical changes in the distance between the beam-splitter and the reference mirror to create an axial scan (A-scan) from the detected signal (51). A-scans are representative of a 1-D line of data within an image. To create a 2-D image (B-scan), A-scans are simply aligned laterally with one another (54). To reduce the signal-to-noise ratio (SNR) of B-scans allowing for better segmentation of retinal anatomy, scans can be averaged, whereby repeat scans of the same region are taken to produce a final composite image. The obvious trade-off in acquiring a clearer image is an increase in acquisition time (55).

Superior images are the product of spectral domain (SD) systems, whereby the reference mirror is a fixed distance from the beam-splitter (54). In such setups, the photodetector is replaced by a spectrophotometer which records spectral domain signals from the incident ray, I_D, having first passed through a diffraction grating (53). To acquire an A-scan, the SD signal must be transformed into a spatial domain signal- a Fourier transform is used to achieve this (51) (56).

As SD-OCT is free from the limitations that come with the moving reference arm used in TD-OCT, A-scan acquisition rate improves from approximately 400/s to 29,000/s, allowing B-scans to be taken in just 1/29s (27) (54). Using this method, greater optical resolutions of 7μm axially and 14μm laterally can be made with a SD-OCT machines (see Figure 3.2) (57). Faster acquisition also allows SD-OCT to take scans both of volume and a larger field-of-view (FOV) (27); up to 48 B-scans per second can be taken and aligned to form a 3D image of the retina (see Figure 3.3) (57), with which the macular can be segmented to obtain a volume measurement in mm^3. Macular volume scans present the opportunity to directly capture neuronal degeneration as 34% of the average macular thickness comprises the inner retinal complex (i.e. ganglion cell layer, inner plexiform and nuclear layers) (58). Decreases in macular volume would therefore suggest neuronal loss in the RGC layer.

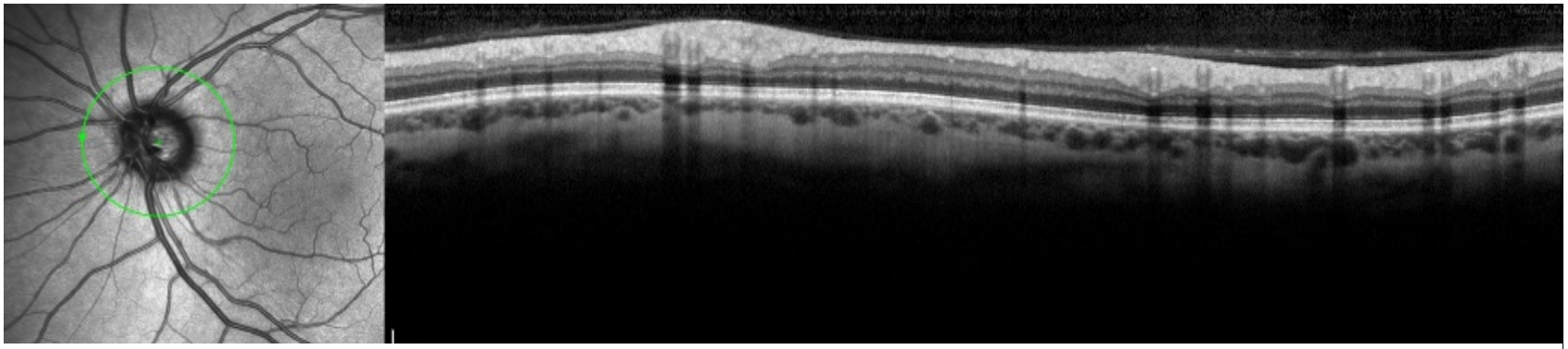

Figure 3.2: Example of a peripapillary SD-OCT scan acquired with the Heidelberg Spectralis. The left shows an infrared SLO image which traces the path of the SD-OCT scan in green around the OD. The right shows an SD-OCT image: the pale top layer is the RNFL, within which there are blood vessels shown that cast a shadow axially through the scan.

Segmentation of OCT scans is commonly achieved automatically with proprietary software supplied by device manufacturers that separates the cell layers and gives thickness measures in micrometres. Peripapillary scans offer RNFL measurements taken at a radius of 3.4mm from the centre of the optic disk (as manually identified by the operator) (57). The thickness measures are then divided into 8 regions for analysis: global (G), superior temporal (TS), inferior temporal (TI), temporal (T), superior nasal (NS), inferior nasal (NI), nasal (N) and the papillomacular bundle (PMB). PMB is a measure created for the investigation of neurodegenerative diseases as it pertains specifically to information from the fovea- the region most effected by ON (59).

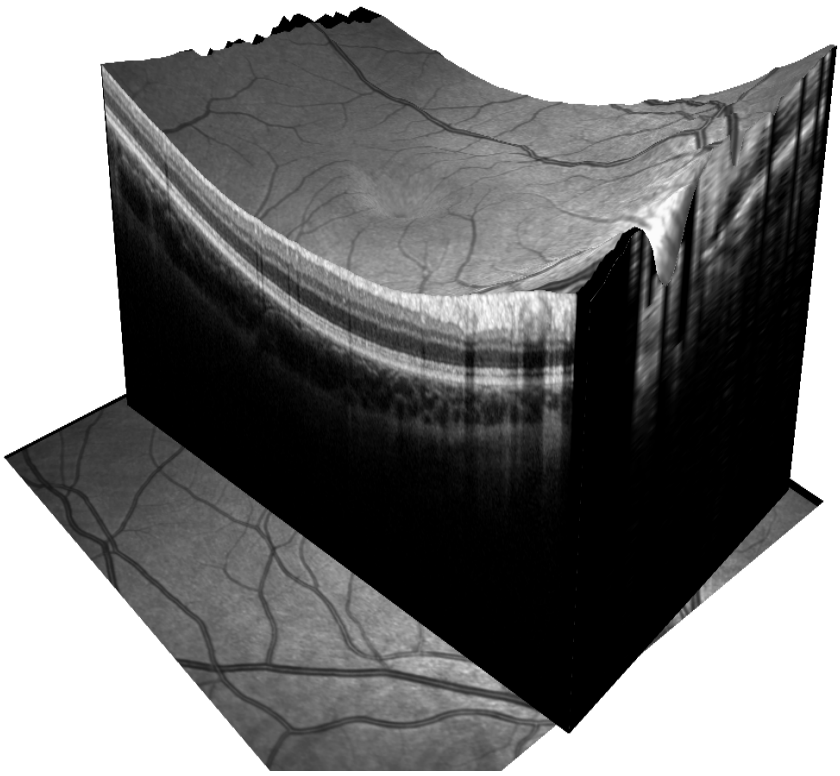

Figure 3.3: A visualisation of macular volume acquired using a Heidelberg Spectralis. On the upper surface we can see the blood vessels which emanate from the OD, whilst from the side there is shown one of the 48 B-scans which make up a 3D image of the macular.

To ensure multiple scans taken from the same patient at different timepoints can be compared longitudinally, OCT devices use registration techniques to align scans using the anatomical landmarks of the retina. The Heidelberg SPECTRALIS (Heidelberg Engineering, Heidelberg, Germany) simultaneously images the eye with 2 beams of light. One beam will map over 1000 points of the eye in order to continuously track eye movement, whilst the other beam uses this mapping as a reference to image the retina regardless of blinks or movements from the participant (60). This registration technique allows for high degrees of repeatability not only between scans, but between each individual eye movement (intraclass correlation coefficient (ICC) = 0.99) (61).

3.3 Scanning Laser Ophthalmoscopy

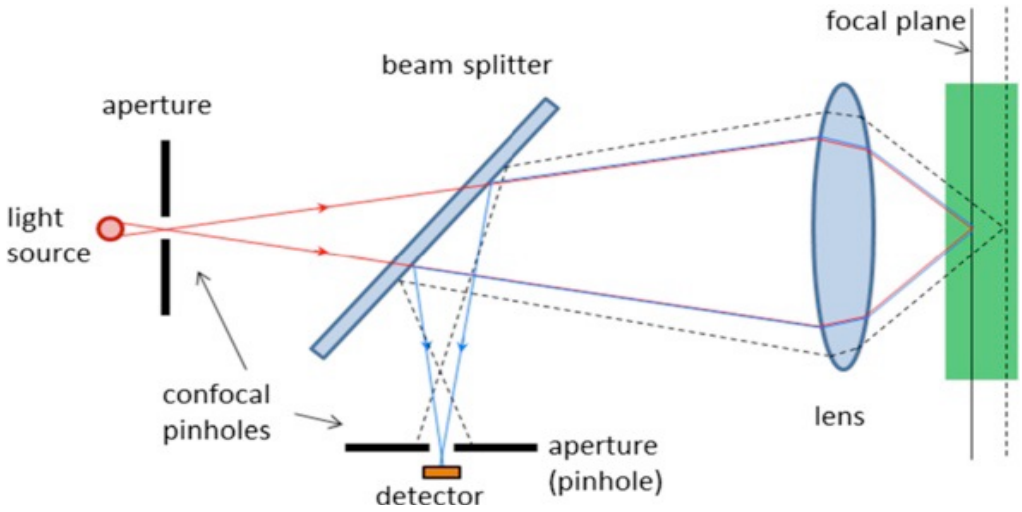

Figure 3.4: Schematic of the principles of SLO (53)

The scanning laser ophthalmoscope (SLO) offers high-resolution images of the surface of the retina, using an infrared light source along with the principles of confocal microscopy (53). A laser (such as one with a wavelength of 820nm) is directed through the pupil illuminating a

small region of the retina, approximately 10μm in diameter. Once a reflected signal has been detected and recorded, the beam is then moved to an adjacent position where another signal is measured. In this sense, each image is taken pixel by pixel in a raster pattern. Due to the confocal setup, only those signals which reflect from very close to the focal plane can be detected, which results in a higher imaging resolution (typically 5μm) than can be achieved with fundus camera systems (typically 7-10μm).

With fundus photography, a poorly dilated pupil can represent a significant obstacle to good-quality image capture (a problem exacerbated by the bright flash a patient experiences), but the use of infrared light alongside a confocal scanning protocol minimises the effect in SLO. Furthermore, infrared light penetrates deeper into the retina than the flash of light in fundus photography (53). This enables for useful information to be ascertained regarding the health of cell layers as deep as the RPE but it is not capable of quantifying the thickness of cell layers as OCT does.

Scans are taken in as little as 24ms allowing SLO to be utilised for video capture. The FOV available in SLO varies, but rarely reaches above 60° (53). For this reason, it is mostly employed for imaging the central anatomical landmarks e.g., fovea and optic disk. However, the high-resolution images generated do present an opportunity to investigate the peripapillary blood vessels and any subsequent changes which may occur to them as a result of neurodegenerative disease.

3.3.1 Ultra-wide field imaging

Figure 3.5: Stitching three fundus camera images together to create a larger FOV

Typical fundus image capture is limited by the small FOV offered by standard fundus camera and SLO devices. While this is adequate to view the posterior pole containing the central anatomical landmarks, it is inefficient at imaging the peripheral retina, its vasculature and pathology. Multiple fundus images can be computationally stitched together in a mosaic to render an image with a larger FOV (see Figure 3.5), but transitions between images are sometimes broken or badly aligned making measurements of vascular features such as vessel width and tortuosity unreliable. Ultra-wide field SLO (UWF-SLO) combats this by capturing a single image with a much larger FOV in one go without the need for pupil dilation, specialist contact lenses or lens attachments.

Much like SLO, UWF-SLO images are created using a confocal, pixel-by-pixel approach. Two lasers are used for imaging: red (with a wavelength of 635nm) and green (with a wavelength of 532nm) (62). In tandem, both lasers are swept across an ellipsoidal mirror Figure 3.6 (63)). Whilst each laser is directed through one of the mirror's focal points, the participant's head is positioned against the device so that the second focal point lies on the participant's retina. From here, the lasers move across the retina much like a conventional SLO.

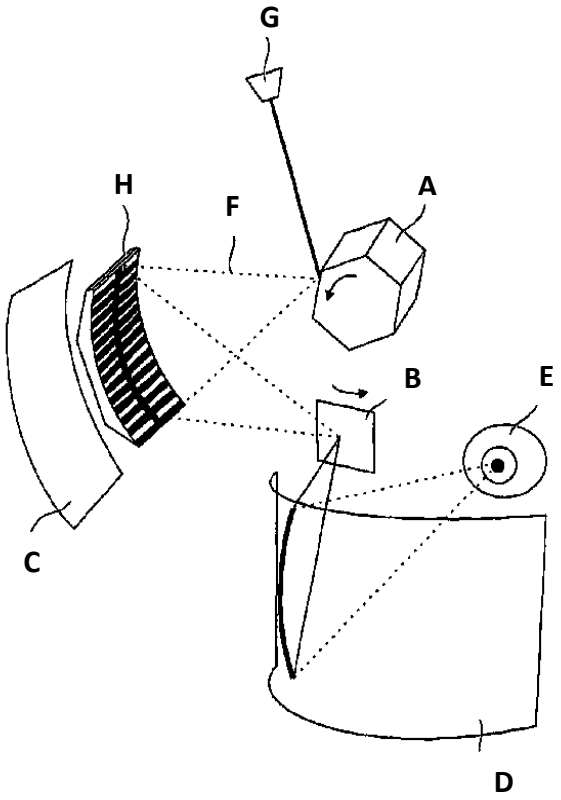

Figure 3.6: Schematic of an Optos UWF scanner system (97). A) High speed rotating polygon mirror. B) A second, low speed mirror. C) Ellipsoidal mirror. D) Main ellipsoidal mirror. E) Patients eye. F) Scanning beam. G) Light source. H) Reference object.

With just a 0.4s exposure time this technique enables capture of a pseudo-colour image (as there is no blue channel to create a true RGB image) whilst keeping patient discomfort at a minimum (62). With a maximum FOV of 200° (82% of the retina) UWF-SLO produces a

wealth of information on the retinal vasculature (63). However, artefacts such as eyelashes do limit coverage, and the superior/inferior regions of the retina may appear distorted in comparison to nasal/temporal regions. Although the resolution is less than with other types of fundus image (20μm vs. 7-20μm) and the participant experiences a bright flash of light, the FOV is much larger than that of SLO or fundus photography and scanning is not as affected by pupil contraction due to its confocal scanning mechanism (62).

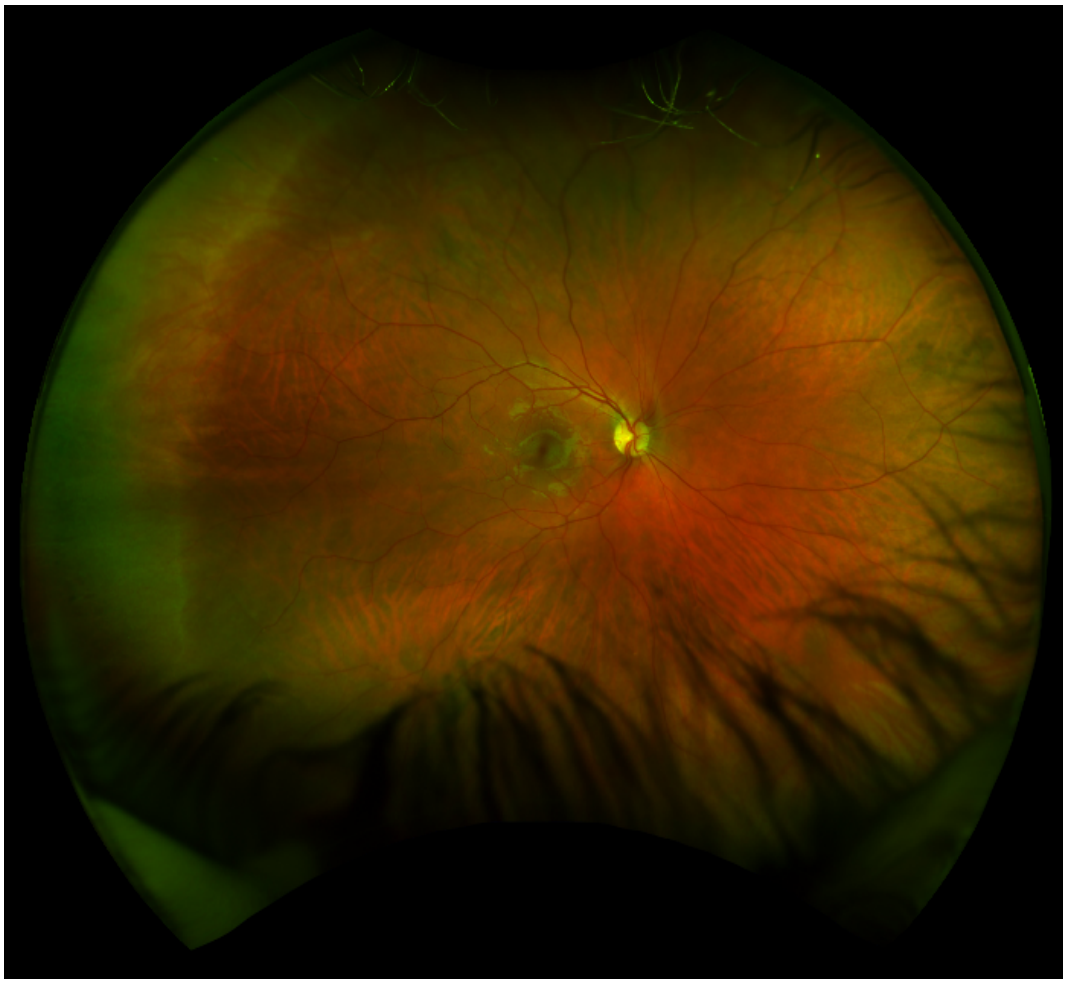

Figure 3.7: UWF-SLO image of the right eye once stereographically projected

Due to the spherical shape of the eye, mapping of a 3D surface onto a 2D plane creates difficulties when preserving qualities such as distance, area and orientation. As the incident beam travels a shorter distance to reach the periphery of the retina, the absolute area these

pixels represent on a 2D image will be smaller than those pixels located closer to the fovea. As such, there is an 'enlargement factor' associated with a pixel's angular location upon the retina (64). In imaging devices with small FOVs, the distortion has a negligible effect on measurements; it is only when considering large FOVs that this must be accounted for. Figure 3.7 displays an image which has been stereographically projected to conserve angles, which in turn compromises measures such as area and distance (much as a map of the world distorts the sizes of countries whilst in turn conserving shape). If distance measurements are to be made, appropriate mathematical translations provided by the manufacturer (which set a default axial length of 24mm) must be accounted for in any calculations (65). These calculations are based on theoretical formulations which have been tested and verified through the *in vivo* measurement of the Argus II retinal implant, the dimensions of which are precisely known prior to implantation (65).

UWF-SLO has proved a useful tool when investigating diseases which manifest themselves in peripheral regions of the retina e.g., retinal vasculitis, retinal detachment and diabetic retinopathy, and as such has remained a tool largely focused on these conditions (63) (66). The application of segmentation algorithms which can create reliable maps of retinal blood vessels in UWF-SLO images could be used to quantify indicators of vascular health in the eye such as tortuosity, vessel widths and branching geometry, and as such see UWF-SLO utilised more commonly in a clinical setting (67).

In contrast to OCT, fundus imaging has been under-utilised in biomarker discovery for neurodegenerative diseases. The lack of investigation is likely due to the sparsely available resources that allow for quantification of retinal features; unlike in OCT, SLO manufacturers do not provide segmentation software and as such, applications must be custom built. With the advent of novel computer algorithms to reliably segment the retinal vasculature in SLO and UWF-SLO images, it is now possible to investigate changes to the peripheral retinal vasculature in relation to neurodegenerative disease (68).

3.4 Visual acuity

Figure 3.8: Low contrast letter acuity chart (LCLA) (41)

With visual symptoms, such as those associated with ON, being more common in patients with MS, visual function should be considered clinically when assessing a patient's disability status. The leading outcome measure of visual disability in patients with MS is low-contrast visual acuity (LCVA), which attempts to quantify changes in retinal function through examining a patient's ability to read from a Sloan letter chart (Figure 3.8) (41).

Patients are required to sit approximately 3 metres from a backlit chart in a darkened room. One eye at a time, the patient identifies, from the top down, as many letters as possible from two charts; one full-contrast (100%) and another low-contrast (2.5%). As each chart progresses, the size of the letters decreases to not only test contrast sensitivity, but also measure a patient's sensitivity to various spatial frequencies (41). Once completed, each eye is given a

score based on how many letters (out of a potential 70) the patient correctly identified- this simple measure allows for linear statistical analysis but is still comparable to the logMAR system used by ophthalmologists when assessing ETDRS (Early Treatment Diabetic Retinopathy Study) - the current gold standard in research and clinical settings (41) (69). The test has an interrater reliability of 0.86 to 0.95 and is the most sensitive measure of visual dysfunction in MS currently available; a difference in score of 7 is considered clinically significant (41).

Clinical studies pertaining to LCVA suggest the test acts as a measure of damage to the inter-neural connections in the complex visual pathway and a recent review by Balcer et al. found that LCVA was a useful measure in determining impairment and disability from MS. LCVA has been found to correlate with EDSS, but also to decrease where EDSS score remains stable (41). This could suggest that LCVA may be able to discern changes to disability to which other measures are not sensitive (20). Axonal loss measured with OCT has also been found to correlate with a reduced LCVA score in both patients with and without clinical history of ON (42).

3.5 Summary

There are many modalities with which to capture images of the retinal anatomy, thus allowing investigation of the changes that may occur in patients with MS and other diseases. Much of the current research has relied on the ability of OCT to capture cross sectional images of the retina and subsequently measure thinning of the RNFL and a loss of ganglion cells. Such measures have been associated with brain atrophy and thus considered as a potential method of tracking disease progression (70). However, little research has been conducted on potential changes to the retinal vasculature, which may act as a useful surrogate for similar changes in the brain. With the advent of novel computer algorithms, which are tailor made to quantify vascular measures (e.g., vessel calibre, tortuosity etc.) in UWF-SLO images, comes the opportunity to investigate the vascular network in the retina of patients with MS, particularly

in the periphery.

Chapter 4

Materials and Methods

4.1 Introduction

This study was a preliminary investigation into possible changes which occur to the retinal blood vessels of patients with MS, and how these fit with known changes in RNFL thickness and macular volume. Multiple modalities of imaging were used to capture both the retinal cell layers and retinal vasculature, alongside visual acuity to quantify retinal function. This chapter will set out how the study addresses its hypotheses using a methodological, ethical and reliable approach to data collection and image analysis.

4.2 Study design

As investigating the peripheral retinal vasculature in patients with MS is a novel concept, there were no similar studies from which to estimate an effect size and perform subsequent power calculations. Importantly, this study aimed to provide just such data so that an estimate of the likely sample size needed for larger prospective studies could be calculated. Initial recruitment targets were therefore based on realistic expectations of how many individuals could be recruited from within the Anne Rowling Regenerative Neurology Clinic (ARRNC), Little France, Edinburgh, based on preceding MS studies run from within the clinic and their rates of recruitment. Thus, a target of 100 patients with MS, comprising 25 participants from each of the four MS subtypes, were to be enrolled with a further 100 age and sex matched HVs to act as a control group (recruited through word-of-mouth and staff emails sent to the local research community). Should a spouse or family member regularly accompany a participant with MS to their clinical consultations, they would also be approached to enrol in the study as a HV.

Competent and consenting patients with MS were recruited opportunistically; during a clinical consultation in the ARRNC with either a neurologist or MS specialist nurse the patient was approached regarding the opportunity to enrol in this study and given an information sheet to read. Potential participants were not approached directly by myself so as to not apply undue pressure to participate in the study or to breach patient confidentiality. Should the patient declare an interest in participating they were then introduced to me and I would answer any questions and detail the study more thoroughly. Patients were made aware that all identifying information would be removed from images prior to being exported from the ARRNC for analysis, and their participation in the study kept anonymous. It was also explained that they were free to withdraw from the study whenever they wished. All images would be reviewed by a clinical ophthalmologist for incidental findings and should any be found the patient would be contacted through their GP to take any necessary action. Exclusion criteria included any individuals who had undergone retinal surgery (other than laser vision correction), had severe myopia (i.e. -10 or more) or any pathologies which would compromise my ability to make accurate measurements with OCT or UWF-SLO images in at least one eye.

If an eligible patient wished to commit to the study, written consent was obtained. The imaging protocol then started with OCT as it required the greatest amount of sustained concentration from a participant and scanning at the end of a session could risk patient fatigue and failure to complete. A decision was made in this study not to dilate pupils as this may reduce the number of participants willing to enrol, and a comparison of RNFL thickness measured in dilated and non-dilated eyes showed no significant difference with SD-OCT (71). VA tests were performed prior to UWF-SLO capture as this device emits a bright flash of light which may affect a participant's performance in LCVA tests. Once baseline scans were acquired at this initial session, follow-up scans for participants with MS were taken alongside future clinical consultations so as to not inconvenience the participant with additional visits to the clinic. These would typically be every 3, 6 or 12 months. For HVs, follow up scans were arranged at approximately 6-month intervals at a convenient time for the participant.

4.3 Recruitment

Characteristics	Patients with MS (N = 72)	Healthy Volunteers (N = 80)
Median Age	44	38
Age range	20-79	23-73
Male	19	19
Female	53	61
History of ON (No. patients)	16	0
History of ON (No. Eyes)	19 (OD 9, OS 10)	0
Relapse-remitting	62	N/A
Primary progressive	2	N/A
Secondary progressive	7	N/A
Disease-modifying therapies*	46	N/A

Table 4.1: The demographic of people who took part in the study. ON = Optic Neuritis, OS = Left eye, OD = Right eye. *These include: Fingolimod, Tecfidera, Dimethylfumerate, Copaxone, Plegridy, Alemtuzimab and Tysabri. One MS participant's disease subtype was unable to be determined from their electronic correspondence.

All imaging was completed within the ARRNC between July 2015 and September 2017. Final recruitment numbers are shown in table 4.1. Only one of the healthy controls within this study was recruited as the spouse of an MS participant- this was mostly due to a lack of spousal company during clinical consultations. However, when approached to participate, healthy spouses were often rushed for time or put-off by the necessity to come in for follow-up scans. Information on participants with MS relating to their disease was identified by research nurses in the ARRNC using historic electronic patient correspondence. This included the initial date of MS diagnosis for each participant as well as any clinical history of ON, current disease-modifying medication and the most recently available EDSS score.

The length of disease ranged from 1.7 to 38.5 years. 46 MS patients were being treated with

disease modifying therapies during the time of their participation in the study, 12 of which were prescribed Fingolimod (a drug associated with an increased risk of macular oedema) (15). Recent EDSS scores could only be found for 2 participants (scores of 0 and 7). Median age was slightly lower in the group of HVs when compared to participants with MS (38 and 44 respectively), with the group of individuals with MS having a greater age range. An equal number of male participants were scanned in both the HV and MS groups, although more female HVs were scanned than females with MS. This was a consequence of the large number of responses from females (mostly young PhD students from the local research community) volunteering to be involved in the study. Of the MS participants, 8 right eyes and 10 left eyes had at least one previous episode of ON.

Follow-up scans were successfully attained for 65 participants with MS and 72 HVs. The healthy controls for which follow-up scans were not attained had either moved away, making scanning unfeasible, or could no longer be contacted- most likely because they no longer worked/studied within the local research community. Follow-up scans for participants with MS were reliant on those individuals returning to the clinic for their scheduled clinical consultations, the dates and times of which were given to the research team in advance. In some circumstances, these individuals would miss their appointment or would simply opt for an over-the-phone consultation due to a lack of any progression in their symptoms. Patients were not contacted with respect to scheduling an extra clinic visit just for the purposes of having a follow-up scan for the study.

The number of scans for each individual within the MS group ranged from 1 to 5, with the time difference between baseline and final scan ranging from 196 to 672 days. HVs were scanned between 1 and 3 times during their participation in the study, the time difference between baseline and final scan ranging from 227 to 802 days.

4.4 OCT imaging procedure

OCT imaging was completed with a Heidelberg SPECTRALIS (Heidelberg Engineering, Heidelberg, Germany). Prior to scanning, participants were given a brief introduction to what the OCT device does and how it works as well as simple instructions to be followed during the scan such as where to direct their gaze. Effort was made to ensure each participant was comfortable resting their head in the correct position by adjusting the height of the apparatus. A small internal blue light was used to help fixate the participant's gaze in the desired position for a given scan. Should a participant have trouble fixating on the dot (either because they were partially sighted or fatigued by the scanning), external red LED antennas were used to help direct a participant's gaze to the correct orientation. Participants were free to blink during the scanning and if at any point they felt uncomfortable, a short break and adjustment of the apparatus was offered. In chronological order, the scans taken were as follows:

- Horizontal line scan- a straight line which runs from the centre of the optic disk, through the foveal dip. Automatic real time (ART), which is a measure of how many scans are averaged to compile a single image with the SPECTRALIS, was set at 100 as per the manufacturer's recommended acquisition protocol. Scans are averaged using the registration techniques laid out in the previous chapter.
- Vertical line scan- a line which runs perpendicular to the horizontal line scan, once again passing through the foveal dip. ART set at 100 as per the manufacturer's recommendation.
- Posterior pole scan- a volume scan which allows for measures of macular volume, comprising multiple line scans perpendicularly aligned across the macula. ART for each individual line scan was set at 12, as per the manufacturer's protocol.
- Peripapillary scan- a line scan which is taken in a circular fashion around the optic disk, with a radius of 3.4mm. ART set at 100. This was taken last as it was the only scan requiring the participant to fixate on the light appearing at the side of their vision towards their nose, so as to centre the image on the optic disk rather than the fovea.

In volume scans the ART was set lower than in 2D scans as the increase in SNR that comes with higher ART would not compensate for the large amount of time it would take to complete the acquisition; patients with MS would often begin to feel fatigued during the scanning process and struggle to remain fixated for long time periods. Moreover, segmenting the macular in volume scans is often simpler than segmenting single cell layers such as the RNFL, as the boundaries are much better defined. This in turn allows for a smaller SNR for the acquired image. For each scan, a participant would have multiple images taken for each eye; the best scan was selected through careful assessment of three areas:

- Quality score- this is a measure of signal strength given by the manufacturer's propriety software. Scans with a score less than 25 were deemed too poor to gather accurate and precise thickness values of individual cell layers. It has been shown that signal strength in SPECTRALIS OCT scans are negatively associated with RNFL thickness measures (poor quality scans overestimate thickness values) (72).
- ART score– though with line scans the ART was set at 100, this was not always attainable if the patient was restless, blinked frequently or had mild cataracts. This was due to the real-time tracking algorithm employed by the SPECTRALIS described in the previous chapter. As such, the scan which had the largest ART score generally had the greatest definition between cell layers and was selected for analysis (see Figure 4.1) (73). Studies have shown that an increased ART score is associated with better reproducibility and reduced short term and day-to-day variability in RNFL thickness measures made using the SPECTRALIS device (74).
- Quality of segmentation- largely, the quality of the segmentation was dependent on the signal strength and ART score. However, on some occasions, artefacts or misaligned scans would cause erroneous segmentation by the software (see Figure 4.5). If so, the image with the most accurate segmentation of cell layers (or macular in volume scans) as determined by operator inspection was selected for analysis.

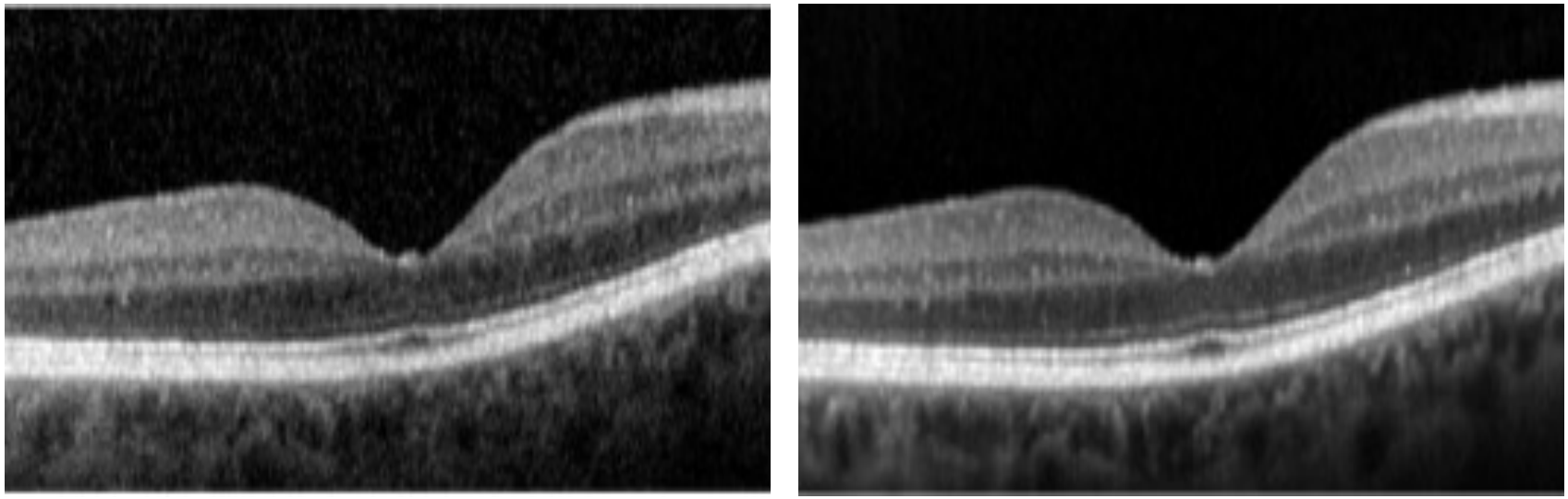

Figure 4.1 Two OCT images from the same individual depicting different ART scores. The left scan was created from 2 B-scans whilst the right scan was comprised of 96 B-scans (73).

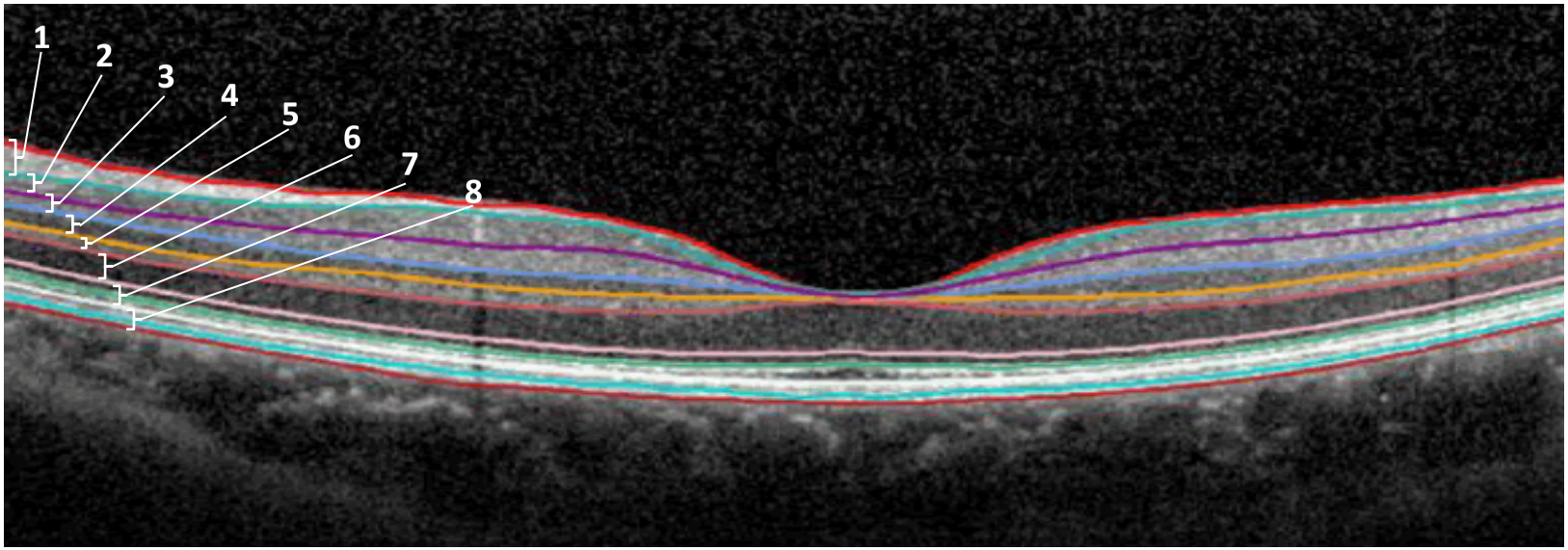

Figure 4.2: An example of the segmentation output from a Spectralis device, showing the different retinal layers from top to bottom: 1) RNFL, 2) ganglion cell layer, 3) inner plexiform layer, 4) inner nuclear layer, 5) outer plexiform layer, 6) outer nuclear layer, 7) photoreceptors and 8) retinal pigment epithelium (98)

A degree of post-processing was required with the OCT scans. The accuracy of regional peripapillary RNFL thickness measurements are dependent on correct identification of the fovea (as regions are created using fovea and optic disk position). Though foveal segmentation is automated, it was checked by the operator and adjusted if necessary. An example of correct foveal segmentation is shown in Figure 4.3 with a blue line which connects the centre of the optic disk to the centre of the fovea. Also shown in Figure 4.3 are the RNFL thickness measures in μm for each region produced by the device's own analysis software (HEYEX, software version 6.5, Heidelberg Engineering, Heidelberg, Germany). It was equally important that the fovea was correctly identified for macular volume scans (see Figure 4.4). Once again this is a semi-automated process, with manual fine-tuning of the position essential. Foveal position was deemed correct when the pixel directly in the centre of the measurable area was located at the place of minimal retinal thickness (in line with the foveal dip).

To eliminate any errors in segmentation, the operator would assess the quality of segmentation visually in all scans. To minimise human error, the segmentation (if seen as inaccurate) would be run automatically a second time with the device's software; the robust image analysis algorithms used to segment the scans had a high rate of reproducibility (ICC = 0.988 for mean RNFL thickness) making it favourable over manual segmentation (75). Should the results still be considered erroneous, minimal manual corrections were made by the operator to correct the segmented area to one which was deemed more accurate by visual inspection (see Figure 4.5). Small segmentation errors were common around the retina's surface blood vessels as the lumens of these vessels lay within the RNFL, and the subsequent reflection of incident infrared light causes vertical shadows down to the choroid, disrupting segmentation slightly. Unless this caused any egregious errors (10 pixels or more), they were left uncorrected as it would take a considerable amount of time for the operator to correct all of them and would thus be impractical. Errors which required manual correction were rare and often due to subtle artefacts or poor scan quality, but nevertheless had to be manually refined to improve accuracy (76). Secondly, intervention by the operator was kept to a minimum as automatic segmentation

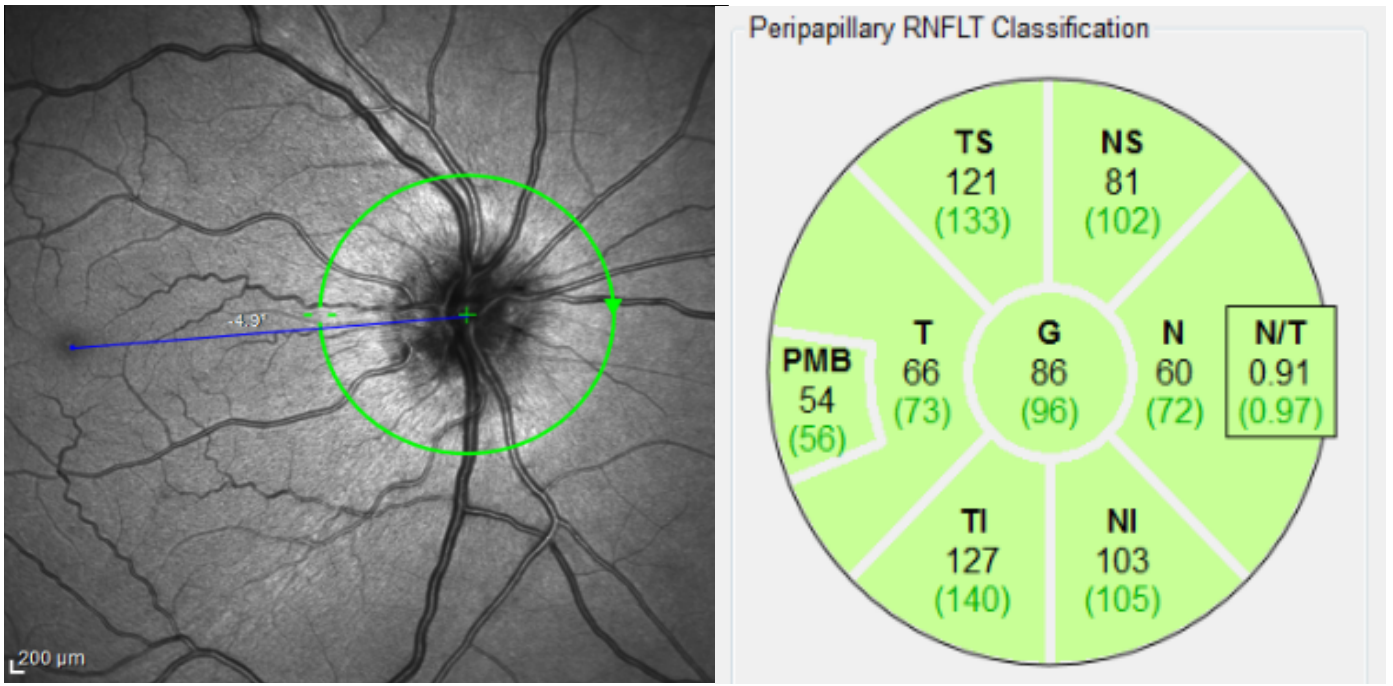

Figure 4.3: Left- manual identification of the fovea, with the green circle tracing the path of a peripapillary OCT scan. Right- subsequent segments automatically produced by the proprietary software on the Heidelberg SPECTRALIS device. Numbers in black represent µm measures of peripapillary RNFL thickness for the retina displayed. Numbers in green are the mean RNFL thickness values in µm for each region, determined from a sample population.

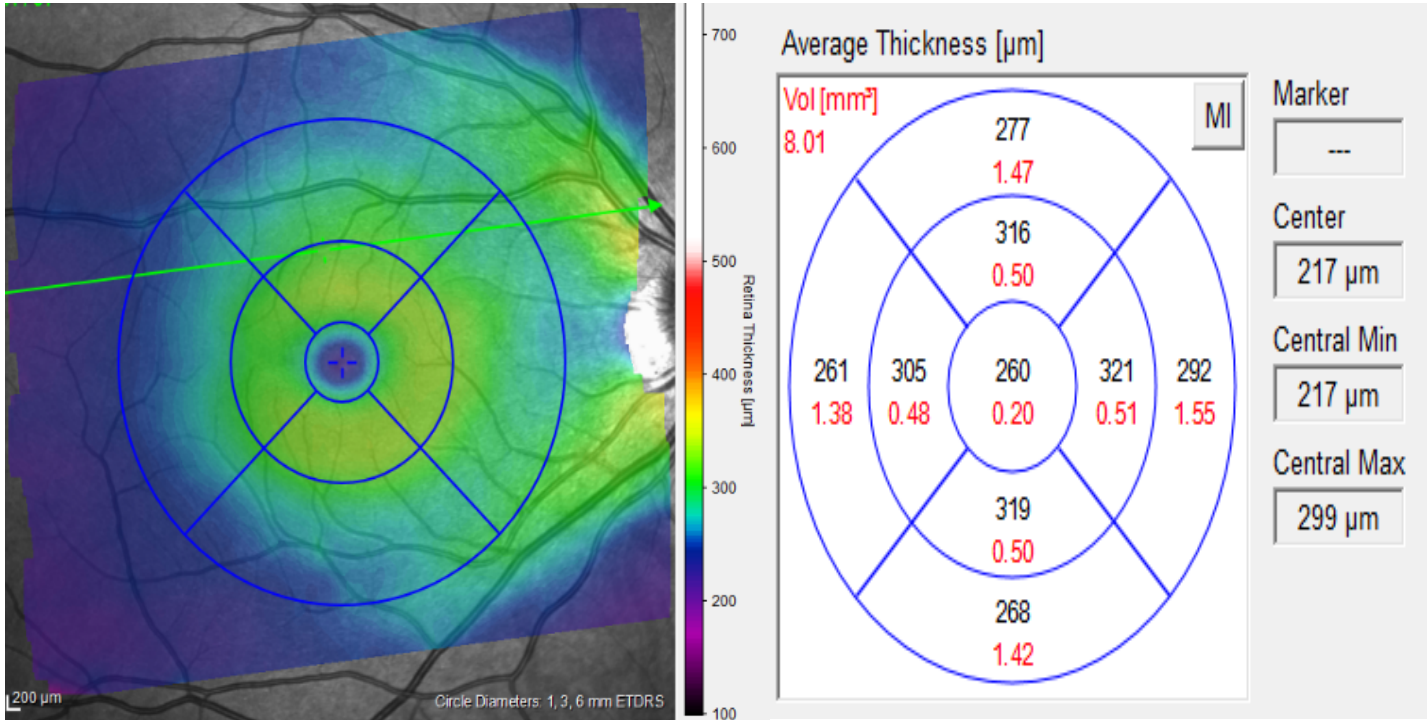

Figure 4.4: Left: Thickness heat map of the macular Right: Regional thicknesses of the macular, with 'center' value manually moved to the fovea

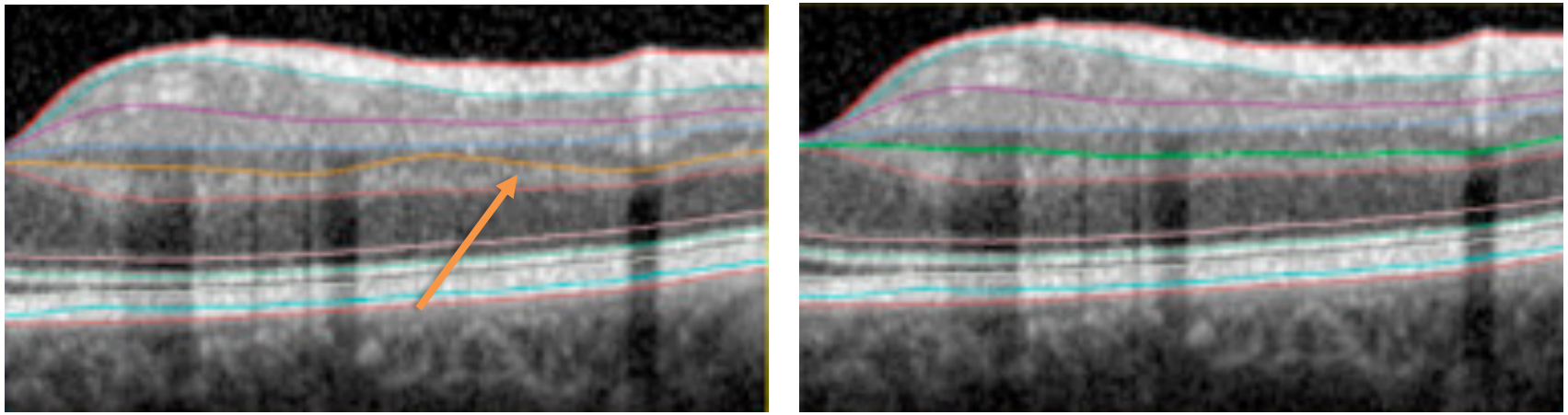

Figure 4.5 OCT image depicting an incorrect segmentation of the inner nuclear layer on the left, as highlighted by the orange arrow and line. On the right: a segmentation of the inner nuclear layer once manually corrected, shown with the green line (99).

around blood vessels in a follow-up scan were likely to be comparable to segmentation in baseline scans, therefore being a more consistent approach than manually correcting segmentations when investigating longitudinal changes in the data (75).

Once a baseline scan is taken for a person, it is set as a reference for all of their future scans; whenever a participant has a new scan, the SLO image of the fundus is automatically registered to the baseline image so that the new OCT scan is acquired in the same location and orientation as the original. All previously manual interventions such as fovea-placements are then automatically aligned with the original scan allowing for a direct longitudinal comparison. Reproducibility and repeatability measures of mean retinal thickness are reported by the manufacturer with standard deviations of 1.6μm and 1.1μm respectively (57). Outliers, i.e. suspiciously thick or thin measurements, were identified using box plots for each of the three participant groups: HVs, participants with MS but no clinical history of optic neuritis i.e. MS (no ON) and participants with MS and a clinical history of optic neuritis: MS (ON).

4.5 UWF SLO imaging procedure

UWF-SLO scans were acquired using an Optos Daytona (Optos, Dunfermline, Scotland). Participants were given brief instructions specific to this imaging procedure and made aware of the bright flash they would experience when the image is taken. To acquire the best possible images, participants were asked to keep both eyes open regardless of which eye was being scanned. If participants struggled to assume the correct head position for scanning, I would intervene and with their permission gently guide the participant's head accordingly.

Participants had two images of each eye taken and the best image from each eye was selected for analysis. Image quality was determined by how clearly both the optic disk and fovea could be viewed and the amount of peripheral vasculature that was visible. Images were exported in non-compressed TIFF format (to preserve detail) and sent for stereographic projection which re-maps the image to account for the curvature at the back of the eye, conserving angular dimensions about the fovea. Projected images were then assessed for quality of the projection; a file containing the "Maximum percent error in area measurement" which was automatically created for each image was made available by Optos. Should this value be above 1, the image was declared poorly projected, upon which manual identification of the fovea was made. The coordinates of the fovea were then used to re-project the image with the aim of producing a better projection with an error of <1. If the error remained above the threshold of 1, then the image was discarded as converting pixel measurements made of the vasculature into mm measurements relies on the accurate re-mapping of the retinal image (65). If an image was successfully projected, it was then prepared for analysis by segmenting the retinal vasculature.

To enable the best possible segmentation of the retinal vasculature, a mask was created manually to crop out features such as eyelashes and the eyelid that would interfere with this process and lead to artefacts. Though this reduces the usable FOV of the image, the resulting region of interest (ROI) will still be considerably larger than that of a conventional fundus camera or SLO. The masks were designed to maximise the amount of visible peripheral

vasculature, whilst mitigating against artefacts. Some artefacts (mostly eyelash) were still included in the useable ROI if excluding them meant also excluding a large percentage of the retinal vasculature. Then the image is segmented to produce a binary map of the blood vessels detectable on the surface of the retina (Figure 4.6) (68).

While this map will subsequently be used for quantifying vessel widths, it is not a perfect representation of the vascular network; accuracy of the algorithm has been reported as 0.965 ± 0.006 (68). Some smaller vessels fail to be segmented due to the lower resolutions inherent to UWF-SLO imaging, and the vessel network itself may contain inaccuracies at complicated junctions or vessel crossings. Therefore, a skeletonised version of the binary map (with vessels represented with only a 1-pixel diameter) was created whereby vessels are connected within a graph structure by individual ‘nodes’, which either represent the start/end of a vessel, a vessel crossing or a junction at which a vessel bifurcates. Next, each image’s skeleton was subjected to manual corrections, completed by myself as the sole operator.

Figure 4.6: a) UWF-SLO image of a study participant b) Corresponding binary map of the segmented retinal vessels produced from the image in a).

The purpose of the manual correction step was to create as accurate a representation of the vascular network as was possible whilst minimising the likelihood of erroneous vessel measurements. This first meant the deletion of false positives which were actually representations of something other than the retinal vasculature e.g., eyelashes, drusen, choroidal vessels. In Figure 4.7, the effects of a blonde fundus are shown, whereby choroidal vessels are observable through the retina and are subsequently segmented unintentionally due to their similar appearance to retinal vessels e.g. their width and piecewise linear structure. For measurements of retinal vessels to be accurately quantified, it was important to remove false positives from the vessel skeleton.

Segments were also corrected manually when two vessels that lied parallel to one another were represented as a single vessel rather than two distinct structures, which would prevent accurate width measurements (Figure 4.8). Similarly, it was common for vessels close to the optic disk to run parallel to one another without a distinguishable gap between them, meaning when it came to measure the width of these vessels, the resulting analysis would be incorrect. In this scenario, both vessel segments were deleted until the separate vessel paths could be resolved.

In some circumstances, a small portion of a vessel would fail to be segmented. Though this may seem insignificant, when vessel paths are later identified (stretching from the optic disk to the outer periphery) such scenarios would lead to two distinct and separate structures rather than one complete vessel tree, essentially splitting a vessel path in half (Figure 4.9). As the main advantage of UWF SLO imaging is its ability to view the peripheral retina to give measurements of long vessel paths, this inaccuracy was corrected wherever possible. On small scales vessels are piecewise linear, so such corrections are merely straight-line paths. However, if the distance between the two segmented pieces of vessel is too large, joining the two segments with a straight line may not be representative of the true path taken by the vessel. As such, connecting vessel segments together was only completed where the distance was

Figure 4.7: a) Skeletonised binary map overlaid onto a UWF-SLO image with falsely segmented choroidal blood vessels b) The same image with choroidal vessels removed manually

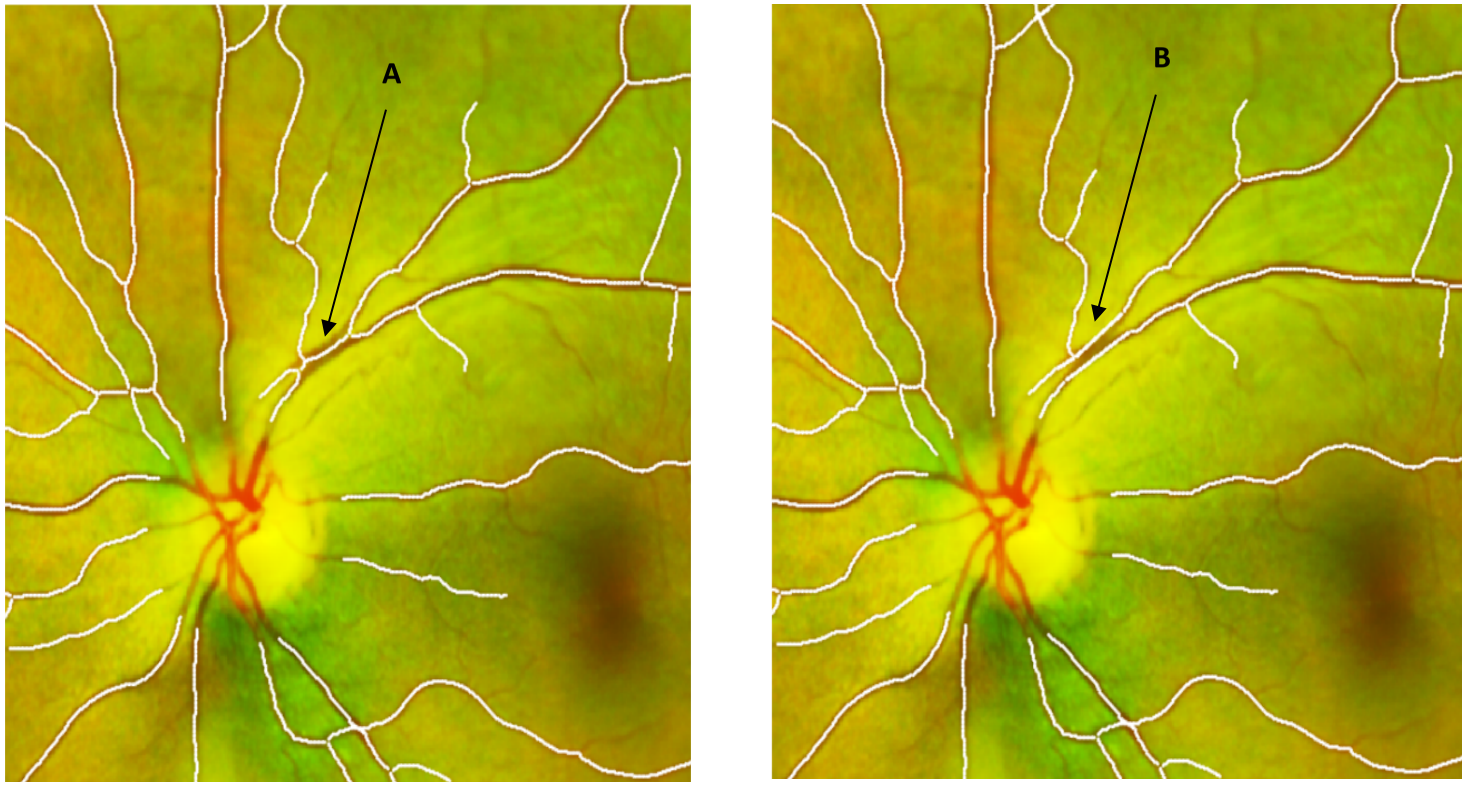

Figure 4.8: **a**) Erroneous segmentation whereby two vessels are represented as one **b**) Corrected segmentation where there are now two distinct vessels

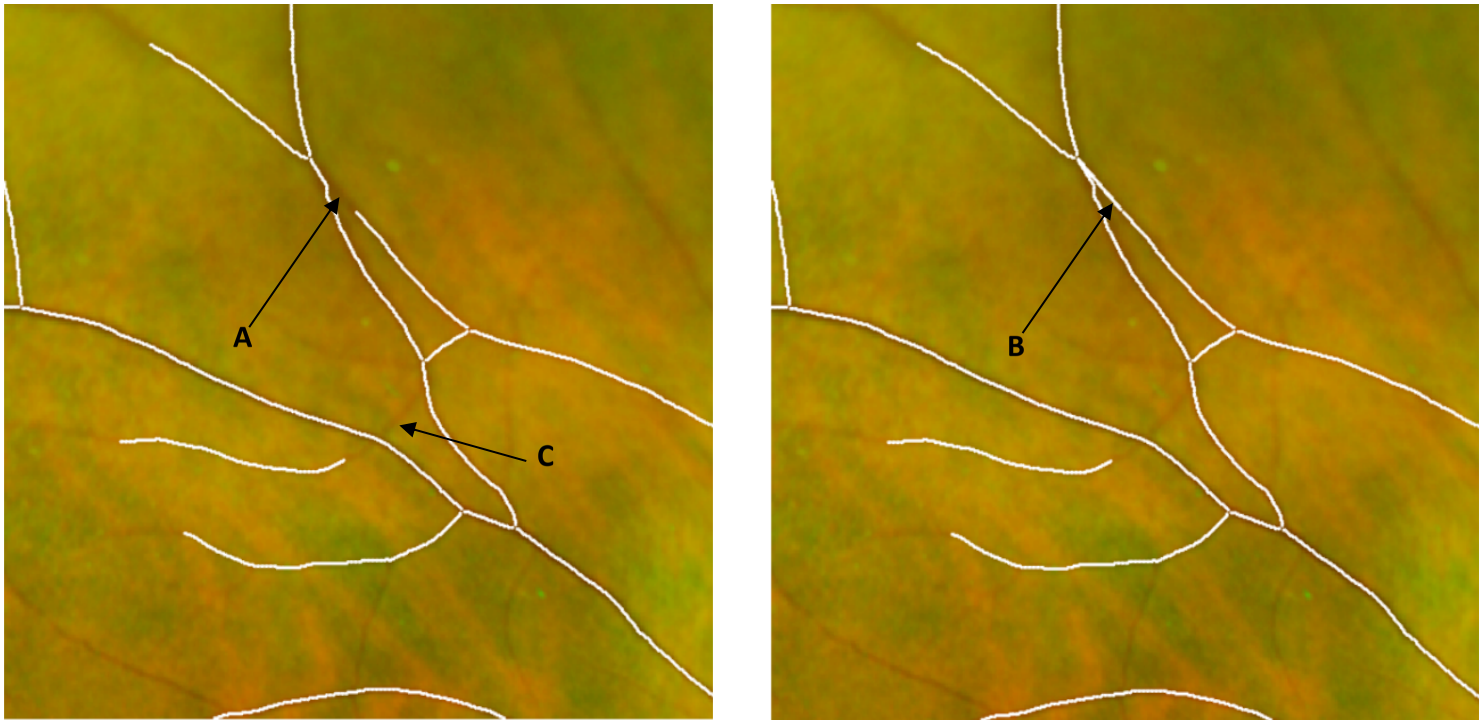

Figure 4.9: **a**) Vessel with a gap in its path **b**) Vessel is now connected and path is complete **c**) Gap in vessel is too large to accurately correct

small enough that a straight line could be considered a viable representation of the vessel's true path.

Vessel segments that were falsely connected were separated at a crossing or junction by creating a new node- what was once a single vessel will be two vessel segments that connect to a newly created node (Figure 4.10). Having corrected the skeletonised vessel map, myself as the operator then manually identified segments as being either arteries or veins to create separate arterial and venular trees. These are essentially networks, whereby each vessel can be traced from its original parent segment (next to the optic disk) to its end node in the periphery of the retina.

Distinguishing between the two vessel types can sometimes be speculative and open to interpretation, however by using the following rules an accurate classification can mostly be achieved by a trained observer.

- A crossing of two vessels will never consist of two vessels of the same type i.e. one will always be a vein and the other an artery.
- Veins appear thicker and darker than arteries due to transporting deoxygenated blood.
- Veins and arteries generally alternate when emanating from the optic disk.

Finally, the processed images were used to identify which vessels to use for biomarker analysis. Due to the longitudinal nature of the dataset, it was important to ensure the same vessels were being analysed consistently for each participant's follow-up scans, regardless of difference in image quality, orientation or length of vessel path. Each image was split into four quadrants: nasal inferior, nasal superior, temporal inferior and temporal superior. Quadrants were made by creating a line from the centre of the optic disk to the

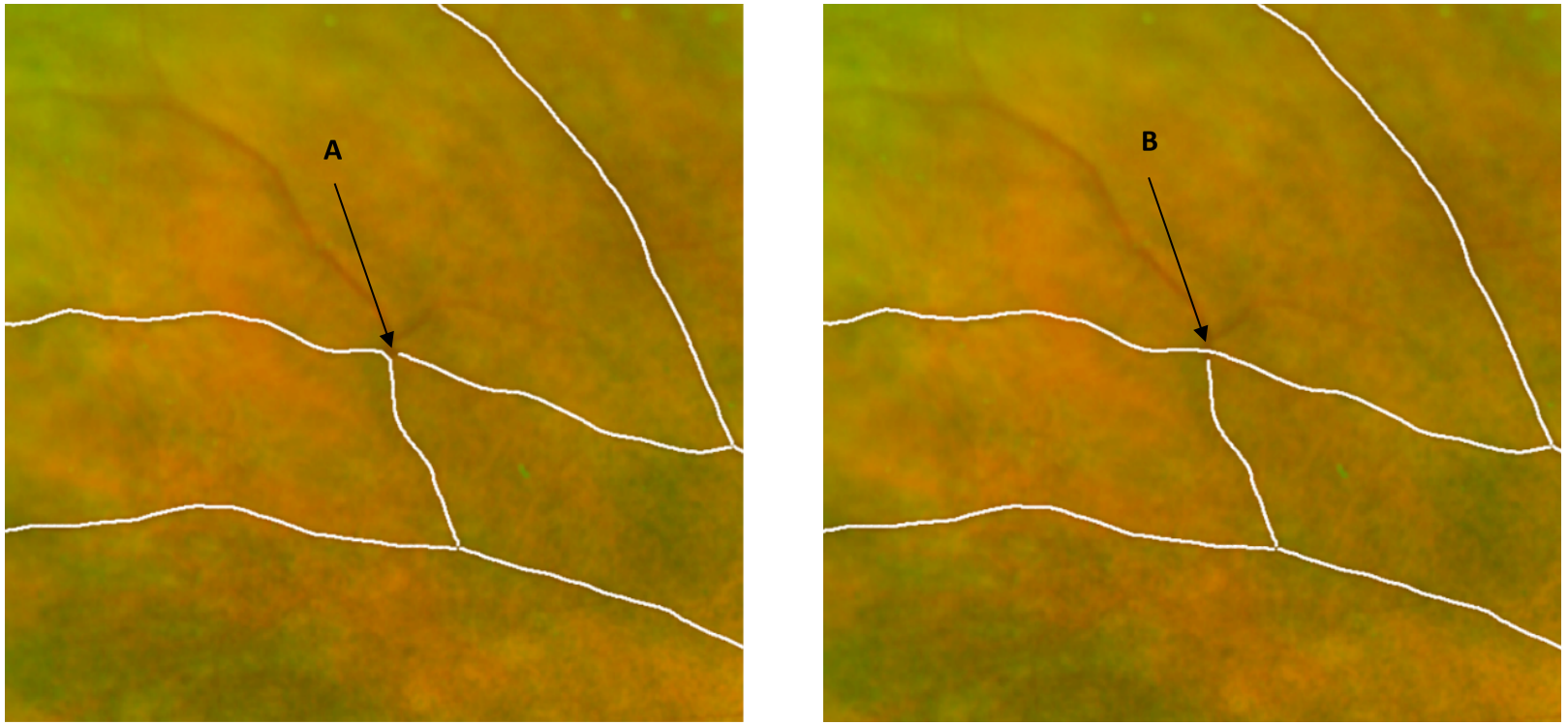

Figure 4.10: **A**) Erroneous vessel path identified at junction **B**) Vessel path corrected

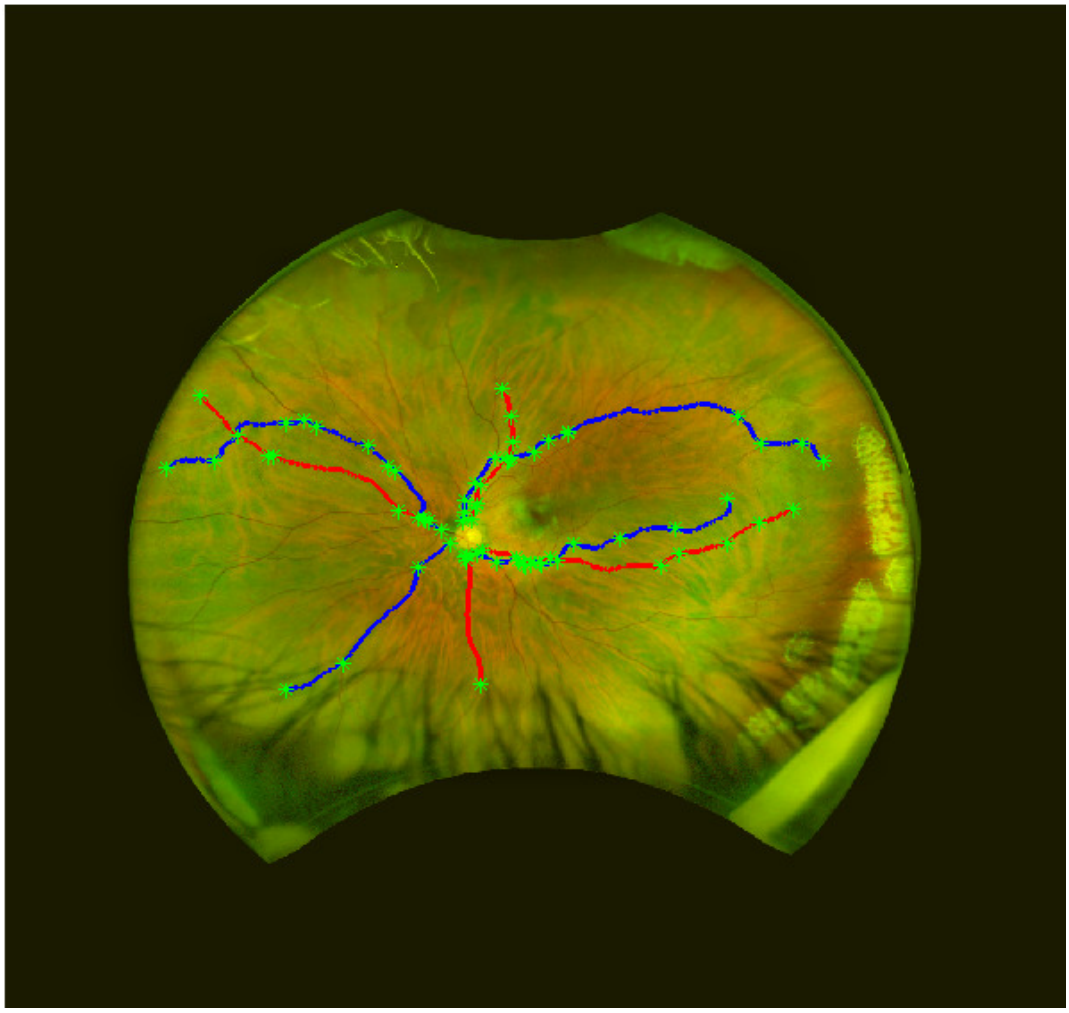

Figure 4.11: Example of the 8 vessels selected for analysis in a participant. Veins are coloured blue and arteries red, with the nodes (i.e. crossings, bifurcations, start and end points) plotted as green crosses.

centre of the fovea for superior/inferior hemispheres and another line perpendicular to this for the nasal and temporal regions. For each image, a maximum of 8 vessels were selected- 4 veins and 4 arteries. Vessels were selected such that each artery/vein originated from within one quadrant of the retina. If there were multiple vessels to choose from within a given quadrant, the vessel path selected would be the one which had the longest path regardless of which quadrant the vessel path ended in. If there was a choice between two vessels of approximately equal path length, the vessel which ended closest to the centre of the quadrant in which it began was selected. The same vessel was selected for each follow-up image, therefore if a vessel had

a large path length but was obstructed within one of the follow-up images of the same participant, a shorter vessel which appeared in every image was instead selected.

As vessel widths decrease as a function of their path length (from the optic disk to the periphery), care was taken to create a standardised vessel width measure from within a specific location on the retina. To enable direct comparison between participants, only select portions of each of the 8 main vessels were used when measuring vessel calibre. Any pixel from a selected vessel which lay between 6.5 and 8.5 optic disk radii away from the optic disk centre was used for vessel width analysis (see Figure 4.12). Prior to width measurements being taken a spline refinement algorithm was incorporated to smooth the edges of the vessels (77) (68). Estimates of the true vessel width were then calculated using gaussian-fit adaptations and an algorithm by Lupascu *et al*. which utilises cross-sectional intensities of the vessels alongside bagged decision trees (78). Width measures were taken from each quadrant separately so as to determine any anatomical changes specific to particular regions of the retina (as shown in RNFL data). Further to this, measurements taken from participants with a history of ON were separated for each eye so as to investigate the potential changes to retinal blood vessels caused by oedema during ON. All vessel width measures were converted from pixel to millimetres using an algorithm supplied by Optos that accounts for a pixel's global position on the retina with respect to the fovea (79).

Graphical representations of the raw data produced from this targeted approach, such as those shown in Graph 4.1, highlighted a clear positive skew in vascular width measurements for all four quadrants. Width measures which were found to be beyond the 95% confidence interval for each quadrant were therefore investigated manually and the majority of these were discovered to be representative of erroneous segmentations around vessel crossings or bifurcations, which in turn caused a larger width measure than was deemed accurate by visual inspection. Such points were removed from the UWF-SLO dataset and the remaining width measures were assumed to be accurate and included in the analysis.

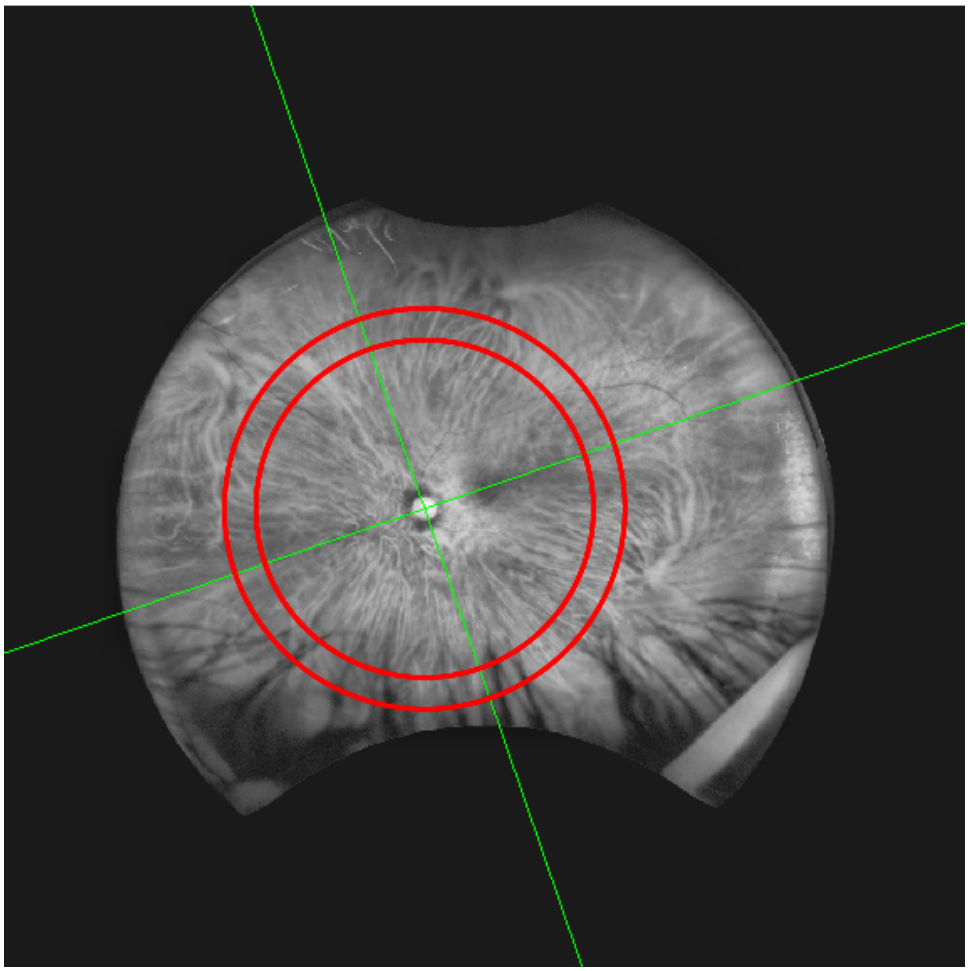

Figure 4.12: A visual representation of the region from which vessel widths are measured in UWF-SLO data; the area between the rings lies between 6.5 and 8.5 OD diameters from the OD centre. Green lines mark the boundaries of each quadrant, created from a line which bisects to centre of the OD and the centre of the fovea.

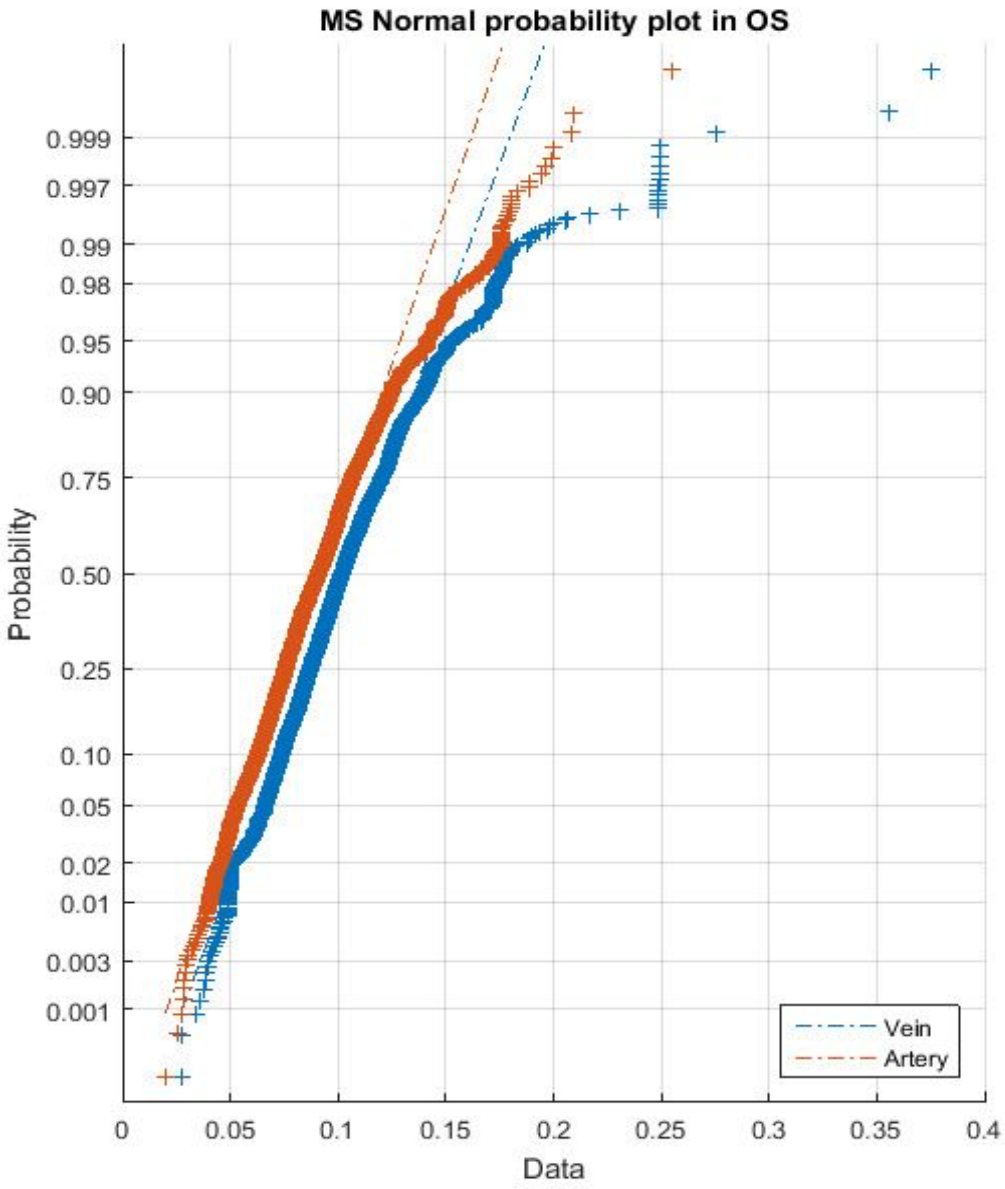

Graph 4.1: Normal probability plot for vessel width measurements in the left eye (OS) showing a positive skew in both arteries and veins

4.6 Visual acuity procedure

Visual acuity was measured for each participant whenever possible. If a participant was without spectacles worn for myopia, then the test was abandoned. Whilst sat 3 metres away from a backlit 100% Sloan letter chart, participants were first asked to read the characters, from the top, one eye at a time. For consistency, the eye not being tested was covered with an opaque object. Participants would continue to the following line providing they identified 3/5 letters correctly. Scores were tallied before changing the chart to one which measured 2.5% LCVA. From here, the process was repeated with instructions for the participant to take their time, and not to worry if letters came in and out of focus. During the process, lights in the room were switched off to allow for the greatest contrast between characters on the charts. As visual acuity data was collected manually at the time of each participant's visit to the ARRNC, no data was excluded for use in analysis upon inspection of outliers.

4.7 Statistical methods

The data were analysed statistically using MatLab and the Statistics Toolbox (Release 2015a, The MathWorks, Inc., Natick, Massachusetts, United States). Normality of the data collected was tested using a selection of objective and subjective approaches. For participant groups with a sample size $N>50$ (e.g., HV, MS (no ON)) a Lilliefors test was utilised, which rejects the null hypothesis that data is normally distributed at the 5% significance level. Due to the low number of participants generally ($N<100$) in each group, the p-values produced were not deemed enough to be used definitively as a test for normality. Therefore, the data were also visually assessed using box plots to look at symmetry and histograms to identify Gaussian distribution curves, while normal probability plots aided in uncovering any inherent skews/lack of normality. In circumstances where $N<10$, such as in the MS (ON) group, data points were too few to reliably assess normality and were treated as being non-normal during statistical analysis.

Where data was found to be normally distributed, a two-sample t-test was used separately for

each eye to identify significant differences between the retinal parameters measured from each participant group: HV, MS (no ON) and MS (ON). For sample distributions where N>30, confidence intervals for differences in the mean where calculated using the central limit theorem: the standard deviation of a sample distribution is approximately equal to that of the sampling distribution's (80). In cases where N<30 e.g. MS (ON), confidence intervals were estimated: a t-distribution represented the shape of the sampling distribution, under the assumption that the group distribution was normally distributed. In non-normal datasets, differences in the median value were instead investigated using the Wilcoxon rank sum test, as this does not rely on the assumption of a Gaussian distribution within the datasets being compared. 95% confidence intervals (CIs) were calculated using a bootstrap function, which creates a distribution of the difference in medians between 1000 resampled groups and ranks these values from lowest to highest and provided an estimate of the 95% CIs of the actual dataset.

To determine the effects of potentially confounding variables in the retinal parameters measured, the data was analysed using multivariate linear regression models in correspondence with similar studies of OCT data (33) (42) (35). Despite a tendency in the literature to adjust for intraocular variations within regression models, or to assume left and right eyes to have a high degree of intercorrelation, this study kept eye data separate so as to investigate lateral asymmetry, which has been found in RNFL thickness measures of healthy individuals (81). Due to the low sample size of participants with a clinical history of ON (OD: N = 9, OS: N = 10), only MS participants without a clinical history of ON were included in this analysis. As per regression models put forward by comparable studies, *age* was considered as one of the possible predictors along with two binomial variables: *disease* (disease vs no disease) and *sex* (female vs male) (27) (82).

To determine the combination of predictors which produced the models which most accurately described the data whilst avoiding overfitting, the model which was both significant and explained the greatest variation in the data (i.e. had the largest adjusted R-squared value) was

identified. Should no model be significant, then selection was based on the adjusted R-squared value alone. The coefficients produced by the selected models were then used to assess the effect that each predictor has on the measured anatomical changes in the retina, along with their significance. In order to assess the robustness of each model, they were verified subjectively; the residuals from a model were tested for normality (to ensure a linear model is correct for characterising the data) via box plots, histograms and normal probability plots, and the model was run again once the most influential data points had been removed. Influential points were identified as those having a Cook's distance which was greater than 3 times the mean Cook's distance for the dataset from which it came (83). Remodelling once these points had been removed allowed an understanding of whether a model was robust or susceptible to a large degree of change towards a few highly influential pieces of data.

MS (no ON) data was isolated to investigate the potential of *length of disease* (from date of diagnosis to date of baseline scan) to act as a predictor of retinal anatomical measures. *Age* and *sex* were again considered as possible predictors when constructing these models. For macular volume, an additional predictor, *fingolimod*, which identifies individuals who are being treated with Fingolimod during their enrolment within the study, was also included as a possible predictor, as taking this drug has been associated with an increased macular volume (84) (85).

Though the intervals between follow-up scans were approximately 3, 6 or 12 months apart, for use in statistical analysis the intervals were too irregular for a direct comparison of changes in the retinal anatomy between different participants. As such, any changes seen in the anatomy of each participant were standardised as a rate-of-change per year, a technique mirroring that of another study found in the literature which imaged participants longitudinally at irregular intervals (35). This approach allows for participant-to-participant comparison regardless of the time elapsed between baseline and follow-up scans. For each individual who had received at least one follow up scan, a first order polynomial was fitted to their follow-up data, and the gradient of this line was used for calculating rate-of-change per year. Despite

some participants receiving scans over a period of time which is greater than two years, any changes which occurred in the retina over this period of time (rather than over the entire disease course) were predetermined to be piece-wise linear in their nature, hence the use of a first order polynomial. This is not to say that the pattern of change over an entire lifetime would necessarily fit a linear model, but it was deemed an appropriate approximation for this study. All follow-up scans for each participant (not just the baseline and final follow-up scan) were used to fit the polynomial so as to gain the most accurate measure of rate-of-change and to reduce the potential bias of observational errors. Outliers in the calculation of rate-of-change were investigated to ensure their validity when included in the dataset, or removal if found to be erroneous.

This method was also applied to visual acuity data; the annual drop in score from Sloan letter charts were calculated using a first order polynomial with all follow-up data from each participant. What constitutes a clinically significant change in visual acuity has previously been investigated and argued in the literature. The test/re-test differences in someone with stable visual functionality can be substantial, and as such only seemingly large changes are seen as significant. Some studies suggest a 2-line (10 letter) difference to be beyond the reach of test-retest variability, thus constituting a measurable change in visual functionality (86). However, a recent study similar to this one suggests that a drop of 5 letters in HCVA and 7 letters in LCVA is unlikely to be due to testing error and as such this criterion was adopted here (42).

Due to the very nature of follow-up scans, *age* and *length of disease* varies as a function of time from baseline to final study visit (by more than 2 years for some participants). Although this would be normalized throughout the participant groups if all follow-up scans were taken at the same time intervals, due to the irregular scanning visits previously mentioned, the amount of variation in *age* and *length of disease* for each participant is dependent on the length of time between scans. As such, *age* used for follow-up regression analysis was the age of the participant at exactly half way between their baseline and final scan, and likewise for *length*

of disease. This helped to standardise time-dependent variables so as to have a more accurate representation of their effects on the rate-of-change in the retinal anatomy, should they be found to have an effect.

4.8 Summary

This is the first study to investigate the retina's peripheral vasculature and the potential effects of MS on its health. Analysis of UWF-SLO images was made possible through the use of semi-automated algorithms which produce reliable measures of arterial and venous width. The study was planned to address its hypotheses in a reliable and methodological manner, having recruited HVs and patients with MS who underwent identical scanning procedures at multiple time points, to collect baseline and longitudinal data on anatomical changes to the retina. Care was taken to ensure the scans were both taken and analysed following a strict protocol which would allow for direct group and participant comparisons. Alongside UWF-SLO imaging, OCT scans and visual acuity scores were recorded during a participant's visit so as to investigate reproducibility of the results of previous studies on the effect of MS on the retina's anatomy and functionality. With consent, patient records were used to identify clinical data such as date of diagnosis and clinical history of ON, to be used in regression analysis at baseline and follow-up.

Chapter 5
Baseline Data Analysis

5.1 Introduction

This chapter details the analysis of baseline data by the methods described in chapter 4; analysis was aimed at addressing hypotheses 1 and 2 as outlined in chapter 1. Namely, whether macular volume, RNFL thickness and vessel width were statistically significantly different when comparing certain retinal regions from each of the three participant groups. Linear regression models are used to highlight any anatomical changes associated with *disease* without the potentially confounding factors of *age* and *sex*.

5.2 Data cleaning

Due to an excess of HVs, the youngest 8 females from within the control group were excluded from analysis. This reduced the difference in the median age of the two group demographics by 2 years and created an identical ratio of female:male HVs as that of the MS group. Exclusion of this data was purely on the basis of age and sex; table 5.1 shows the final demographics used for baseline analysis. For a small number of participants, a good-quality OCT image capture was not successful with the Heidelberg SPECTRALIS: one healthy control suffered from age-related macular degeneration and some individuals with MS were not able to sustain focus for the entire scanning procedure. Manual inspection of outliers resulted in one individual's baseline data being excluded from the study as they were suffering from ON at the time of the scan and the resulting oedema was causing a swelling of the retina. As such, this individual's first follow-up scan (once the symptoms of oedema had subsided) was instead used as baseline data within the MS (ON) group.

Characteristics	Patients with MS (N = 72)	Healthy Volunteers (N = 72)
Median Age	44	41
Age range	20-79	24-73
Male	19	19
Female	53	53
History of ON (No. patients)	16	0
History of ON (No. Eyes)	19 (OD 9, OS 10)	0
Relapse-remitting	62	N/A
Primary progressive	2	N/A
Secondary progressive	7	N/A
Disease-modifying therapies*	46	N/A

Table 5.1: Adjusted group demographics for analysis. ON = Optic Neuritis, OS = left eye, OD = right eye. *These include: Fingolimod, Tecfidera, Dimethylfumerate, Copaxone, Plegridy, Alemtuzimab and Tysabri. One MS participant's disease subtype was unable to be determined from their electronic correspondence.

	Multiple Sclerosis		Optic Neuritis		Healthy volunteers	
	OS	OD	OS	OD	OS	OD
Baseline scans of usable quality	60	59	10	8	72	71

Table 5.2: Number of OCT baseline images for each participant group which were of good enough quality for analysis

The final number of usable OCT scans are shown in table 5.2. Likewise, as the UWF-SLO has a fixed focal point the imaging procedure was sensitive to patient movement meaning not all images were of a good enough quality to analyse. Even when an image captured is of a suitable quality once projected, with both the OD and the fovea visible, a portion of the image may still be obstructed by eyelashes or eyelids that prevents analysis of the retinal vessels. Tables 5.3 and 5.4 display the number of UWF-SLO images for both MS and HV groups that have vessels present in each of the quadrants, which were then able to be segmented and used for analysis.

	Number of images from which arterial data could be taken for each individual quadrant					
	Healthy Volunteers		MS (no ON)		MS (ON)	
Region	OS	OD	OS	OD	OS	OD
Temporal Inferior	64	57	54	53	9	5
Temporal Superior	68	70	56	61	10	8
Nasal Inferior	55	58	35	46	7	4
Nasal Superior	68	70	54	58	9	8

Table 5.3: The number of images for each group from which arterial data could be taken, from each of the four quadrants

	Number of images from which venous data could be taken for each individual quadrant					
	Healthy Volunteers		MS (no ON)		MS (ON)	
Region	OS	OD	OS	OD	OS	OD
Temporal Inferior	65	62	54	55	9	8
Temporal Superior	66	70	58	61	10	8
Nasal Inferior	57	64	37	50	8	7
Nasal Superior	69	72	55	59	10	8

Table 5.4: The number of images for each group from which venous data could be taken, from each of the four quadrants

5.3 OCT analysis

Data for HV and MS (no ON) groups were judged to be normally distributed in both eyes. Mean RNFL thickness was found to be thinner in the MS (no ON) group than in HVs (see Table 5.5), with a significant mean global reduction measured in both eyes at baseline (left eye (OS): -10µm, $p<0.001$; right eye (OD): -11µm, $p<0.001$), corresponding to a 10% and 11% drop in the left eye and right eyes respectively (see Table 5.7) . The largest reduction within my dataset was observed by an unpaired samples Student's t-test in the inferior temporal regions and was 15µm ($p<0.001$) in left eyes and 13µm ($p<0.01$) in right eyes. Significant differences were likewise observed in the temporal region (OS: -11µm, $p<0.001$; OD: -12µm, $p<0.001$) and the superior temporal region (OS: -10µm, $p<0.01$; OD: -9µm, $p<0.05$) of both sets of eyes. The temporal region (OS: -16%, OD: -17%) of the MS (no ON) group saw a greater difference in RNFL thickness as a percentage of the HV's RNFL thickness than all over regions in both eyes, including the temporal inferior region (OS: -10%, OD: -9%). Nasally the mean RNFL thickness in the MS (no ON) group was reduced when compared to HVs at baseline, although these differences were less pronounced, with only the superior nasal (OS: -9µm, $p<0.05$; OD: -9µm, $p<0.05$) and nasal (OS: -8µm, $p<0.01$; OD: -11µm, $p<0.001$) regions showing a significant difference. A significant reduction in macular volume was also observed in MS patients (OS: -0.22mm^3, $p<0.01$; OD: -0.3mm^3, $p<0.001$) when compared to HVs, corresponding to a 3% and 4% drop in volume for left and right eyes. 95% CI's were negative (showing a decrease in thickness or volume) for all regions within the MS (no ON) group except the inferior nasal region in both sets of eyes.

A reduction of the RNFL was observed by Mann-Whitney U test to be greatest in eyes which had a clinical history of ON (see Table 5.6). Once again, the temporal regions played host to the largest reduction when compared to HVs, with the greatest difference in the temporal region of the left eye (-30.5µm, $p<0.001$), and the superior temporal region of the right eye (-23µm, $p<0.05$). Although the temporal region of the left eye measured the greatest difference

in terms of percentage (-43%) of median HV RNFL thickness, it was the superior nasal region which showed the greatest percentage difference (-22%) in the right eye. Differences between the HV and MS (ON) groups were significant in all circumstances but the inferior temporal region of the right eye. When compared to participants with MS (no ON), the reduction was only found to be significant via Mann-Whitney U test in the temporal region of the left eye (p-value < 0.05). Greater anatomical changes associated with ON were also reflected in macular volume, where the loss of volume when compared to HVs was found to be significant in both eyes (OS: -0.64mm^3, p<0.001; OD: -0.52mm^3, p<0.05), corresponding to a 7% and 6% lower macular volume in the left and right eye respectively. Once more, although a greater loss of macular volume was seen in the MS (ON) group than in the MS (no ON) group, the difference was only found to be significant between these two groups in the left eye (p-value < 0.05).

Region	Mean RNFL thickness (µm ± SE)		The difference from mean HV baseline RNFL thickness in µm (95% CI)			
	Healthy Volunteers		MS (no ON)		MS (ON)	
	OS	OD	OS	OD	OS	OD
Global	98 ± 1.2	99 ± 1.3	-10*** (-14, -5)	-11*** (-15, -7)	-19 (-30, -10)	-18 (-34, -2)
Temporal	70 ± 1.3	71 ± 1.5	-11*** (-16, -7)	-12*** (-17, -7)	-23 (-37, -9)	-19 (-37, -1)
Temporal Inferior	145 ± 2.3	142 ± 2.4	-15*** (-23, 7)	-13** (-22, -5)	-29 (-47, -10)	-24 (-51, 4)
Temporal Superior	136 ± 1.9	136 ± 2.3	-10** (-17, -3)	-9* (-15, -2)	-21 (-36, -7)	-19 (-35, -2)
Nasal	74 ± 1.7	78 ± 2	-8** (-13, -3)	-11*** (-16, -6)	-14 (-22, -6)	-15 (-29, -1)
Nasal Inferior	110 ± 2.9	113 ± 3	-5 (-14, 4)	-8 (-17, 0)	-19 (-33, -4)	-23 (-43, -3)
Nasal Superior	108 ± 2.3	99 ± 2.2	-9* (-17, -1)	-9* (-16, -3)	-14 (-29, 2)	-12 (-35, 11)

Mean macular volume (mm^3 ± SE)		The difference in from mean HV baseline macular volume in mm^3 (95% CI)			
Healthy Volunteers		MS (no ON)		MS (ON)	
OS	OD	OS	OD	OS	OD
8.68 ± 0.04	8.66 ± 0.04	-0.22** (-0.35, -0.08)	-0.3*** (-0.44, -0.17)	-0.57 (-0.9, -0.23)	-0.35 (-0.74, 0.04)

* p <0.05, ** p <0.01, *** p <0.001

Table 5.5: The difference in mean baseline RNFL thickness for MS participants when compared to the baseline RNFL thickness of HVs using an unpaired samples Student's t-test, in each peripapillary region, as well as for macular volume. SE = standard error. CI = confidence interval. OS = left eye, OD = right eye, ON = optic neuritis.

	Median RNFL thickness in µm (IQR)		The difference from median HV baseline RNFL thickness in µm (95% CI)			
	Healthy Volunteers		MS (no ON)		MS (ON)	
Region	OS	OD	OS	OD	OS	OD
Global	98 (13)	99 (14)	-8*** (-14.5, -4)	-10*** (-15.5, -5)	-24*** (-30, -7.5)	-16** (-37, -1)
Temporal	70.5 (15)	71 (14)	-11.5*** (-19, -4.5)	-12*** (-19, -6)	-30.5*** (-38, -8)	-15* (-46, 4)
Temporal Inferior	141.5 (25)	142 (23.75)	-10.5*** (-26, -2)	-16** (-25, -0.5)	-27** (-47, -3.5)	-21 (-54, 13)
Temporal Superior	139 (26)	137 (27.75)	-11** (-24.5, -2)	-10** (-21, -3)	-26.5** (-42.5, -7)	-23* (-39, -3)
Nasal	72.5 (20.5)	74 (18.75)	-6.5** (-16.5, -1)	-9*** (-15, -3.5)	-15** (-21, -1.5)	-15* (-25, -3)
Nasal Inferior	106.5 (31)	109 (30)	-3.5 (-13.5, 6)	-3.5 (-15, 6)	-18* (-27, -4.5)	-22* (-42, 4)
Nasal Superior	106 (26)	97 (22)	-10* (-18,5, 2)	-5* (-12, 1)	-16.5* (-27.5, 2)	-21* (-28, 16)

Median macular volume in mm^3 (IQR)		The difference from median HV baseline macular volume (mm^3)			
Healthy Volunteers		MS (no ON)		MS (ON)	
OS	OD	OS	OD	OS	OD
8.63 (0.54)	8.63 (0.52)	-0.23** (-0.42, -0.03)	-0.25*** (-0.47, -0.05)	-0.64*** (-0.84, -0.21)	-0.52* (-0.78, 0.24)

* p <0.05, ** p <0.01, *** p <0.001

Table 5.6: The difference in median baseline RNFL thickness for MS participants when compared to the baseline RNFL thickness of HVs using the Mann-Whitney U test, in each peripapillary region, as well as the difference in macular volume. IQR = interquartile range. CI = confidence interval. OS = left eye, OD = right eye, ON = optic neuritis.

% change between mean HV baseline RNFL thickness and the MS (no ON) group		
	OS	OD
Global	-10	-11
Temporal	-16	-17
Temporal Inferior	-10	-9
Temporal Superior	-7	-7
Nasal	-11	-14
Nasal Inferior	-5	-7
Nasal Superior	-8	-9

% change between median HV baseline RNFL thickness and the MS (ON) group		
	OS	OD
Global	-24	-16
Temporal	-43	-21
Temporal Inferior	-19	-15
Temporal Superior	-19	-17
Nasal	-21	-20
Nasal Inferior	-17	-20
Nasal Superior	-16	-22

Table 5.7: The percentage change between the mean and median RNFL thickness of the HV group and the two MS groups

5.4 UWF-SLO analysis

UWF-SLO vessel width data for HV and MS (no ON) groups was judged to be normally distributed. The full results for each participant group's mean vessel thickness for both arteries and veins is displayed in Table 5.8. In both eyes, the mean arterial width for MS (no ON) was significantly reduced when compared to HVs (OS: -7%, OD: -10%) when using an unpaired samples Student's t-test in the inferior nasal quadrant (OS: -0.005mm, $p<0.05$; OD: -0.007mm, $p<0.05$): this also being the quadrant which showed the greatest differences in mean arterial width between HV and MS (ON) groups and the only region for which 95% CIs were both negative. In all other regions the differences measured lacked statistical significance, and in no region was the percentage change greater than in the inferior nasal region (see Table 5.10).

Differences between the MS (no ON) and HV groups in the mean width of retinal veins were likewise found to be greatest in the inferior nasal quadrant (OS: -6%, OD: -6%)) in both absolute and percentage difference, although only in the right eye was the difference found to be significant (OS: -0.005mm, $p=0.06$; OD: -0.005mm, $p<0.05$). Left eye data measured a reduction in the mean thickness of retinal veins in every quadrant, however right eye data measured reductions in only the nasal quadrants, with no change in the superior temporal quadrant and a small increase in thickness for the MS (no ON) group in the inferior temporal quadrant. In no region were 95% CIs both negative, although in three regions (including the inferior nasal) the upper interval was estimated at zero. No significant differences were found in either eye between HVs and MS (ON) participants when comparing median arterial or venous width, as shown in Table 5.9. The pattern of reduced vessel width in participants with MS was not seen in the MS (ON) group, with only half of the tested quadrants showing a reduction in median vessel width- the other quadrants either showing an increase in thickness or no change at all.

	Mean arterial thickness (mm ± SE)		The difference from mean HV baseline arterial thickness in mm (95% CI)			
	Healthy Volunteers		MS (no ON)		MS (ON)	
Region	OS	OD	OS	OD	OS	OD
Temporal Inferior	0.095 ± 0.002	0.096 ± 0.002	-0.003 (-0.009, 0.003)	-0.005 (-0.011, 0.001)	0 (-0.009, 0.008)	-0.007 (-0.019, 0.006)
Temporal Superior	0.104 ± 0.002	0.104 ± 0.002	-0.003 (-0.008, 0.003)	-0.002 (-0.007, 0.004)	-0.004 (-0.011, 0.003)	+0.002 (-0.009, 0.013)
Nasal Inferior	0.072 ± 0.002	0.07 ± 0.002	-0.005* (-0.01, -0.001)	-0.007* (-0.012, -0.002)	-0.004 (-0.016, 0.007)	+0.009 (-0.001, 0.018)
Nasal Superior	0.079 ± 0.001	0.077 ± 0.001	-0.001 (-0.005, 0.003)	-0.003 (-0.007, 0.001)	-0.001 (-0.011, 0.01)	+0.004 (-0.004, 0.012)

	Mean vein thickness (mm ± SE)		The difference from mean HV baseline vein thickness in mm (95% CI)			
	Healthy Volunteers		MS (no ON)		MS (ON)	
Region	OS	OD	OS	OD	OS	OD
Temporal Inferior	0.114 ± 0.002	0.109 ± 0.002	-0.004 (-0.009, 0.001)	+0.001 (-0.006, 0.007)	-0.007 (-0.018, 0.004)	-0.012 (-0.026, 0.002)
Temporal Superior	0.118 ± 0.003	0.118 ± 0.002	-0.002 (-0.009, 0.005)	0 (-0.006, 0.005)	+0.004 (-0.008, 0.016)	+0.003 (-0.012, 0.017)
Nasal Inferior	0.084 ± 0.001	0.082 ± 0.002	-0.005 (-0.01, 0)	-0.005 (-0.01, 0) *	-0.008 (-0.02, 0.004)	-0.002 (-0.017, 0.013)
Nasal Superior	0.092 ± 0.001	0.092 ± 0.002	-0.003 (-0.007, 0.001)	-0.004 (-0.009, 0)	0 (-0.008, 0.008)	+0.002 (-0.006, 0.01)

*p <0.05, **p <0.01, ***p <0.001

Table 5.8: The difference in mean baseline vessel thickness for MS participants when compared to the baseline vessel thickness of HVs using an unpaired samples Student's t-test, in four quadrants. SE = standard error, CI = confidence interval, OS = left eye, OD = right eye, ON = optic neuritis

	Median arterial thickness in mm (IQR)		The difference from median HV baseline arterial thickness in mm (95% CI)			
	Healthy Volunteers		MS (no ON)		MS (ON)	
Region	OS	OD	OS	OD	OS	OD
Temporal Inferior	0.098 (0.019)	0.093 (0.016)	-0.003 (-0.009, 0.005)	-0.004 (-0.009, 0.006)	-0.004 (-0.012, 0.006)	-0.005 (-0.022, 0.008)
Temporal Superior	0.1 (0.016)	0.104 (0.015)	+0.002 (-0.004, 0.006)	0 (-0.006, 0.007)	+0.001 (-0.009, 0.004)	+0.004 (-0.009, 0.014)
Nasal Inferior	0.07 (0.015)	0.069 (0.015)	-0.003 (-0.011, 0.001)	-0.005* (-0.01, -0.002)	-0.001 (-0.023, 0.013)	+0.009 (0.001, 0.015)
Nasal Superior	0.08 (0.014)	0.079 (0.014)	0 (-0.006, 0.004)	-0.005 (-0.01, 0.001)	-0.003 (-0.012, 0.015)	+0.004 (-0.006, 0.01)

	Median vein thickness in mm (IQR)		The difference from median HV baseline vein thickness in mm (95% CI)			
	Healthy Volunteers		MS (no ON)		MS (ON)	
Region	OS	OD	OS	OD	OS	OD
Temporal Inferior	0.111 (0.02)	0.111 (0.021)	-0.002 (-0.008, 0.005)	+0.001 (-0.009, 0.009)	-0.005 (-0.016, 0.012)	-0.008 (-0.026, 0.001)
Temporal Superior	0.117 (0.018)	0.119 (0.022)	-0.002 (-0.009, 0.004)	+0.002 (-0.005, 0.005)	+0.007 (-0.006, 0.013)	-0.006 (-0.014, 0.021)
Nasal Inferior	0.085 (0.012)	0.082 (0.015)	-0.006* (-0.012, -0.001)	-0.005* (-0.011, -0.001)	-0.004 (-0.023, 0.004)	0 (-0.018, 0.011)
Nasal Superior	0.092 (0.012)	0.092 (0.018)	0 (-0.005, 0.004)	-0.002 (-0.008, 0.002)	0 (-0.006, 0.01)	+0.003 (-0.006, 0.011)

* p <0.05, ** p <0.01, *** p <0.001

Table 5.9: The difference in median baseline vessel thickness for MS participants when compared to the baseline vessel thickness of HVs using a Mann-Whitney U test, in four quadrants. IQR = interquartile range, CI = confidence interval, OS = left eye, OD = right eye, ON = optic neuritis.

Vessel type	% change between mean HV baseline vessel thickness and the MS (no ON) group		
		OS	OD
Arteries	Temporal inferior	-3	-5
	Temporal superior	-3	-2
	Nasal Inferior	-7	-10
	Nasal Superior	-1	-4
Veins	Temporal inferior	-4	1
	Temporal superior	-2	0
	Nasal Inferior	-6	-6
	Nasal Superior	-3	-4

Vessel type	% change between median HV baseline vessel thickness and the MS (ON) group		
		OS	OD
Arteries	Temporal inferior	-4	-5
	Temporal superior	+1	+4
	Nasal Inferior	-1	+13
	Nasal Superior	-4	+5
Veins	Temporal inferior	-5	-7
	Temporal superior	+6	-5
	Nasal Inferior	-5	0
	Nasal Superior	0	+3

Table 5.10: The percentage change between the mean and median vessel thickness of the HV group and the two MS groups

5.5 Visual acuity analysis

Visual acuity data was not judged to be normally distributed for the MS (no ON) and HV groups. Comparisons of each group's mean HCVA and LCVA scores showed little differences between participant groups- differences became evident when comparing the median scores of each participant group, as shown in Table 5.11. The MS (no ON) group was found to have a smaller median HCVA score in both the left (HV: 56, MS: 50, p-value < 0.001) and right (HV: 55, MS: 52, p-value < 0.05) eyes when compared to the HV group. A similar result was observed for LCVA scores in both the left (HV: 27, MS: 21, p-value < 0.01) and right (HV: 25, MS: 19, p-value < 0.001) eyes. The range of scores was greatest in the MS (no ON) group for both HCVA and LCVA score, as although the highest scores were similar in all participant groups, participants with MS (no ON) would more frequently score poorly when reading from both 2.5% and 100% Sloan letter charts.

	Median visual acuity scores for each participant group (range)					
	Healthy Volunteers		MS (no ON)		MS (ON)	
Snellen chart	OS (N=68)	OD (N=68)	OS (N=51)	OD (N=50)	OS (N=6)	OD (N=8)
Full contrast (100%)	56 (14-65)	55 (32-65)	50 (0-63)	52 (0-65)	47 (4-60)	55 (33-65)
Low contrast (2.5%)	27 (0-39)	25 (0-39)	21 (0-40)	19 (0-40)	6 (0-28)	21 (0-33)

Table 5.11: The difference in median baseline visual acuity scores for MS participants when compared to the baseline visual acuity scores of healthy volunteers when using a Mann-Whitney U-test, in each eye. OS = left eye, OD = right eye, ON = optic neuritis, N= number of participants

The MS (ON) group was not found to have a significant difference in their HCVA scores in either eye when compared to the HV group when using a Mann-Whitney U test. However, LCVA scores were found to be significantly reduced in the left eye (HV: 27, MS (ON): 6, p < 0.01), but not in the right eye (HV: 25, MS (ON): 21, p = 0.1). Medians scores for HCVA and

LCVA were not found to be significantly different between MS participants and participants with a clinical history of ON in either eye.

5.6 Baseline regression analysis

5.6.1 Baseline OCT

Globally, the predictors *disease* and *age* produced the multivariate model which was most representative of the RNFL thickness data in both eyes (OS: adjusted R-squared = 0.15, $p<0.001$, OD: adjusted R-squared = 0.19, $p<0.001$). This was also the case in all nasal regions (see Table 5.12). However, the temporal regions were less consistent e.g., the temporal region itself was best described by the univariate model of *disease* as the only predictor (OS: adjusted R-squared=0.15, $p<0.001$, OD: adjusted R-squared=0.15, $p<0.001$). The only region for which the *sex* of a participant added predictive power was the inferior temporal of the left eye (adjusted R-squared=0.09, $p<0.01$), but macular volume was best described by all three predictors in both eyes (OS: adjusted R-squared=0.08, $p<0.01$, OD: adjusted R-squared=0.15, $p<0.001$). All models were found to be significant ($p<0.01$), except when modelling the inferior nasal region of both eyes.

Table 5.13 displays the coefficients for the best fitting model within each region. The effect of *disease* was comparable to the difference in mean values between HV and MS (no ON) groups at baseline and was found to be significant ($p<0.05$) in all regions except the inferior nasal, in which the models themselves were not significant. The greatest reduction in RNFL thickness attributed to *disease* was again seen in the inferior temporal (OS: -14μm, $p<0.001$; OD: -12μm, $p<0.001$) and temporal (OS: -11μm, $p<0.001$; OD: -12μm, $p<0.001$) regions. *Disease* was also found to correlate with a reduced macular volume in both eyes (OS: -0.207mm^3, $p<0.01$; OD: -0.29mm^3, $p<0.001$).

	Adjusted R-Squared value for three linear regression models					
	Disease, age and sex		Disease and age		Disease	
Region	OS	OD	OS	OD	OS	OD
Global	0.144***	0.187***	0.148***	0.193***	0.128***	0.166***
Temporal	0.14***	0.15***	0.142***	0.153***	0.146***	0.154***
Temporal Inferior	0.092**	0.075**	0.089***	0.078**	0.089***	0.064**
Temporal Superior	0.043*	0.055*	0.049*	0.06**	0.052**	0.042*
Nasal	0.08**	0.111***	0.084**	0.118***	0.067**	0.105***
Nasal Inferior	0.003	0.014	0.011	0.022	0.003	0.02
Nasal Superior	0.066**	0.062*	0.068**	0.063**	0.034*	0.052**
Macular Volume	0.075**	0.146***	0.068**	0.137***	0.066**	0.13***

p-values: * <0.05, **<0.01, ***<0.001

Table 5.12: Adjusted R-squared values for three linear regression models using the predictors *age*, *sex* and *disease*. The model highlighted in grey for each region was selected for coefficient analysis. OS = left eye, OD = right eye.

Although *age* was included as a predictor in all but one region, it was only found to be a significant attributor to RNFL reductions globally (OS: -0.18μm/year, p-value <0.05; OD: -0.19μm/year, p-value<0.05), as well as in the superior nasal region of the left eye (-0.38μm/year, p<0.05). Likewise, macular volume and the inferior temporal region of the left eye both included *sex* as a predictor, but despite the models suggesting females have a reduction in macular volume and RNFL thickness, *sex* was not found to be a significant predictor. In the regions which played host to the largest changes in RNFL thickness (global and all temporal regions) the regression model's residuals appeared normal, suggesting that linear modelling was indeed appropriate for describing the data. The superior nasal region of the right eye also appeared normal although no other nasal region shared this normality, indicating that the models were less suited to describing data from these regions.

		Results for linear regression models			
		OS		OD	
Region		Coefficient	p-value	Coefficient	p-value
Global	*Disease*	-9	<0.001	-10	<0.001
	Age	-0.18	<0.05	-0.19	<0.05
Temporal	*Disease*	-11	<0.001	-12	<0.001
Temporal Inferior	*Disease*	-14	<0.001	-12	<0.01
	Age	-0.15	0.35	-0.3	0.08
	Sex	5.59	0.22	N/A	N/A
Temporal Superior	*Disease*	-10	<0.01	-8	<0.05
	Age	N/A	N/A	-0.26	0.06
Nasal	*Disease*	-7	<0.01	-10	<0.001
	Age	-0.19	0.06	-0.18	0.1
Nasal Inferior	*Disease*	-4	0.34	-8	0.09
	Age	-0.26	0.15	-0.19	0.28
Nasal Superior	*Disease*	-8	<0.05	-8	<0.05
	Age	-0.38	<0.05	-0.21	0.11
Macular Volume	*Disease*	-0.207	<0.01	-0.29	<0.001
	Age	-0.003	0.25	-0.004	0.16
	Sex	-0.106	0.17	-0.118	0.14

Table 5.13: Linear regression model coefficients and their associated significance values for each eye. OS = left eye, OD = right eye

A comparison of the adjusted R-squared values for the raw data and the remodelled data (with influential points removed) are shown in Table 5.14, alongside their associated p-values. No model that previously lacked significance subsequently gained significance when remodelled. In the right eye, the adjusted R-squared value was only improved when remodelling macular volume data, which was again best represented by all three predictors. However, in the left eye all nasal regions along with the inferior and superior temporal regions benefitted from a higher adjusted R-squared value when highly influential data points were removed. Within the nasal

Adjusted R-Squared values for models with and without influential points

	OS				OD			
	Raw data		Remodelled data		Raw data		Remodelled data	
Region	Adjusted R-squared	p-value	Adjusted R-squared	p-value	Adjusted R-squared	p-value	Adjusted R-squared	p-value
Global	0.148	<0.001	0.116	<0.001	0.193	<0.001	0.17	<0.001
Temporal	0.146	<0.001	0.122	<0.001	0.154	<0.001	0.14	<0.001
Temporal Inferior	0.092	<0.01	0.102	<0.01	0.078	<0.01	0.053	<0.05
Temporal Superior	0.052	<0.01	0.055	<0.01	0.06	<0.01	0.047	<0.05
Nasal	0.084	<0.01	0.123	<0.001	0.118	<0.001	0.113	<0.001
Nasal Inferior	0.011	0.18	0.014	0.16	0.022	0.09	0.021	0.11
Nasal Superior	0.068	<0.01	0.09	<0.01	0.063	<0.01	0.059	<0.01
Macular volume	0.075	<0.01	0.071	<0.05	0.146	<0.001	0.166	<0.001

Table 5.14: Comparing model statistics for raw and remodelled data (with influential points removed). OS = left eye, OD = right eye.

region itself, *age* was deemed to be a significant predictor in remodelled data along with *disease* (see Table 5.15), whereas previously it indicated a trend rather than significance (p = 0.06). The greatest change in the effect of *disease* on RNFL thickness was in the nasal region of the left eye and the inferior temporal regions of both eyes. However, the coefficients of the remodelled data largely remained similar to that of the raw data, suggesting that linear modelling of the raw data was sufficiently robust to account for influential data points.

Table 5.16 displays the results from modelling the MS (no ON) group with *length of disease*, *age* and *sex* as predictors of RNFL thickness and macular volume. Few models were found to be significant when using permutations of these 3 predictors and the adjusted R-squared values

Region		Results for linear regression model once influential data points are removed					
		OS			OD		
		Raw data coefficient	Remodelled data coefficient	p-value	Raw data coefficient	Remodelled data coefficient	p-value
Global	*Disease*	-9	-9	<0.001	-10	-10	<0.001
	Age	-0.18	-0.13	0.15	-0.19	-0.14	0.11
Temporal	*Disease*	-11	-10	<0.001	-12	-11	<0.001
Temporal Inferior	*Disease*	-14	-16	<0.001	-12	-10	<0.05
	Age	-0.15	-0.14	0.41	-0.3	-0.24	0.17
	Sex	5.59	4.2	0.36	N/A	N/A	N/A
Temporal Superior	*Disease*	-10	-10	<0.01	-8	-8	<0.05
	Age	N/A	N/A	N/A	-0.26	-0.2	0.1
Nasal	*Disease*	-7	-9	<0.001	-10	-11	<0.001
	Age	-0.19	-0.24	<0.05	-0.18	-0.13	0.26
Nasal Inferior	*Disease*	-4	-4	0.35	-7	-8	0.07
	Age	-0.26	-0.28	0.13	-0.21	-0.13	0.48
Nasal Superior	*Disease*	-8	-9	<0.05	-8	-8	<0.05
	Age	-0.38	-0.41	<0.01	-0.21	-0.2	0.15
Macular volume	*Disease*	-0.207	-0.222	<0.01	-0.29	-0.303	<0.001
	Age	-0.003	-0.002	0.43	-0.004	-0.005	0.13
	Sex	-0.106	-0.07	0.39	-0.118	-0.11	0.17

Table 5.15: A comparison of raw data coefficients and remodelled data coefficients in each eye, alongside the remodelled coefficient's p-value.

selected are shown in Table 5.17. Of the models which were significant, *length of disease* was found to correlate with a thinner RNFL in the global (-0.45μm/year, p-value < 0.05), temporal (-0.6μm/year, p-value<0.05) and the inferior temporal (-1.27μm/year, p-value<0.01) regions for the right eye. In no other region was *length of disease* found to be a significant predictor, yet in all regions except the inferior and superior nasal regions of the left eye, *length of disease* was found to positively correlate with a thinner RNFL.

	Adjusted R-Squared value for three linear regression models					
	Length of disease, Age, Sex		*Length of disease, Age*		*Length of disease*	
Region	OS	OD	OS	OD	OS	OD
Global	-0.025	0.025	-0.008	0.037	0.006	0.052*
Temporal	-0.001	0.065	-0.008	0.065	-0.002	0.073*
Temporal Inferior	0.023	0.083*	0.003	0.095*	0.012	0.103**
Temporal Superior	-0.04	-0.016	-0.022	-0.013	-0.007	0
Nasal	-0.021	-0.026	-0.003	-0.025	0.002	-0.012
Nasal Inferior	-0.012	-0.022	-0.014	-0.021	-0.015	-0.012
Nasal Superior	0.034	0.032	0.035	0.016	-0.01	-0.005
Macular Volume	0.038	0.096*	0.026	0.074	0.031	0.059*

p-values: * <0.05, **<0.01, ***<0.001

Table 5.16: Adjusted R-squared values for three models, investigating how *length of disease* affects RNFL thickness and macular volume. The model highlighted in grey for each region was selected for coefficient analysis. OS = left eye, OD = right eye

Despite the regression model for macular volume being significant when using *age*, *sex* and *length of disease* as predicators, none of these were found to be significant themselves. However, *length of disease* appears to also positively correlate with a reduced macular volume in patients with MS (OS: -0.009mm^3/year, p= 0.29; OD: -0.013mm^3/year, p=0.12). The rate of reduction due to MS was greater than that attributed to aging (OS: -0.005mm^3/year, p=0.29; OD: -0.008mm^3/year, p=0.13) when modelling macular volume. Fingolimod was initially included as a predictor for those that were prescribed it during the course of the study, however in no region was it found to either be significant or increase the predictive power of the models, so it was excluded from the final regression analysis to avoid overfitting.

Results for linear regression model					
		OS		OD	
Region		Coefficient	p-value	Coefficient	p-value
Global	*LoD*	-0.29	0.25	-0.45	<0.05
Temporal	*LoD*	-0.4	0.18	-0.6	<0.05
	Age	0.17	0.32	N/A	N/A
	Sex	5	0.24	N/A	N/A
Temporal Inferior	*LoD*	-0.84	0.09	-1.27	<0.01
	Age	0.27	0.34	N/A	N/A
	Sex	11	0.15	N/A	N/A
Temporal Superior	*LoD*	-0.32	0.45	-0.33	0.31
Nasal	*LoD*	-0.26	0.3	-0.13	0.6
Nasal Inferior	*LoD*	0.12	0.8	-0.22	0.6
	Age	-0.34	0.23	N/A	N/A
	Sex	-8	0.3	N/A	N/A
Nasal Superior	*LoD*	0.05	0.92	-0.05	0.88
	Age	-0.5	0.06	-0.32	0.09
	Sex	N/A	N/A	-8	0.17
Macular Volume	*LoD*	-0.009	0.29	-0.013	0.12
	Age	-0.005	0.29	-0.008	0.13
	Sex	-0.164	0.20	-0.193	0.14

Table 5.17: Coefficients and significance values for models in each eye. OS = left eye, OD = right eye, LoD = length of disease

5.6.2 Baseline UWF-SLO

The adjusted R-squared values when using the predictors *age*, *sex* and *disease* to model for vessel width in each peripapillary quadrant of the retina are shown in table 5.18, with the model selected for further coefficient analysis highlighted in grey. The model with the largest adjusted R-squared value when modelling for arterial data was that of the inferior nasal region of the right eye (adjusted R-squared: 0.095, $p<0.01$). However, much like the regression models created for OCT data, adjusted R-squared values were generally very small and the models which best describe vessel width varied from region to region and between the left and right eye. Despite this, arterial width models were found to be significant with exception of the superior nasal quadrant in both sets of eyes and the superior temporal quadrant of the left eye. In the venous width modelling (Table 5.20), only the univariate model for inferior nasal data in the right eye was found to have significance. Unlike RNFL thickness data, *age* was more often considered a positive contributor to the model when using vessel width as a response variable.

As shown in Table 5.19, a reduced mean arterial thickness in the MS (no ON) group can be seen when compared to the HVs in all models, although the coefficients of *disease* were only found to be significant in the inferior nasal quadrant (OS: -0.0053mm, p-value < 0.05; OD: -0.0079mm, p-value < 0.01) where the difference was greatest. When included as a predictor in the regression models, *age* was found to be associated with a reduced arterial thickness (per year) with exception of the inferior nasal quadrant of the right eye. Though *age* was not significant in the superior nasal quadrant it was close to significance in the inferior temporal region of the right eye (-3e-04mm/year, p-value = 0.05), and as a predictor *age* was significant in all other regions for which it was included. *Sex* was not found to be a significant confounder when included in the models but was consistent in describing females as having thicker mean arterial widths in all models for which it was a predictor.

Adjusted R-Squared value for three models of arterial data						
	Disease, age and sex		*Disease and age*		*Disease*	
Region	OS	OD	OS	OD	OS	OD
Temporal Inferior	0.041*	0.038	0.045*	0.042*	0	0.017
Temporal Superior	0.019	0.049*	0.027	0.042*	-0.001	-0.005
Nasal Inferior	0.03	0.095**	0.039	0.086**	0.046*	0.061**
Nasal Superior	-0.002	-0.005	-0.006	0	-0.007	0.006

p-values: * <0.05, **<0.01, ***<0.001

Table 5.18: Adjusted R-squared values for three linear regression models. The model highlighted in grey for each quadrant was selected for coefficient analysis. OS = left eye, OD = right eye.

Results for linear regression models of arterial data					
		OS		OD	
Region		Coefficient	p-value	Coefficient	p-value
Temporal Inferior	*Disease*	-0.0018	0.55	-0.0044	0.15
	Age	-0.0003	<0.05	-3e-04	0.05
Temporal Superior	*Disease*	-0.0015	0.57	-7e-04	0.8
	Age	-2e-04	<0.05	-3e-04	<0.01
	Sex	N/A	N/A	0.0042	0.16
Nasal Inferior	*Disease*	-0.0053	<0.05	-0.0079	<0.01
	Age	N/A	N/A	2e-04	<0.05
	Sex	N/A	N/A	0.0044	0.16
Nasal Superior	*Disease*	-0.0005	0.78	-0.0027	0.18
	Age	-1e-04	0.33	N/A	N/A
	Sex	0.0026	0.22	N/A	N/A

Table 5.19: Coefficients and significance values for arterial models in each eye. OS = left eye, OD = right eye

Adjusted R-Squared value for three models for veins						
	Disease, age and sex		*Disease and age*		*Disease*	
Region	OS	OD	OS	OD	OS	OD
Temporal Inferior	0.032	-0.019	0.004	-0.01	0.012	-0.008
Temporal Superior	-0.004	0.014	-0.01	0.002	-0.004	-0.008
Nasal Inferior	0.042	0.027	0.033	0.035	0.028	0.027*
Nasal Superior	-0.0066	0.0016	0.001	0.008	0.008	0.016

p-values: * <0.05, **<0.01, ***<0.001

Table 5.20: Adjusted R-squared values for three linear regression models. The model highlighted in grey for each quadrant was selected for coefficient analysis. OS = left eye, OD = right eye.

Results for linear regression model in vein data					
		OS		OD	
Region		Coefficient	p-value	Coefficient	p-value
Temporal Inferior	*Disease*	-0.0042	0.12	1e-04	0.81
	Age	0	0.77	N/A	N/A
	Sex	0.0066	<0.05	N/A	N/A
Temporal Superior	*Disease*	-0.0021	0.56	4e-04	0.9
	Age	-1e-04	0.6	-2e-04	0.16
	Sex	0.0053	0.19	0.0053	0.11
Nasal Inferior	*Disease*	-0.0051	<0.05	-0.0054	<0.05
	Age	1e-04	0.22	1e-04	0.16
	Sex	0.0038	0.18	N/A	N/A
Nasal Superior	*Disease*	-0.0029	0.16	-0.0043	0.08

Table 5.21: Coefficients and significance values for vein models in each eye. OS = left eye, OD = right eye

Baseline regression models for venous data also showed *disease* to correlate with a reduced vessel width in all quadrants of the left eye and both nasal quadrants of the right eye. The greatest difference between the MS (no ON) and HV groups where once again found in the inferior nasal quadrant of the retina, with significance and similar coefficients for both eyes (OS: -0.0051, p-value < 0.05; OD: -0.0054, p-value < 0.05), despite neither model being significant. Unlike arterial data, *age* was not found to be a significant confounder in any model and the effect of *age* on mean vein width was inconsistent throughout the quadrants. Once again, being female was found to associate with wider vessels (between 0.0038mm-0.0066mm), although *sex* was only a significant predictor in the inferior temporal quadrant of the left eye (0.0066mm, p-value < 0.05).

The remodelled data, once influential data points had been removed, is presented in Tables 5.22 and 5.23. While the residual plots for each model were assessed to be normal on visual inspection and therefore indicate that linear regression models suitably represent the data, in some quadrants the adjusted R-squared values were improved when the data was remodelled. For example, right eye data for venous width saw both nasal models benefit from a higher adjusted R-squared value as well as gaining significance, whereas the inferior temporal quadrant of the OS arterial data lost significance when remodelled. Despite 3 of the 4 arterial quadrant models being improved in the right eye by remodelling, only the superior nasal quadrant gained significance.

Comparing the remodelled coefficients with those from the raw dataset for arterial width data (see Table 5.22) saw three circumstances where the remodelled coefficient of *disease* changed from a negative to a positive value, indicating a thickening of the arteries in individuals with MS (no ON), however all three of these coefficients have large p-values and lack evidence of a statistically significant effect. *Disease* coefficients that were significant or close to significance changed little in the remodelled data, and no disease coefficient which previously lacked significance gained significance when remodelled. Where *age* was included as a

Adjusted R-Squared values for arterial models with and without influential points

	OS				OD			
	Raw data		Remodelled data		Raw data		Remodelled data	
Region	R-squared	p-value	R-squared	p-value	R-squared	p-value	R-squared	p-value
Temporal Inferior	0.045	<0.05	0.034	0.06	0.042	<0.05	0.042	<0.05
Temporal Superior	0.027	0.07	0.028	0.07	0.049	<0.05	0.055	<0.05
Nasal Inferior	0.046	<0.05	0.051	<0.05	0.095	<0.01	0.097	<0.01
Nasal Superior	-0.002	0.43	-0.003	0.46	0.006	0.18	0.018	0.08

Results for arterial linear regression models once remodelled

		OS			OD		
Region		Raw data Coefficient	Remodelled data coefficient	p-value	Raw data coefficient	Remodelled data coefficient	p-value
Temporal Inferior	*Disease*	-0.0018	1e-04	0.98	-0.0044	-0.0041	0.21
	Age	-0.0003	-0.0003	<0.05	-3e-04	-3e-04	0.06
Temporal Superior	*Disease*	-0.0015	-5e-04	0.86	-7e-04	8e-04	0.75
	Age	-2e-04	-2e-04	<0.05	-3e-04	-3e-04	<0.01
	Sex	N/A	N/A	N/A	0.0042	0.0028	0.36
Nasal Inferior	*Disease*	-0.0053	-0.0055	<0.05	-0.0079	-0.0085	<0.01
	Age	N/A	N/A	N/A	2e-04	2e-04	0.16
	Sex	N/A	N/A	N/A	0.0044	0.0042	0.17
Nasal Superior	*Disease*	-0.0005	0.0008	0.68	-0.0027	-0.0036	0.08
	Age	-1e-04	-1e-04	0.52	N/A	N/A	N/A
	Sex	0.0026	0.003	0.17	N/A	N/A	N/A

Table 5.22: Comparing model statistics for raw and remodelled arterial data (with influential points removed), as well as the coefficients produced from both raw data and remodelled data (with associated p-values for each remodelled coefficient)

Adjusted R-Squared value for venous models with and without influential points

	OS				OD			
	Raw data		Remodelled data		Raw data		Remodelled data	
Region	R-squared	p-value	R-squared	p-value	R-squared	p-value	R-squared	p-value
Temporal Inferior	0.032	0.08	0.035	0.08	-0.008	0.81	-0.009	0.84
Temporal Superior	-0.004	0.47	-0.014	0.7	0.014	0.19	0.014	0.2
Nasal Inferior	0.042	0.08	-0.011	0.56	0.035	0.05	0.044	<0.05
Nasal Superior	0.008	0.162	0.008	0.17	0.016	0.08	0.0316	<0.05

Results for venous linear regression models once remodelled

		OS			OD		
Region		Raw data Coefficient	Remodelled data coefficient	p-value	Raw data coefficient	Remodelled data coefficient	p-value
Temporal Inferior	*Disease*	-0.0042	-0.0046	0.1	7e-04	6e-04	0.84
	Age	0	0	0.78	N/A	N/A	N/A
	Sex	0.0066	0.0068	<0.05	N/A	N/A	N/A
Temporal Superior	*Disease*	-0.0021	-0.0076	0.84	4e-04	0.0017	0.58
	Age	-1e-04	-1e-04	0.5	-2e-04	-2e-04	0.09
	Sex	0.0053	0.0038	0.38	0.0053	0.0038	0.29
Nasal Inferior	*Disease*	-0.0051	-0.0031	0.2	-0.0054	-0.0058	<0.05
	Age	1e-04	1e-04	0.41	1e-04	2e-04	0.14
	Sex	0.0038	1e-04	0.75	N/A	N/A	N/A
Nasal Superior	*Disease*	-0.0029	-0.003	0.17	-0.0043	-0.0055	<0.05

Table 5.23: Comparing model statistics for raw and remodelled venous data (with influential points removed), as well as the coefficients produced from both raw data and remodelled data (with associated p-values for each remodelled coefficient)

predictor for arterial data, the coefficients remained the same in all quadrants but lost significance in the inferior nasal quadrant of the right eye. Finally, where included as a predictor, the effect of being female resulted in an increase in arterial thickness, but once more the coefficients were not judged to be significant. With the exception of quadrants where the disease coefficient was not significant in either the raw or remodelled data, the remodelled data suggests that linear regression models were still appropriate and robust in representing the data collected.

For venous width data (see table 5.23), the *disease* coefficient in the nasal superior quadrant of the right eye showed evidence of an effect, which was previously not apparent in the raw-data models. Contrary to this, in the inferior nasal quadrant of the left eye, the disease coefficient lacked evidence of an effect when remodelled. However, unlike arterial data the effect of *disease* on vein width remained consistent in each of the quadrants, though some changes were seen in the magnitude of this effect, the biggest being in the superior temporal quadrants of both eyes. The effect of *age* as a predictor (where included) also remained consistent within each quadrant, as was the case with *sex* although the magnitude of the change in the three models for which *sex* was included was smaller in all the remodelled datasets.

The MS (no ON) data was separated and modelled with three predictors: *length of disease*, *age* and *sex*. An additional binomial predictor representing whether an individual was prescribed Fingolimod during the extent of the study was also included in the analysis but in no circumstances did its inclusion positively contribute to the description of the datasets. The resulting adjusted R-squared values are shown in table 5.24 and 5.26, with the only significant models being from the arterial dataset in the inferior temporal quadrant. When examining the coefficients produced from each model, we see that *length of disease* was only significant in the inferior temporal quadrant of the left eye for arterial data, whilst no other *length of disease* coefficient for any vessel type was similarly significant. The effect of *length of disease* on vessel width was found to be inconsistent across all quadrants, with half of the quadrants suggesting thinner vessels and half suggesting thicker vessels or no change. When included as

a predictor, *age* was determined to be significant again for arterial data in the inferior temporal quadrants of both eyes. Despite a lack of significance in other regions, in all circumstances excluding the inferior nasal quadrants for venous data, *age* had a thinning effect per year on vessel widths. In the three quadrants for which *sex* was included as a predictor, the effect was consistent with previous models in suggesting females as having thicker retinal vessels than males.

	Adjusted R-Squared value for three arterial models					
	Length of disease, Age, Sex		*Length of disease, Age*		*Length of disease*	
Region	OS	OD	OS	OD	OS	OD
Temporal Inferior	0.241***	0.132*	0.256***	0.088*	0.001	-0.013
Temporal Superior	0.005	0.067	0.02	0.043	-0.008	-0.012
Nasal Inferior	-0.034	-0.055	-0.022	-0.033	0.009	-0.022
Nasal Superior	0.041	-0.018	0.06	-0.006	0.044	0.004

p-values: * <0.05, **<0.01, ***<0.001

Table 5.24: Adjusted R-squared values for three linear regression models. The model highlighted in grey for each quadrant was selected for coefficient analysis. OS = left eye, OD = right eye.

		Results for linear regression models in arterial width data			
		OS		OD	
Region		Coefficient	p-value	Coefficient	p-value
Temporal Inferior	*LoD*	6.9e-04	<0.05	3.7e-04	0.29
	Age	-7.5e-04	<0.001	-4.7e-04	<0.05
	Sex	N/A	N/A	0.0105	0.06
Temporal Superior	*LoD*	-1.1e-04	0.73	-7e-05	0.84
	Age	-2.7e-04	0.11	-3.3e-04	0.06
	Sex	N/A	N/A	0.0077	0.12
Nasal Inferior	*LoD*	3.7e-04	0.26	-5e-05	0.87
Nasal Superior	*LoD*	-3e-04	0.15	-2.7e-04	0.28
	Age	-1.4e-04	0.18	N/A	N/A

Table 5.25: Coefficients and significance values for arterial models in each eye. OS = left eye, OD = right eye, *LoD = length of disease*

	Adjusted R-Squared value for three venous models					
	Length of disease, Age, Sex		*Length of disease, Age*		*Length of disease*	
Region	OS	OD	OS	OD	OS	OD
Temporal Inferior	0.024	-0.005	0.042	0.007	0.006	-0.018
Temporal Superior	-0.002	0.042	0.014	0.044	-0.006	0.013
Nasal Inferior	0.054	-0.026	-0.03	-0.011	-0.027	-0.017
Nasal Superior	-0.052	-0.03	-0.032	-0.023	-0.019	-0.013

p-values: * <0.05, **<0.01, ***<0.001

Table 5.26: Adjusted R-squared values for three linear regression models. The model highlighted in grey for each quadrant was selected for coefficient analysis. OS = left eye, OD = right eye.

		Results for linear regression models in venous width data			
		OS		OD	
Region		Coefficient	p-value	Coefficient	p-value
Temporal Inferior	*LoD*	4.5e-04	0.13	6e-05	0.87
	Age	-2.6e-04	0.09	-3.1e-04	0.13
Temporal Superior	*LoD*	-1.6e-04	0.65	5.4e-04	0.1
	Age	-2.6e-04	0.15	-2.8e-04	0.09
Nasal Inferior	*LoD*	-1.7e-04	0.62	5e-05	0.85
	Age	2.3e-04	0.19	1.6e-04	0.26
	Sex	0.011	0.05	N/A	N/A
Nasal Superior	*LoD*	0	0.99	-1.3e-04	0.62

Table 5.27: Coefficients and significance values for venous models in each eye. OS = left eye, OD = right eye, *LoD = length of disease*

5.6.3 Baseline visual acuity

The three variables (*age*, *sex* and *disease*) were used as predictors of LCVA and HCVA scores in order to determine the effects of each on the functionality of someone's retina. The adjusted R-squared values for each model (as shown in Table 5.28) indicate that for HCVA data, using all three predictors was most useful in predicting variation in both eyes. However, the increased effect that MS (no ON) has on LCVA score was reflected in LCVA data being best described by a univariate model of disease alone. All models were significant in their description of the data. The coefficients for *disease* (see Table 5.29) were significant and negative for both HCVA (OS: -5, p-value<0.05; OD: -5, p-value<0.01) and LCVA (OS: -6, p-value<0.01; OD: -6, p-value<0.001) data, being the only significant coefficients found during the modelling. Of the other predictors included, *age* and being female had a negative effect on the HCVA score of a participant.

On assessment of the residuals of the raw data models, all were deemed to be normal supporting the use of linear regression in modelling the datasets. Remodelling of the data with the removal of influential data points showed raw datasets to have a greater adjusted R-squared value and a lower p-value than the remodelled data (see Table 5.30). The coefficients of disease were themselves similar to the raw data models, with an additional drop in LCVA score of 1 letter attributed to disease in left eye when compared to raw data models (Table 5.31). Once more, to investigate how *length of disease* may affect the decline in both LCVA and HCVA in patients with MS (no ON), it was incorporated into modelling of the MS (no ON) data. The resulting adjusted R-squared values were very small (see Table 5.32). The coefficients in the unanimously univariate models selected, though in all cases lacking evidence of an effect, suggested a slight positive correlation between *length of disease* and both LCVA and HCVA score (Table 5.33).

	Adjusted R-Squared value for three models for HCVA and LCVA scores					
	Disease, age and sex		*Disease and age*		*Disease*	
Region	OS	OD	OS	OD	OS	OD
HCVA	0.051*	0.075**	0.049*	0.071**	0.041*	0.064**
LCVA	0.049*	0.079**	0.056*	0.087**	0.062**	0.09***

p-values: * <0.05, **<0.01, ***<0.001

Table 5.28: Adjusted R-squared values for three linear regression models. The model highlighted in grey for each eye was selected for coefficient analysis. OS = left eye, OD = right eye.

		Results for linear regression models of visual acuity data in both eyes			
		OS		OD	
Region		Coefficient	p-value	Coefficient	p-value
HCVA	*Disease*	-5	<0.05	-5	<0.01
	Age	-0.12	0.15	-0.1	0.17
	Sex	-3	0.27	-3	0.23
LCVA	*Disease*	-6	<0.01	-6	<0.001

Table 5.29: Coefficients and significance values for HCVA and LCVA models in each eye. OS = left eye, OD = right eye

Adjusted R-Squared values for HCVA and LCVA models with and without influential points								
	OS				OD			
	Raw data		Remodelled data		Raw data		Remodelled data	
Region	R-squared	p-value	R-squared	p-value	R-squared	p-value	R-squared	p-value
HCVA	0.051	<0.05	0.045	<0.05	0.075	<0.01	0.07	<0.05
LCVA	0.062	<0.01	0.046	<0.05	0.09	<0.001	0.07	<0.01

Table 5.30: Comparing raw and remodelled data coefficients models. OS = left eye, OD = right eye

		Results for linear regression model					
		OS			OD		
Region		Raw data Coefficient	Remodelled data coefficient	p-value	Raw data coefficient	Remodelled data coefficient	p-value
HCVA	Disease	-5	-5	<0.05	-5	-5	<0.05
	Age	-0.12	-0.1	0.22	-0.1	-0.1	0.15
	Sex	-3	-2	0.33	-3	-3	0.18
LCVA	Disease	-6	-5	<0.05	-6	-6	<0.01

Table 5.31: Comparing raw and remodelled data coefficients for HCVA and LCVA scores, as well as the p-values for remodelled coefficients. OS = left eye, OD = right eye.

	Adjusted R-Squared values for three models for HCVA and LCVA scores					
	LoD, age and sex		*LoD and age*		*LoD*	
Region	OS	OD	OS	OD	OS	OD
HCVA	-0.028	-0.064	-0.018	-0.043	0.001	-0.021
LCVA	0.007	-0.05	0.027	-0.033	0.047	-0.013

p-values: * <0.05, **<0.01, ***<0.001

Table 5.32: Adjusted R-squared values for three linear regression models. The model highlighted in grey for each eye was selected for coefficient analysis. OS = left eye, OD = right eye, *LoD = length of disease*

		Results for linear regression model of visual acuity data in both eyes			
		OS		OD	
Region		Coefficient	p-value	Coefficient	p-value
HCVA	*LoD*	0.25	0.31	0.05	0.85
LCVA	*LoD*	0.44	0.07	0.14	0.54

Table 5.33: The coefficients when modelling HCVA and LCVA using *LoD* (*length of disease)* as a predictor, along with their significance levels

5.7 Summary

The findings presented in this chapter offer the first indication of MS affecting the width of peripheral retinal blood vessels, with statistically significant evidence of an effect found in the inferior nasal quadrant. This finding agrees with the small amount of research previously performed on the retinal vasculature close to the optic nerve head in patients with MS, however it further identifies both thinner arteries and veins separately whilst using quadrant-based analysis to identify a profile of vessel width reduction. Comparisons made of baseline data do not indicate whether vascular changes occur over a period of time or acutely at disease onset, which is the motivation for utilising longitudinal data. Baseline analysis also confirmed reports in the literature of RNFL thickness reductions and macular volume loss measured on OCT and a decrease in HCVA and LCVA scores in patients with MS.

Chapter 6

Longitudinal Data Analysis

6.1 Introduction

In order to determine whether the anatomical differences reported in chapter 5 occur longitudinally or over a short time period early in the disease course (as per hypothesis 3), follow-up data was used to investigate the rates-of-change within each of the participant groups, with the results reported in this chapter. Analysis will show the importance of using linear modelling for follow-up data and how the rate-of-change seen in OCT data is found to be accelerated as a result of MS. UWF-SLO data analysis is less conclusive but may indicate a similar longitudinal change as that seen in RNFL thickness and macular volume data on OCT.

6.2 Data cleaning

Of the healthy controls included in this study, two fell pregnant during the time between baseline and follow-up scan. Both these participants presented with a significantly thicker RNFL when scanned during pregnancy: an anatomical change which has been reported, though scarcely, in the literature (87). Due to this thickening of the RNFL, scans from during the pregnancy were excluded from follow-up analysis to maintain a consistent and fair approach to data handling. A postnatal scan was attained for one of these participants, which was included in the analysis under the assumption that any anatomical changes related to pregnancy had then subsided. The total numbers of participants which were scanned at least one further time after baseline are shown in table 6.1. Age range and median age are again slightly larger in the MS group, with more participants in this group having a usable follow-up scan than the HV group. Visual acuity data was collected at every available opportunity but

was dependent on participants remembering to bring any glasses/contact lenses worn during the baseline imaging sessions; vision with corrective lenses was assumed to be consistent (20/20) throughout the study even if a participant had changed their lens prescription, however VA could not be compared for a patient between sessions if they had uncorrected vision for their follow-up reading having had corrected vision for their first.

Characteristics	Patients with MS (N = 69)	Healthy Volunteers (N = 64)
Median Age	44	41
Age range	20-79	24-60
Male	18	14
Female	51	50
History of ON (No. patients)	15	0
History of ON (No. Eyes)	17 (OD 8, OS 9)	0
Relapse-remitting	60	N/A
Primary progressive	2	N/A
Secondary progressive	7	N/A
Disease-modifying therapies*	46	N/A

Table 6.1: Adjusted group demographics for longitudinal analysis. ON = Optic Neuritis, OS = left eye, OD = right eye. *These include: Fingolimod, Tecfidera, Dimethylfumerate, Copaxone, Plegridy, Alemtuzimab and Tysabri

Of the OCT outliers, 3 were caused due to the SPECTRALIS "progression" setting not being activated, causing incongruent positioning of peripapillary regions in follow-up scans. For one participant from the MS (no ON) group this meant they no longer had both baseline and follow-up scans, and their OCT data was excluded from this part of the analysis. The other 2 participants had an adequate number of scans so that even when excluding their baseline scans, they still had enough data for the follow-up analysis. For vessel analysis: despite manual removal of outliers as outlined in chapter 4, and the manual selection of the 8 major vessels used for analysis in each UWF-SLO image, outliers for rate-of-change were still investigated

for each quadrant. Of the outliers, 8 were due to erroneous vessel selection i.e. a different vessel or section of vessel being used to calculate the rate-of-change in width. This was due to one of three things:

- OD diameter varying greatly between scans due to incorrect manual segmentation of the OD. This error would be exaggerated when calculating the ring within which vessel width measurements were being recorded
- Variations in scan quality meaning a vessel was not within the FOV of an image, yet it was in other images
- Subtle variations in the vessel path due to the binary maps not being identical in each image

In such circumstances, the appropriate vessel selection was corrected were possible or removed when not, and the rate-of-change subsequently recalculated. All other suspected outliers were deemed to be valid rates-of-change measurements of vessel width and as such were included in the analysis. Finally, the outliers produced from visual acuity analysis were also investigated manually. Of the outliers, only one participant's data was removed prior to analysis as this individual wore spectacles inconsistently throughout the follow-up sessions meaning their scores could not be compared. All other data was included in the analysis.

6.3 OCT analysis

Though there were several regions with normally distributed RNFL thickness data, this was not true of all regions. For example, inferior nasal, superior nasal and macular volume appeared normally distributed in left eye data for HVs but not for the MS (no ON) group, therefore making direct comparisons with a Student's t-test inappropriate. Table 6.2 displays the median rate-of-change for each peripapillary RNFL region for the HV, MS (no ON) and MS (ON) groups. Despite baseline RNFL data presenting the temporal regions of the retina as

being most effected by MS, the largest annual change in RNFL thickness for the left eye was in the inferior nasal region (OS: -1.06μm/year), with the temporal regions generally showing

	Median rate of change in RNFL thickness in μm/year (IQR)					
	Healthy Volunteers		MS (no ON)		MS (ON)	
Region	OS	OD	OS	OD	OS	OD
Global	0 (1.31)	0.69 (0.98)	-0.29*** (2)	0** (1.96)	-0.31 (2.38)	-0.27* (2.16)
Temporal	0.7 (1.01)	0 (1.67)	0** (2.07)	0 (1.74)	-0.95* (2.1)	-1.56* (1.84)
Temporal Inferior	0 (1.7)	0 (1.84)	-0.11 (3)	0 (2.76)	0 (3.74)	-0.73 (3.91)
Temporal Superior	0.31 (1.89)	0.65 (1.6)	0* (2.49)	-0.05 (3.67)	-0.69 (4.08)	0 (7.68)
Nasal	0 (1.79)	0.76 (1.4)	-0.63* (2.13)	0 (2.36)	-0.39 (2.34)	-0.66 (3.48)
Nasal Inferior	0.05 (2.31)	0.7 (1.8)	-1.06*** (2.4)	0 * (2.35)	-0.75 (3.27)	-0.35 (1.35)
Nasal Superior	0 (2.16)	0.41 (2.19)	-0.53* (3)	0 (2.46)	-0.62 (3.84)	0 (2.38)

Median rate of change in macular volume in mm^3/year (IQR)					
Healthy Volunteers		MS (no ON)		MS (ON)	
OS	OD	OS	OD	OS	OD
0.001 (0.092)	0.012 (0.086)	-0.028** (0.077)	-0.02** (0.087)	-0.028* (0.109)	-0.025* (0.035)

p-values: * <0.05, **<0.01, ***<0.001 when comparing MS (no ON) and MS (ON) groups with HVs

Table 6.2: Median annual RNFL thickness and macular volume changes seen in the three participant groups. OS = left eye, OD = right eye, ON = optic neuritis, MS = multiple sclerosis, SD = standard deviation

smaller annual changes when compared to the nasal regions for individuals in the MS (no ON) group. Left eye data for MS (no ON) did show an annual decrease in all but the temporal and superior temporal regions, however this pattern was not seen in the right eye, where only the superior temporal region showed annual change (OD: -0.05μm/year). A median annual reduction in macular volume was however shown in both eyes of the MS (no ON) group (OS: -0.028mm^3/year OD: -0.02mm^3/year) along with both eyes of the MS (ON) group (OS: -0.028mm^3/year OD: -0.025mm^3/year).

The HV group showed either no change or an annual increase in RNFL thickness and macular volume in both eyes. When comparing the rates-of-change of the MS (no ON) and HV groups statistically via a Mann-Whitney U test, we found there to be a significant difference in values in both sets of eyes globally (OS: $p<0.001$; OD: $p<0.01$) and in the inferior nasal regions (OS: $p<0.001$; OD: $p<0.05$). This was also true of the temporal, superior temporal, nasal and superior nasal regions of the left eye, suggesting an increased rate of thinning in participants with MS (no ON). Despite the low numbers in the MS (ON) group, we still see a significant difference between this group and the HVs in rate-of-change of macular volume and temporal RNFL thickness (this being the region which showed the greatest amount of annual thinning (OS: -0.95μm/year; OD: -1.56μm/year)) in both eyes, as well as globally in the right eye. The median rate-of-change in the MS (ON) group showed annual thinning in all but three regions, and the annual change was greater than seen in MS (no ON) participants in 9 of the 14 peripapillary regions tested.

6.4 UWF-SLO analysis

Some quadrant data was found to be normally distributed, but there were also many sections which were not e.g., all but the superior nasal quadrant of right eye MS (no ON) data. As shown in Table 6.3, the rate-of-change of arterial thickness in the MS (no ON) group was not consistent throughout the peripapillary quadrants; despite baseline data indicating a reduction of vessel calibre for participants with MS (no ON) when compared to the HV group,

longitudinal analysis shows an annual decline in arterial width in 3 of the 8 quadrants investigated. The HV group did however show a median annual thinning of arterial vessels, with all but the inferior temporal region of the left eye indicating a fall in vessel width year on year. The only region for which there was a significant difference ($p<0.01$) in the rate-of-change of arterial thinning was the superior temporal when comparing left eye HV (OS: -3.6e4mm/year) and MS (ON) (OS: 0.0055mm/year) data. As with the MS (no ON) group, MS (ON) data showed a median annual arterial thinning in only a minority of quadrants.

No significant effects were found in the venous data when comparing the three participant groups, where an annual decrease in vessel thickness was seen in only 2 of the MS (no ON) quadrants and 2 of the MS (ON) quadrants (Table 6.4). In both vessel categories, the variation in results is reflected by the large interquartile range (IQR) relative to the small rate-of-change values, and the MS (ON) group's veins did not appear to thin over time despite the lower width values seen in the baseline vessel analysis. The HV group showed an increase in vein width year on year in 5 of the 8 regions.

	Median rate of change of arterial thickness in mm/year (IQR)					
	Healthy volunteers		MS (no ON)		MS (ON)	
Region	OS	OD	OS	OD	OS	OD
Temporal Inferior	9.2e-04 (0.012)	-0.0023 (0.013)	2.7e-04 (0.014)	6.2e-04 0.01)	0.0014 (0.016)	0.0049 (0.012)
Temporal Superior	-3.6e-04 (0.009)	-1.6e-04 (0.013)	-0.001 (0.014)	-0.0018 (0.009)	0.0055** (0.008)	0.0041 (0.011)
Nasal Inferior	-0.002 (0.011)	-0.0014 (0.016)	0.0026 (0.015)	0.0017 (0.013)	5.7e-04 (0.014)	4.3e-04 (0.009)
Nasal Superior	-5.6e-04 (0.007)	-8.8e-04 (0.01)	-3e-04 (0.013)	0.0013 (0.009)	-0.0019 (0.014)	0.0058 (0.012)

p-values: * <0.05, **<0.01, ***<0.001 when comparing MS (no ON) and MS (ON) groups with HVs

Table 6.3: Median annual arterial thickness changes seen in the three participant groups. OS = left eye, OD = right eye, ON = optic neuritis, MS = multiple sclerosis, IQR = interquartile range

	Median rate-of-change of venous thickness in mm/year (IQR)					
	Healthy volunteers		MS (no ON)		MS (ON)	
Region	OS	OD	OS	OD	OS	OD
Temporal Inferior	1.7e-04 (0.011)	3.8e-04 (0.013)	0.0015 (0.016)	7.5e-04 (0.012)	0.0037 (0.018)	-0.0045 (0.02)
Temporal Superior	2e-04 (0.013)	-0.0021 (0.011)	0.0018 (0.014)	-0.0018 (0.011)	0.0024 (0.008)	0.0033 (0.012)
Nasal Inferior	-0.0013 (0.009)	0.5e-0-4 (0.012)	-0.0014 (0.012)	0.0025 (0.013)	-0.003 (0.011)	0.0027 (0.017)
Nasal Superior	-5.4e-04 (0009)	4.2e-04 (0.011)	0.0024 (0.008)	0.0017 (0.008)	0.0021 (0.006)	0.0035 (0.008)

p-values: * <0.05, **<0.01, ***<0.001 when comparing MS (no ON) and MS (ON) groups with HVs

Table 6.4: Median annual venous thickness changes seen in the three participant groups. OS = left eye, OD = right eye, ON = optic neuritis, MS = multiple sclerosis, IQR = interquartile range

6.5 Visual acuity analysis

Normality of the data was not consistently found when analysing the three participant groups which meant Mann-Whitney U tests were used for analysis. HCVA data showed an annual increase in the left eye for both HVs and those in the MS (ON) group (see Table 6.5), whereas left eye data for the MS (no ON) group showed an annual decrease. Right eye data showed median HCVA to be unchanged in the HV group year on year but showed a drop in both MS groups.

Both eyes in the HV group showed an annual rise in LCVA, but the greatest rise was seen in the right eye of the MS (no ON) group, with the left eye in the same group showing no change. The MS (ON) group showed a lack of change in the right eye, but an annual increase in the left eye. Neither of the MS groups showed a significant difference in the rate of change of HCVA or LCVA score for either eye when

compared to the HV group. Once again, IQRs were often large, especially in the MS (no ON) group for LCVA data.

	Median change in visual acuity scores for group demographics (IQR)					
	Healthy Volunteers		MS (no ON)		MS (ON)	
Snellen chart	OS	OD	OS	OD	OS	OD
Full contrast (100%)	1 (5)	0 (8)	-1 (7)	-1 (8)	6 (12)	-1 (3)
Low contrast (2.5%)	1 (6)	3 (8)	0 (17)	5 (12)	4 (2)	0 (11)

p-values: * <0.05, **<0.01, ***<0.001 when comparing MS (no ON) and MS (ON) groups with HVs

Table 6.5: Median annual HCVA and LCVA changes seen in the three participant groups. OS = left eye, OD = right eye, ON = optic neuritis, MS = multiple sclerosis, IQR = interquartile range

6.6 Regression analysis

6.6.1 Longitudinal OCT

The adjusted R-squared values for regression models of longitudinal changes in RNFL thickness and macular volume are shown in table 6.6. As was true with baseline regression models, despite low adjusted R-squared values there were significant models produced for multiple regions: in four circumstances we see a lack of evidence of an effect, three of which are from the temporal regions where data was best represented by a univariate model with *disease/no disease* acting as the lone predictor. However, generally left eye data was better represented by univariate models with only the inferior nasal region including the predictors *age* and *sex*, whereas right eye data was better described by multivariate models in 5 of the 8 datasets.

	Adjusted R-Squared value for three RNFL data regression models					
	Disease, Age, Sex		*Disease, Age*		*Disease*	
Region	OS	OD	OS	OD	OS	OD
Global	0.07**	0.064*	0.078**	0.07**	0.084***	0.045*
Temporal	0.048*	0.022	0.056 *	0.025	0.064**	0.033*
Temporal Inferior	-0.017	-0.011	-0.011	-0.013	-0.006	-0.007
Temporal Superior	0.014	0.008	0.023	0.014	0.028*	0.018
Nasal	0.034	0.022	0.033	0.028	0.036*	0.023
Nasal Inferior	0.053*	0.069**	0.046*	0.077**	0.03*	0.034*
Nasal Superior	0.012	0.052 *	0.018	0.053*	0.026*	0.044*
Macular Volume	0.066 *	0.083**	0.065**	-0.073**	0.071**	0.08**

p-values: * <0.05, **<0.01, ***<0.001

Table 6.6: Adjusted R-squared values when modelling annual changes in RNFL thickness and macular volume. The model highlighted in grey for each region was selected for coefficient analysis. OS = left eye, OD = right eye, ON = optic neuritis, MS = multiple sclerosis, IQR = interquartile range

The subsequent coefficient values from each of the selected models are shown in table 6.7. *Disease* was a significant coefficient in all but the inferior temporal models of both eyes and the superior temporal region of the right eye. The only region for which *disease* did not have a negative coefficient (indicating that disease caused an increase in the annual rate of RNFL thinning) was the inferior temporal region of the left eye. Nasal regions seemed to be more effected by disease than temporal regions when modelling rates-of-change, having the largest absolute coefficients in the inferior nasal regions of the left eye (OS: -1.32, $p<0.05$; OD) and superior nasal region of the right eye (OS: -1.11, $p<0.05$; OD: -1.13, $p<0.01$). An annual global reduction of RNFL thickness in both eyes (OS: -0.98, $p<0.001$; OD: -0.77, $p<0.01$) was also found.

		Results for linear regression models of longitudinal RNFL data			
		OS		OD	
Region		Coefficient	p-value	Coefficient	p-value
Global	*Disease*	-0.98	<0.001	-0.77	<0.01
	Age	N/A	N/A	0.02	<0.05
Temporal	*Disease*	-0.8	<0.01	-0.66	<0.05
Temporal Inferior	*Disease*	0.3	0.56	-0.17	0.66
Temporal Superior	*Disease*	-1.01	<0.05	-1.02	0.08
Nasal	*Disease*	-1.2	<0.05	-0.78	<0.05
	Age	N/A	N/A	0.02	0.21
Nasal Inferior	*Disease*	-1.32	<0.05	-1.06	<0.01
	Age	0.04	0.07	0.04	<0.05
	Sex	0.9	0.19	N/A	N/A
Nasal Superior	*Disease*	-1.11	<0.05	-1.13	<0.01
	Age	N/A	N/A	0.02	0.15
Macular Volume	*Disease*	-0.047	<0.01	-0.042	<0.01
	Age	N/A	N/A	0	0.67
	Sex	N/A	N/A	0.022	0.14

Table 6.7: Coefficient values and their associated p-values from remodelling RNFL thickness and macular volume data with rate-of-change as the response variable. OS = left eye, OD = right eye

When included as a predictor, both *sex* and *age* caused a reduction in the annual rate of RNFL thinning, however *sex* was never a significant predictor and *age* was only significant in the global (OD: 0.02, $p<0.05$) and inferior nasal (OS: 0.04, $p=0.07$; OD: 0.04, $p<0.05$) regions of the right eye. Macular volume was shown to reduce at a higher annual rate for individuals with MS (no ON), with *disease* coefficients being significant in both eyes (OS: -0.047, $p<0.01$; OD: -0.042, $p<0.01$). Neither *age* nor *sex* appeared to have a significant effect on the rate-of-change

of macular volume and the effect of *disease* looks to have been masked when merely calculating the average rate-of-change in the MS (no ON) group as per table 6.2.

As with the baseline data, to verify the use of the models created, the influential data points were removed from the dataset and the remaining data was remodelled, the results from which are displayed in tables 6.8 and 6.9. Adjusted R-squared values remained similar but narrowly improved in 7 of the 16 models. In only one region (nasal region of the right eye) did a model become significant when it otherwise was not in the raw data models. This suggests that the models are again robust enough to describe the data collected irrespective of influential data points. Likewise, the coefficients produced in each region's remodelled data were similar to that of the raw coefficients, with the only coefficient gaining significance after remodelling being *age* in the inferior nasal region of the left eye.

The adjusted R-squared values when using *length of disease* as a predictor for MS (no ON) data are displayed in table 6.10: the values are low and only 3 models were deemed significant, all of which were in the right eye (global, nasal and inferior nasal). The subsequent estimation of each model's coefficients, displayed in table 6.11, shows that in no circumstance was *length of disease* a significant coefficient. *Age* again suggested a decrease in the rate-of-change as a function of time, being a significant coefficient in 3 of the 5 models for which *age* was included. *Sex* was only included as a coefficient in the inferior nasal region of both eyes but showed a mixed effect on the rate-of-change and in neither circumstance was this significant. Modelling with the macular volume data produced no significant *age* or *length of disease* predictors, but followed the trend seen in RNFL data where both caused a decrease in the annual reduction. *Sex* did however produce a significant coefficient in the right eye (OS: 0.053, $p=0.1$; OD: 0.046, $p<0.05$) but in both eyes showed females as having a reduced rate of reduction year on year, thus indicating that men have a more aggressive thinning of their RNFL over time despite females having a smaller macular volume at baseline.

Adjusted R-Squared value for models with and without influential points								
	OS				OD			
	Raw data		Remodelled data		Raw data		Remodelled data	
Region	R-squared	p-value	R-squared	p-value	R-squared	p-value	R-squared	p-value
Global	0.084	<0.001	0.089	<0.01	0.07	<0.01	0.049	<0.05
Temporal	0.064	<0.01	0.05	<0.05	0.033	<0.05	0.038	<0.05
Temporal Inferior	-0.006	0.57	-0.004	0.44	-0.007	0.66	-0.009	0.80
Temporal Superior	0.028	<0.05	0.014	0.11	0.018	0.08	0.012	0.13
Nasal	0.036	<0.05	0.032	<0.05	0.028	0.07	0.042	<0.05
Nasal Inferior	0.053	<0.05	0.06	<0.05	0.08	<0.01	0.09	<0.01
Nasal Superior	0.026	<0.05	0.038	<0.05	0.053	<0.05	0.041	<0.05
Macular Volume	0.071	<0.01	0.064	<0.01	0.083	<0.01	0.068	<0.05

Table 6.8: P-value and adjusted R-squared values produced when remodelling RNFL thickness and macular volume data produced from longitudinal analysis, with influential data points removed. OS = left eye, OD = right eye

Region		Results for linear regression remodelling of longitudinal RNFL data					
		OS			OD		
		Raw data Coefficient	Remodelled data coefficient	p-value	Raw data coefficient	Remodelled data coefficient	p-value
Global	*Disease*	-0.98	-0.97	<0.01	-0.77	-0.63	<0.05
	Age	N/A	N/A	N/A	0.02	0.02	0.06
Temporal	*Disease*	-0.8	-0.69	<0.05	-0.66	-0.58	<0.05
Temporal Inferior	*Disease*	0.3	0.42	0.44	-0.17	-0.09	0.80
Temporal Superior	*Disease*	-1.01	-0.69	0.11	-1.02	-0.89	0.13
Nasal	*Disease*	-1.2	-1.12	<0.05	-0.78	-0.74	<0.05
	Age	N/A	N/A	N/A	0.02	0.03	0.07
Nasal Inferior	*Disease*	-1.32	-1.19	<0.05	-1.06	-1.09	<0.01
	Age	0.04	0.05	<0.05	0.04	0.05	<0.01
	Sex	0.9	0.93	0.18	N/A	N/A	N/A
Nasal Superior	*Disease*	-1.11	-1.02	<0.05	-1.13	-1.06	<0.05
	Age	N/A	N/A	N/A	0.024	0.02	0.24
Macular volume	*Disease*	-0.047	-0.042	<0.01	-0.042	-0.039	<0.01
	Age	N/A	N/A	N/A	0	0	0.63
	Sex	N/A	N/A	N/A	0.022	0.02	0.19

Table 6.9: Comparing the coefficient values and their significance from raw and remodelled data once influential data points have been removed. OS = left eye, OD = right eye

	Adjusted R-Squared value for three models					
	Length of disease, Age, Sex		*Length of disease, Age*		*Length of disease*	
Region	OS	OD	OS	OD	OS	OD
Global	0.003	0.108*	0.01	0.12*	0.02	0.036
Temporal	-0.05	-0.041	-0.031	-0.024	-0.018	-0.006
Temporal Inferior	-0.03	-0.044	-0.035	-0.033	-0.017	-0.015
Temporal Superior	-0.001	-0.015	0.008	-0.011	0.026	-0.008
Nasal	0.015	0.074	0.013	0.086*	0.029	0.033
Nasal Inferior	0.007	0.156**	-0.012	0.127**	-0.016	0.008
Nasal Superior	-0.015	0.002	-0.002	0.02	0.013	-0.018
Macular Volume	0.036	0.038	0	-0.022	0.008	-0.014

p-values: * <0.05, **<0.01, ***<0.001

Table 6.10: Adjusted R-squared values for models when using length of disease as a predictor and rate-of-change as the response variable. The model highlighted in grey for each region was selected for coefficient analysis. OS = left eye, OD = right eye

Results for linear regression models of longitudinal RNFL when using LoD as a predictor					
		OS		OD	
Region		Coefficient	p-value	Coefficient	p-value
Global	*LoD*	0.047	0.15	0.024	0.38
	Age	NaN	NaN	0.041	<0.05
Temporal	*LoD*	0.002	0.94	0.028	0.41
Temporal Inferior	*LoD*	0.013	0.81	0.017	0.71
Temporal Superior	*LoD*	0.075	0.12	0.045	0.47
Nasal	*LoD*	0.102	0.1	0.035	0.34
	Age	NaN	NaN	0.045	<0.05
Nasal Inferior	*LoD*	-0.024	0.75	0.019	0.64
	Age	0.058	0.18	0.063	<0.01
	Sex	1.725	0.16	-1.094	0.1
Nasal Superior	*LoD*	0.071	0.2	-0.019	0.63
	Age	NaN	NaN	0.042	0.08
Macular Volume	*LoD*	0.0015	0.47	0.0001	0.93
	Age	0.0012	0.30	0.0009	0.31
	Sex	0.053	0.1	0.046	<0.05

Table 6.11: The coefficients created from using *length of disease* as a predictor of rate-of-change of RNFL and macular volume data. OS = left eye, OD = right eye, *LoD* = *length of disease*

6.6.2 Longitudinal UWF-SLO

Both arterial and venous data was evaluated with linear regression models so as to eliminate the possible effects of confounding predictors in the median rate-of-change analysis, but over the time scale for which data was collected no models were deemed significant in any region. As shown in tables 6.12 and 6.13, only negative adjusted R-squared values could be produced for 9 of the 16 vessel models, and where values were positive, they were still extremely small.

Tables 6.14 and 6.15 display the coefficients produced from this analysis for arteries and veins respectively. For arterial data, disease had a negative coefficient in 5 of the 8 regions for which data was collected, with both the inferior temporal and superior temporal regions of the left eye showing disease to have no effect at all. *Sex* was included in 3 arterial models and had low p-values relative to other predictors, all with positive coefficients suggesting that being female has the net effect of thickening vessels year-on-year. Of the 3 models for which *sex* was included as a predictor for vein data, the effect of *sex* appeared to be reversed in two of the regions, showing females to have an increased prevalence of vessel thinning annually. As *disease* was not shown to have a significant effect in any region during regression analysis, further examination using *length-of-disease* as a predictor was not completed.

	Adjusted R-Squared value for three models of longitudinal arterial data					
	Disease, Age, Sex		*Disease, Age*		*Disease*	
Region	OS	OD	OS	OD	OS	OD
Temporal Inferior	0.001	-0.025	0.007	-0.017	-0.009	-0.006
Temporal Superior	-0.007	-0.011	-0.001	-0.015	-0.008	-0.008
Nasal Inferior	0.013	0.044	-0.015	0.033	-0.005	-0.01
Nasal Superior	0.009	-0.02	-0.012	-0.015	-0.009	-0.008

p-values: * <0.05, **<0.01, ***<0.001

Table 6.12: Adjusted R-squared values of linear regression models when using rate-of-change of arterial thickness as the response variable. The model highlighted in grey for each quadrant was selected for coefficient analysis OS = left eye, OD = right eye

	Adjusted R-Squared value for three models of longitudinal vein data					
	Disease, Age, Sex		*Disease, Age*		*Disease*	
Region	OS	OD	OS	OD	OS	OD
Temporal Inferior	-0.01	0.013	-0.015	-0.011	-0.006	-0.01
Temporal Superior	0.022	-0.014	0.014	-0.006	-0.004	-0.006
Nasal Inferior	0.015	-0.01	-0.002	-0.014	-0.009	-0.007
Nasal Superior	-0.017	-0.008	-0.01	-0.004	-0.004	-0.006

p-values: * <0.05, **<0.01, ***<0.001

Table 6.13: Adjusted R-squared values of linear regression models when using rate-of-change of vein thickness as the response variable. The model highlighted in grey for each quadrant was selected for coefficient analysis OS = left eye, OD = right eye

		Coefficients for linear regression models when using rate-of-change of arterial width as the response variable			
		OS		OD	
Region		Coefficient	p-value	Coefficient	p-value
Temporal Inferior	*Disease*	0	0.99	-0.0017	0.53
	Age	0.0002	0.11	N/A	N/A
Temporal Superior	*Disease*	0	0.97	0.0005	0.8
	Age	0.0001	0.18	N/A	N/A
Nasal Inferior	*Disease*	-0.0032	0.27	-0.0011	0.65
	Age	-0.0001	0.62	-0.0002	0.05
	Sex	0.0062	0.09	0.0045	0.15
Nasal Superior	*Disease*	-0.0001	0.95	-0.0006	0.73
	Age	-0.0001	0.41	N/A	N/A
	Sex	0.0042	0.08	N/A	N/A

Table 6.14: Coefficient values and their associated p-values when modelling arterial width data produced from follow-up analysis. OS = left eye, OD = right eye

		Results for linear regression model veins			
		OS		OD	
Region		Coefficient	p-value	Coefficient	p-value
Temporal Inferior	Disease	-0.0017	0.51	-0.0006	0.81
	Age	N/A	N/A	-0.0001	0.32
	Sex	N/A	N/A	0.0059	0.07
Temporal Superior	Disease	-0.0009	0.75	0.001	0.57
	Age	0.0002	0.09	N/A	N/A
	Sex	-0.0045	0.17	N/A	N/A
Nasal Inferior	Disease	-0.0014	0.46	0.0015	0.56
	Age	-0.0001	0.23	N/A	N/A
	Sex	-0.0034	0.12	N/A	N/A
Nasal Superior	Disease	-0.0016	0.44	-0.0011	0.45
	Age	N/A	N/A	-0.0001	0.27

Table 6.15: Coefficient values and their associated p-values when modelling vein width data produced from follow-up analysis. OS = left eye, OD = right eye

6.6.3 Longitudinal visual acuity

As seen in table 6.16, no model was significant and very little of the data's variance was described by any of the models created as demonstrated by low adjusted R-squared values. Right eye data were best described by a univariate model of disease alone for both HCVA and LCVA, whereas left eye data was better described with a combination of the variables *age* and *sex*. Despite selecting the models with the highest adjusted R-squared value, none of the coefficients created for either eye was deemed significant (see Table 6.17). The coefficients of disease created for HCVA were the same for each eye, with a reduction of 2 letters per year attributable to disease.

LCVA score appeared to increase by 2 letters per year in both eyes, as a consequence of MS. As with the models themselves, no predictor was found to be significant. *Age* had the effect of increasing HCVA each year as a function of time, but the opposite effect in LCVA. *Sex* was seen to have the largest effect of any predictor, being responsible for a five-letter reduction annually in females.

	Adjusted R-Squared value for three models of HCVA and LCVA data					
	Disease, Age, Sex		*Disease, Age*		*Disease*	
Region	OS	OD	OS	OD	OS	OD
HCVA	-0.002	-0.01	0.01	-0.006	0.008	0
LCVA	0.009	-0.018	-0.012	-0.005	0	0.004

p-values: * <0.05, **<0.01, ***<0.001

Table 6.16: Adjusted R-squared values for models when using HCVA and LCVA as the response variable. The model highlighted in grey for each eye was selected for coefficient analysis. OS = left eye, OD = right eye

		Coefficient results for linear regression models of HCVA and LCVA data			
		OS		OD	
Region		Coefficient	p-value	Coefficient	p-value
HCVA	Disease	-2	0.18	-2	0.32
	Age	0.07	0.28	N/A	N/A
LCVA	Disease	2	0.35	2	0.26
	Age	-0.03	0.76	N/A	N/A
	Sex	-5	0.1	N/A	N/A

Table 6.17: Coefficient values and their associated p-values when modelling HCVA and LCVA data produced from follow-up analysis. OS = left eye, OD = right eye

6.7 Summary

Direct comparisons of each group's rate-of-change data was inconclusive as to the effects of MS on vessel width over time. In no region was rate-of-change of vessel width significantly different between the MS and HV groups, however significant differences were found between them when comparing data collected from OCT. Linear regression modelling did suggest a degree of accelerated vessel thinning in participants with MS but was not conclusive and RNFL data was in-line with previously reported rates-of-change when modelled. Although the lack of observed annual thinning seen in vessel width data may be due to an underpowered study or changes too small to resolve over the scanning period, it may also be because vascular changes occur early in the disease course unlike CNS changes which happen longitudinally.

Chapter 7

Discussion

7.1 Introduction

This study not only reproduces results which have previously been reported on the reduction of RNFL thickness and macular volume in patients with MS, but provides the first evidence of changes to the retina's peripheral vasculature caused by MS. This discovery may lend credence to the theory that MS is first caused by an inflammatory response of the blood vessels in the brain. This chapter discusses the results presented in the preceding chapter, highlighting the strengths and limitations of the study described throughout this thesis.

7.2 Study participants

The number of individuals with RRMS far exceeded those of any other subtype. This was likely due to the nature of progressive subtypes and the opportunistic recruitment strategy employed in this study; patients frequenting the clinic were more likely to be receiving treatment and in need of regular review. As progressive subtypes do not currently have any form of effective disease modifying treatment, patients available for recruitment were more likely to have RRMS for which there are some therapies. Another likely cause is that Fingolimod (a second line therapy that can be prescribed to RRMS patients) has macular oedema listed amongst its possible side effects. Subsequently, individuals prescribed Fingolimod undertook baseline and follow-up OCT scans throughout their treatment as a precautionary measure to identify any signs of oedema. These individuals would already be familiar with part of my scanning procedure or would have to undertake scanning as part of their patient-centred care, so may have been more comfortable with participating in the study. Despite previous studies reporting that different MS subtypes have a different rate and profile

of thinning of the RNFL, subtype was not integrated into the regression models created for this study due to the overwhelming dominance of RRMS patients in recruitment numbers (88) (89). More targeted participant recruitment would aid future investigations into the differences in retinal anatomy between disease subtype, but this less-opportunistic approach would likely result in a lower rate of recruitment and need more time to reach its objectives than my study.

As mentioned in Chapter 4, not all participants received follow-up retinal scans and of those that did, not all of the scans were of a sufficiently high quality for analysis. HVs received fewer follow-up scans than those in the MS groups. This is likely because MS participants adhered to their scheduled clinical appointments more fervently, the clinic sessions being focused around their medical wellbeing rather than being purely research related. Scheduling follow-up scans for HVs required a greater degree of organisational effort to encourage people back to the clinic, whilst some HVs moved to locations too far away to reasonably travel back to the clinic for follow-up.

7.3 OCT

Although this study has lower participant numbers compared to larger investigations into the effect of MS on the retina, the results resonate with the changes previously reported in the literature. Differences seen between the MS groups and the HVs were great enough as a percentage of overall RNFL thickness/macular volume that our participant numbers had adequate power to often provide statistical significance with both Students t-tests and Mann-Whitney U tests. This was also true of the MS (ON) group, which saw the greatest difference in RNFL thickness despite a lack of normality and low participant numbers ($N<11$). Temporal regions showed the greatest difference but all regions except the inferior nasal showed a significantly thinner RNFL in the MS (no ON) group when compared to HVs. Global differences (OS: -10μm, $p<0.001$; OD: -11μm, $p<0.001$) were consistent with a large multi-centre study of 414 MS patients, although was larger than that reported by a recent systematic review and meta-analysis which saw a 7.41μm thinner RNFL in 4109 eyes (90) (29). The

profile of differences seen, with greater reductions measured in the temporal regions of the retina, is typical of MS; thinning in the temporal region is the most reliable measure of both physical and cognitive disability in MS when compared to thinning in other quadrants (91). My results show a similar range of temporal RNFL thickness reduction (OS: -11µm, $p<0.001$; OD: -12µm, $p<0.001$) as presented by Antonio-Santos et al. (-11µm $p<0.0001$) and Henderson et al. (-12.8µm to -22.9µm) (92) (31).

The reduced RNFL thickness in the left eye of MS (ON) participants was found to be larger than the global reduction reported by Petzold et al. in their meta-analysis of 2063 eyes (-24µm vs -20.1µm respectively), although the difference was not as large in the right eye (-16µm) and this meta-analysis was focused on changes measured with TD-OCT devices (27). As reported by Costello et al. the effect of ON is compounded after repeated attacks in the same individual, and with such small numbers of participants comprising the MS (ON) group in this study, individuals who have suffered from ON on more than one occasion could skew the data to a large extent (93). Likewise, this may also help explain the difference seen between the left and right eyes in the median analysis; with $N<10$ for both eyes, a lack of intraocular correlation is not unexpected. By studying the historical correspondence of those in the MS (ON) group and incorporating the number of ON episodes for each eye into a regression model, this data could be better characterised and potentially explain the interocular variations that were observed. Despite these small numbers, in all regions except the inferior temporal the difference in median RNFL thickness was found to be significant when compared to that of HV's. A significant reduction in macular volume was also observed in MS (no ON) participants when compared to HVs, with left eye data correlating well with Burkholder's reported 10µm reduction in RNFL thickness for every $0.2mm^3$ reduction in macular volume (30).

Linear regression modelling went on to suggest that the majority of the differences seen between the groups were due to *disease* rather than *age* or *sex*, although in some models these

predictors were also significant. Initially the MS and HV groups had relatively even demographics, which may explain why linear modelling showed similar results to the direct comparisons of each group's average RNFL thickness or macular volume. However, having split the MS group into MS (no ON) and MS (ON), it was still vital to model the data to be sure of the role disease played in explaining the differences between the groups. Although the low adjusted R-squared values produced when modelling OCT data may suggest the absence of one or more confounders from the models, reports for similar studies do not suggest any additional important predictors (35); all models were found to be significant ($p<0.01$), except when modelling the inferior nasal region of both eyes, indicating that the models had descriptive value with *disease* being the most consistently significant predictor. Scatter plots such as the one displayed in Graph 7.1 suggest that a large variance within the datasets may be responsible for the low adjusted R-squared values presented in this thesis.

The general lack of predictive power when using *length of disease, age* and *sex* as predictors of MS (no ON) data may be due to the huge variability in disease progression that is found between individuals with MS; *length of disease* is not a particularly reliable measure of disease activity because MS does not follow a single pattern of progression over time but is widely variable between patients and disease subtypes (3). Without regular MRI scans with which to view new/active plaques on the brain, or regular EDSS/MSFC assessments to quantify disease progression, such a predictive model would be difficult to create. A study which used said measures found a reduced rate of axonal thinning is associated with "no evidence of disease activity" in patients with MS, indicating that the rate of thinning is dependent on the disease status of an individual (94). Including EDSS/MSFC assessments into the retinal scanning sessions would provide informed data which may be useful for linear regression modelling, but it would also extend the sessions by a considerable amount of time at the inconvenience of the participant and would require experienced assessors to carry out.

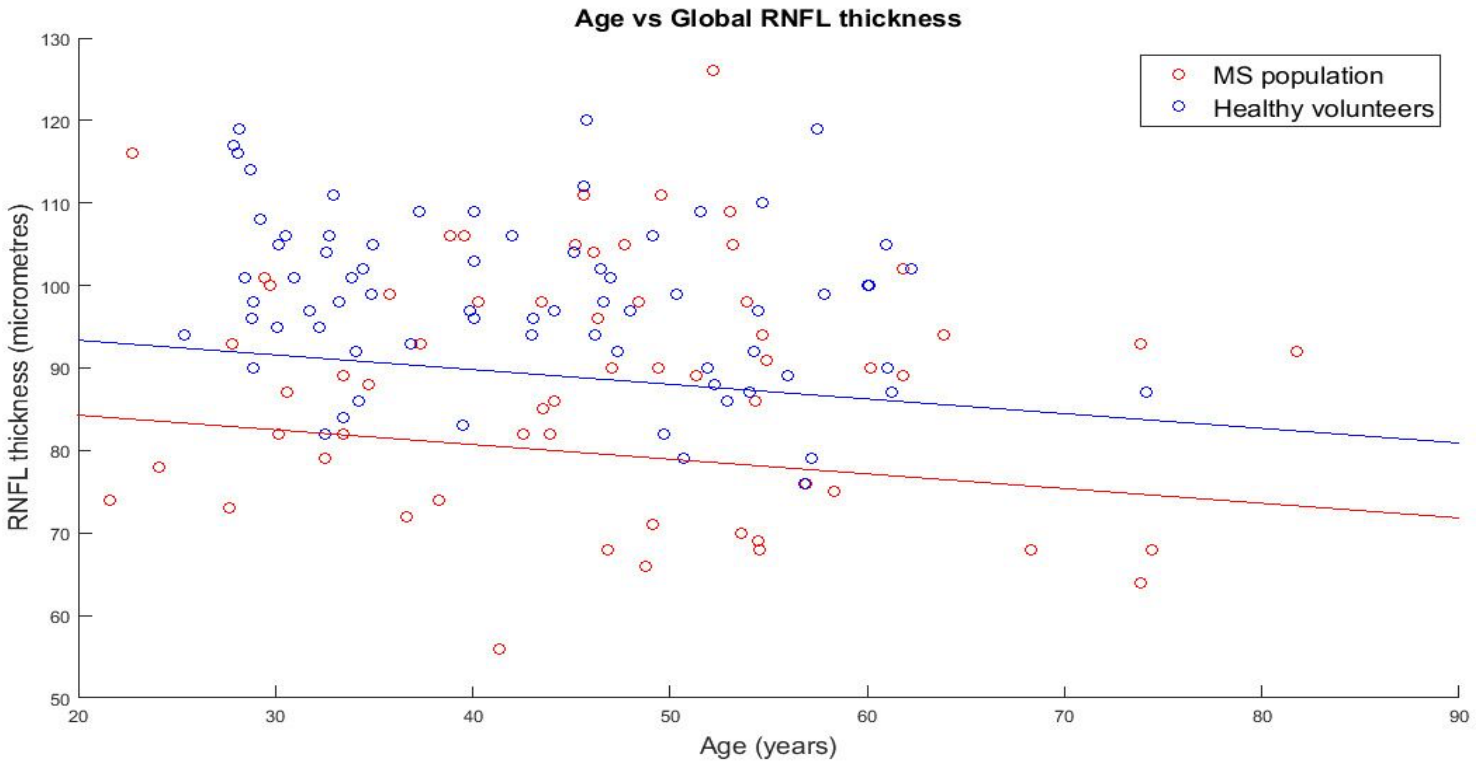

Graph 7.1: A plot displaying the large levels of variance when investigating global RNFL thickness as a function of age. Two lines of best fit show the general decline for patients with MS and HVs as age increases

Longitudinal data provided less conclusive results in assessing the rate-of-change of RNFL thickness and macular volume when using unpaired samples Student's t-tests. This is likely due to the effect size being much smaller; comparing results at baseline will show compounded differences which have occurred year-on-year, whereas annual changes are both smaller and more susceptible to small changes caused by erroneous segmentation. Changes which occur over these time periods may also be smaller than the resolution of the device used to capture images (i.e. 7μm axial resolution for SD-OCT devices vs 1.1-2.9μm reduction in global RNFL thickness every 2 years), resulting in only extreme changes being detected or considered clinically significant. The low rate-of-change values seen suggests that the pace with which anatomical changes occur in the retina is slow (approximately 6-7 years for a measurable change), regardless of disease status. Large IQRs indicate a high variability in the rate at which changes occur between participants of the same group, with some participants having negative rates-of-change and thus thinning over time, whilst others have a thickening. This variation is visualized in Graph 7.2, which displays a box plot of the median annual rate-of-change in RNFL thickness seen in each group for left eye data; the participants from the MS (no ON) group appear on average to have either no annual change or an annual rate of thinning. Results which suggest a thickening were unexpected as even in HVs, annual thinning of the RNFL and loss of macular volume may be anticipated as a result of aging (36). However, the changes associated with age may again be too small to accurately measure with the resolution of the device used, and the data may represent the normal range of variation in retinal anatomy expected from multiple images acquired in different sessions.

These results did not concur with those found in the literature relating to the annual change expected in RNFL thickness as measured in longitudinal analysis (see chapter 2) (33) (34) (33). Several key differences can be found between this study and the previous reports: two of

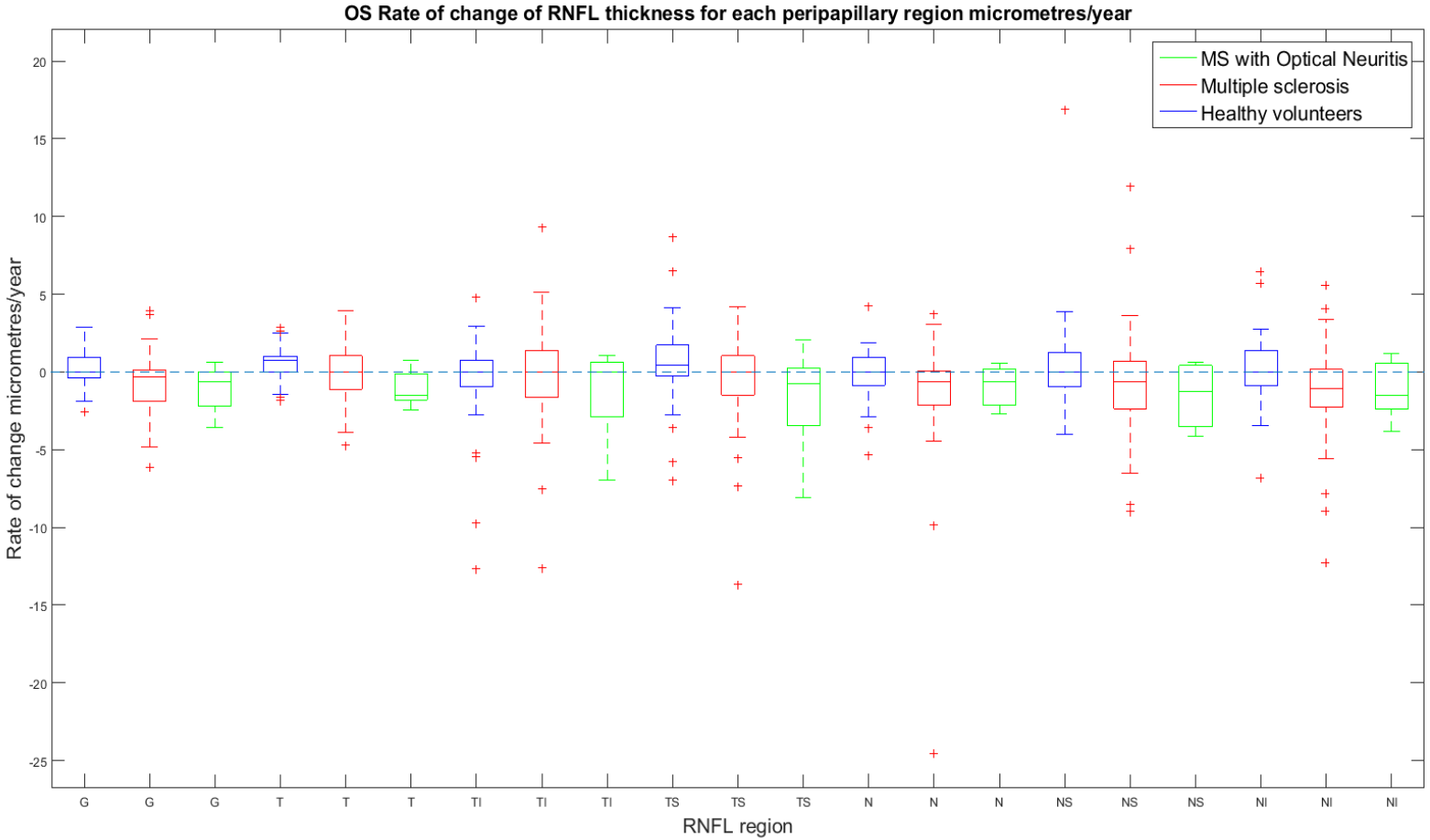

Graph 7.2: Box plot which shows the annual rate-of-change in RNFL thickness for each participant group in the peripapillary OCT regions. OS = left eye

the studies used TD-OCT to collect data which lacks the resolution and hence resolving power of SD-OCT to measure small changes and has a lower inter-rater and test-retest reliability (42) (35). One of these studies did however report a similar reduction in macular volume annually as found in the MS (no ON) group from this study (35). In the third study, which used a SPECTRALIS device and had a high number of RRMS patients, separate analysis of individuals with a clinical history of ON was not carried out, although no significant difference was found in participants who had previously suffered ON when compared to those who had not (33). My results conflict with this finding, with the annual rate of thinning being largest in the MS (ON) in 75% of circumstances. This would suggest that not only does RNFL thinning occur each time an individual suffers from ON, but that the effects of ON continue over time as patients have an increased rate of RNFL thinning.

The likeliest reason for my results differing from those reported elsewhere and, in some cases, indicating a thickening of the RNFL is the low number of scans (in some cases as few as two) taken during the course of the study. Such subtle changes to RNFL thickness over a two-year period will be unsubstantial in comparison to the errors in segmentation or limitations of the device's resolution. As such, in circumstances where there are just two scans for a participant the longitudinal results would be easily skewed by small errors This is despite the SPECTRALIS having good repeatability and ICC measures as discussed in chapter 3. Without being able to extend the study time (to increase the measurable change in RNFL thicknesses), one solution would be to take many more scans throughout the two-year period in order to create a more accurate gradient of change. This would require more of a patient burden and perhaps discourage individuals from participating in the study. Therefore, a more preferable potential solution would be to scan the eye multiple times using the OCT device during each session and average the scan results for each individual (supposing the scans are of sufficient quality). This would lead to greater accuracy, results which are less prone to error and therefore provide a more reliable source for rate-of-change.

Results from my linear regression analysis were closer to those reported by other longitudinal studies (33) (34) (33). My results suggest that age-related thinning of the RNFL occurs at a greater pace annually when individuals are younger and gradually slows over time. They also indicate that the median rate-of-change presented might be affected by some confounding variable in the HV group, as rates-of-change were found to be positive on average indicating a thickening of the RNFL over time rather than a thinning due to age. Such a missing confounder may not be restricted to just HV data, as the coefficients of disease estimated by the models created here are larger than the median rates-of-change calculated for the MS (no ON) group.

The adjusted R-squared values when using *length of disease* as a predictor were once again low with only 3 models being significant, all of which were in the right eye (global, nasal and inferior nasal). The subsequent estimation of each model's coefficients shows that in no circumstance was *length of disease* a significant coefficient. However, in all but two models the coefficient was positive which suggests, much like *age*, that the annual rate of RNFL thinning associated with MS (no ON) occurs at a greater rate early in the disease course and plateaus over time. The decline in the rate of thinning found in right eyes in this study is similar to that reported by Balk et al, although the left eye was found to have a larger decline in the rate of thinning year-on-year in the global region (33).

7.4 UWF-SLO

Differences were seen when comparing baseline vessel width (within 6.5 and 8.5 optic disc radii from the centre of the optic disc) from HV and MS (no ON) groups providing evidence to confirm hypothesis 1, although the degree of change was dependent on the region from which measurements were taken. Most notably, vessels in the nasal quadrants of the retina seem most effected in the MS (no ON) group, being the only region that saw significant differences in vessel thickness. The location of the greatest vascular differences between these two groups is not the same as changes seen in the RNFL data. This may be because blood

vessels in the temporal region form a more complex network with a greater amount of bifurcations and vessel crossings as capillaries supply a rich quantity of oxygenated blood to the macular. Such a complex network might lead to more errors in the segmentation of blood vessels and may therefore cover up any subtle changes in vessel width. On the other hand, the differences between retinal quadrants may be an accurate representation of anatomical/pathological changes which occur within specific locations of the retina. Despite the pattern of differences, in the majority of quadrants, despite a lack of significance, both arteries and veins appeared to have a slightly reduced width in the MS (no ON) group when compared to HVs. Although no other study has investigated the retinal vasculature in peripheral regions as this one has, the reduced vessel widths measured here is complimentary to Bhaduri's study of blood vessels in close proximity to the OD (40).

Evidence of an effect was not found when comparing the HV group and the MS (ON) group. With the relatively small differences expected in vessel width compared to the changes seen in RNFL thickness, along with the very low numbers of participants with a clinical history of ON ($N<10$), statistical tests applied to MS (ON) would likely lack meaningful power or reliability. Regardless, the results seem to resonate with what has been previously reported in the literature (40), although it has also been reported that blood flow is reduced specifically in the optic nerve head region in patients with a clinical history of ON (40) (95). This finding may not translate to peripheral regions of the retinal vasculature.

My linear regression analysis seemed to further highlight the effect of MS on vessel width whilst considering *age* and *sex* as confounders. In arterial data, modelling generally showed slightly smaller effect sizes attributable to *disease* than when directly comparing the MS (no ON) and HV groups. This was not the case for the inferior nasal region, which saw *disease* bearing a greater effect in the linear models. *Age*, which was a significant predictor in the superior temporal and inferior nasal quadrants (when included in the models) was also negative in most cases, suggesting that vessels get thinner as one gets older. The modelling of vein data showed little change to the results from a direct comparison of the MS (no ON) and

HV groups, which may be because *age* does not appear to play the same role in the thinning of veins as it does with arteries (never being a significant predictor). Although the differences in vessel thickness were seen to be significant in some regions, it should be noted that even the greatest difference seen between the participant groups was smaller than the resolution of the imaging device used, as reported by the manufacturer (7μm difference found between HV and MS (no ON) groups in the inferior nasal quadrant vs a smallest resolvable object of 14μm). This would limit the current ability of UWF-SLO to create screening procedures for individual patients. Nevertheless, over a study population of 144 participants the compounded effect of vascular change provides new insight into how the peripheral vasculature changes in patients with MS.

The disparity between the raw-data and remodelled coefficients of *disease*, especially those of the arterial dataset show a degree of sensitivity to influential data points which was not present in the RNFL regression models. This is likely due to the effect size in retinal vessels being smaller than that of RNFL thickness measures; with low numbers of participants, influential data points will have an exaggerated effect on the regression models. However, the *disease* coefficients still suggest that MS (no ON) does show a reduced retinal blood vessel thickness when compared to HVs. In order to determine whether this effect is progressive and occurs at a certain rate throughout the disease, the MS (no ON) data was once again modelled separately. Modelling of the MS (no ON) group when using *length of disease* as a predictor alongside *age* and *sex* showed a mixed effect attributable to *length of disease*. This may be due to the small effect sizes seen in the vessel width data in the MS (no ON) group, as well as the flawed assumption that *length of disease* is an accurate measure of disease severity. On the other hand, this modelling could suggest that changes to vessel anatomy occur early in the disease course along with initial inflammatory responses within the brain; the initial breach of the BBB may be mirrored in the BRB, and the inflammatory effects of this may cause an immediate reduction in blood vessel width.

Longitudinal analysis showed no consistent trends when comparing the rate-of-thinning of vessels of the three groups through unpaired samples Student's t-tests. Similarly, no regression models were found to be significant when attempting to describe the data and the resulting adjusted R-squared values were extremely small. This may indicate that linear regression was an inappropriate tool for explaining variations in the data and more complex approaches are needed. This was supported by the lack of normal residuals produced from the models. However, upon examining the coefficients themselves: although direct comparisons between the participant group's median annual change in vessel thickness showed little sign of individuals with MS having an increased rate-of-thinning, linear regression analysis indicates this might be masked by confounding variables, as was true of RNFL data. *Disease* shows an annual increase in the rate of arterial thinning in 5 of the regions modelled, with two regions showing no annual change. Likewise, modelling of vein data shows *disease* as causing an increased rate of vessel thinning in six of the eight models created, again in conflict with the results produced from directly comparing the three groups. Although none of the coefficients for any predictor were significant in this part of the analysis, this may well be due to a lack of power as changes in vessel width are small, there were low participant numbers, or the timescale was too short, rather than *disease* having no clear effect on the rate-of-change of vessel thinning. Of the other predictors included, *age* had a mixed effect but produced a negative coefficient in six of the nine models for which it was included, suggesting that (unlike RNFL and macular volume) the rate at which *age* causes thinning of the vessels increases as individuals get older.

7.5 Visual acuity

Visual acuity is at present a widely used tool for determining the retinal function of an individual as it is quick, simple to understand and requires little expense. However, it can be difficult to create a controlled environment that is suitably consistent when undertaking testing, hence the large degree of change required before determining a drop of VA score which is of clinical significance. For example, though blinds were used to block sunlight

entering through the clinic window in this study, the level of illumination within the room would still vary to large amounts depending on the outside environmental brightness on any given day. In an ideal environment a constant level of illumination would have to be maintained to accurately compare participant scores. Secondly, social factors could potentially play a large role in how consistent each participant is in the effort and time they dedicate to providing an accurate VA score. Whereas retinal scanning mitigates this to some degree, VA is reliant on a participant trying their best to focus on the letters every time they are tested, which may conflict with their wishes should they be feeling rushed for time or tired. Despite these limitations, significant differences were seen between the three groups at baseline, as was expected.

The reduction in HCVA found in the MS (no ON) group when compared to the HV group was above the 5-letter limit for clinical significance in the left eye, although right eye data only produced a 3 letter decline in score. While the difference between these two groups in HCVA was both significant and greater than 5-letters, in both eyes the fall in LCVA score narrowly missed the 7-letter drop to declare clinical significance. As mentioned, the highest scores were similar in both groups, however the scores in the MS (no ON) group had a larger range, thus indicating that although MS participants can perform well when viewing Sloan letter charts, they are more likely to have a low score than HVs. The lower median values seen in the MS (no ON) group correlates well with the reduction in RNFL thickness and macular volume also seen in this group. The large differences seen between the HV and MS (ON) group in RNFL thickness and macular volume were not reflected when comparing HCVA scores, with neither eye showing a significant difference despite a 9-letter decrease in median score for the left eye in the MS (ON) group. Left eye data was however significant when comparing LCVA scores, although the small drop in LCVA score for right eye data lacked evidence of an effect. The lack of evidence seen is likely due to the low participant numbers in the MS (ON) group as such large changes in RNFL thickness and macular volume would be expected to reduce the functionality of the retina.

The significant 5-letter reduction in HCVA score was also seen in both eyes when linear regression models were used to isolate the effect of disease. Despite the inclusion of *age* and *sex* as predictors, *disease* was the only coefficient to be significant, although the effect of *age* correlating inversely with retinal functionality was an expected phenomenon. Once again, LCVA score narrowly missed the 7-letter decline associated with clinical significance, although the coefficient was itself significant in both eyes. Surprisingly, *length of disease* proved to have a positive coefficient when used as a predictor for MS (no ON) data. Though this did lack significance, one would expect VA score to diminish with the length of time someone has lived with MS, however this result may yet again indicate the fallacious assumption that *length of disease* correlates with disease activity in MS.

Follow-up data analysis, including regression models, produced mixed results. HCVA data saw a small annual decrease in score for the MS (no ON) group in both eyes, however both HVs and the MS (ON) group saw circumstances where an increase in HCVA occurred annually. Regression models did seem to indicate that MS was responsible for a 2-letter decrease in score year-on-year. LCVA score was found to conflict with the assumption that retinal function would diminish annually in MS participants, as regression models suggested LCVA to increase annually by 2 letters in MS. *Age* was also found to contribute to an increase in HCVA score annually, although the changes predicted were small. None of the models produced were significant. With the bar set high for a clinically significant change in both LCVA and HCVA score due to the nature of testing, it is unlikely that an individual would have such a dramatic reduction in their retinal functionality between scanning sessions unless they experienced an episode of ON. This analysis may therefore show the inappropriate nature of using rate-of-change as a method of determining drop-off in retinal functionality. Over a longer time period, a more comprehensive approach to the data may be to examine the percentage of each group that have a clinically significant change in their VA scores, as presented by previous research (see chapter 2).

7.6 Future work

Vascular analysis in this study showed evidence that the blood vessels of the retina are anatomically altered as a consequence of MS, but to what extent is uncertain as this study was ultimately underpowered. Table 7.1 presents the power level for each of the vascular changes seen. Although differences between the HV and MS (no ON) groups were significant, none were above the 0.8 power threshold- arterial widths in the inferior nasal region of the right eye had the greatest power of 0.77.

Future studies should be designed to confirm the differences seen at baseline between HV and MS (no ON) groups. Assuming the differences in vessel width seen are accurate, in order to prove statistically these differences, the numbers of participants needed for each of the four quadrants are shown in table 7.2, with power set to 0.8 and a significance level of 0.05. The

	Power level when comparing the vessel widths of HV and MS (no ON) groups			
	Arteries		Veins	
Quadrant	OS	OD	OS	OD
Inferior Temporal	0.23	0.44	0.33	0.06
Superior Temporal	0.093	0.11	0.17	0.05
Inferior Nasal	0.62	0.77	0.60	0.47
Superior Nasal	0.07	0.30	0.26	0.37

Table 7.1: Given the number of participants who had usable scans in each quadrant, the power level for both vessel classifications are presented for the effect size seen in this study

	Number of participants from both HV and MS (no ON) groups needed to create a power level of 0.8 when comparing vessel widths			
	Arteries		Veins	
Quadrant	OS	OD	OS	OD
Inferior Temporal	304	129	200	8172
Superior	1291	996	471	70332
Inferior Nasal	66	56	72	123
Superior Nasal	2739	241	276	192

Table 7.2: With power = 0.8 and significance = 0.05, the number of participants needed to provide evidence of change within each quadrant for the two vessel classifications are shown

number of participants needed to prove the findings in the inferior nasal quadrant of the retina are feasible, especially when comparing arterial widths. However, the numbers needed to provide evidence in the other quadrants are too large to reasonably expect to recruit. As such, future work using UWF-SLO imaging should focus on confirming the findings specific to the inferior nasal quadrant. The use of higher resolution imaging techniques (e.g., infrared SLO and fundus photography) may be able to discern changes in vessel thickness to a greater precision and thus confirm the reduction in vessel width seen in the other quadrants of the retina without such high participant numbers, although would struggle to image the peripheral retina. This higher precision may also be beneficial in identifying small changes which occur longitudinally throughout the disease course, and thus determine whether the vascular changes seen occur as a function of time. Incorporation of axial measurements should also be considered to improve accuracy of vessel width measures; when measuring the area of the Argus II retinal implant *in vivo* and comparing this to the known values, the accuracy of the measurement was 10.21% when axial length is unaccounted for and 1.93% when accounted for (65). Investigating vascular measures other than just vessel width (e.g., fractal dimension of the vascular branching pattern and vessel tortuosity) may also uncover differences between HVs and MS participants- pilot analysis could be completed on the data already collected in this study. To better understand the correlation of disease severity with anatomical changes in the retina, clinical information including EDSS/MSFC and MRI analysis would be a valuable asset in stratifying participants.

Future studies should also be designed with a more proactive strategy for recruiting MS participants from each of the disease subtypes, as this would allow for better patient stratification and the potential for regression models that better describe the data. Models may also be improved by scanning participants at set intervals rather than relying on rate-of-change calculations. This would allow for a more direct comparison between the participant groups to be made. One of the limitations of this study is the small timescale over which scans were taken relative to potential length of the disease course (approximately 2 years vs median of 30

years between diagnosis and death), especially given the slow rate at which changes to the retinal anatomy appear to occur (6). By increasing the length of time over which data is collected, analysis may offer evidence of when vascular changes occur in the disease course- a question which should be central to future studies. Specifically, prospective investigations must look to determine whether changes occur over the entire disease course or are only the result of initial disease mechanisms. Collecting data over a longer timescale should not prove to be problematic for MS participants as the chronic nature of the disease requires regular consultations with a neurologist. However, recruiting HVs for the same length of time might prove more problematic as individuals may relocate or become unavailable for follow-up scans. One possible solution could be to more actively encourage the friends and family members of MS participants to volunteer as presumably they would remain committed to a study for a greater period of time. Linear regression models may however be less effective at describing longitudinal changes over larger timescales, as is shown by both *length of disease* and *age* causing a progressively smaller amount of thinning each year, suggesting that thinning plateaus over time. As such, more sophisticated statistical analysis is likely needed to characterise the data.

An effort to fully automate vessel analysis in UWF-SLO images would be extremely beneficial in encouraging researchers to investigate changes to retinal vasculature. Despite its benefits, the analysis software used for this study does require a large investment of operator time which may discourage other clinicians and researchers. Automating vessel analysis would also increase the feasibility of using UWF-SLO devices as a screening tool for MS, and reduce experimental errors associated with human intervention. Ultimately, future work should be directed towards the creation of a screening method which can identify the early anatomical changes associated with MS and offer early intervention for those at risk of developing symptoms. Integrating all the vascular measures mentioned alongside information from OCT and visual acuity data could be a useful predictive tool for use in logistical regression models

which determine the likelihood of an individual developing MS given changes to their retinal anatomy.

Chapter 8

Conclusion

The opening chapters of this thesis explained the importance of diagnosing and treating patients with MS as early as possible and how retinal imaging could be of benefit by providing a patient friendly tool for viewing the CNS and microvasculature. Building on the examples of previous studies which have touted retinal imaging as a potentially useful biomarker for disease progression, this longitudinal pilot investigation was designed to address the three hypotheses set out at the beginning of this thesis:

1. An individual diagnosed with MS will have quantifiable differences to their retinal vasculature at baseline imaging compared to healthy controls
2. An individual diagnosed with MS will have quantifiable differences to their RNFL thickness and macular volume as measured by OCT
3. An individual diagnosed with MS will have quantifiable changes to their retinal vasculature which occur longitudinally and correlate with disease progression and worsening severity

The novel discovery of evidence showing thinner blood vessels in the inferior nasal quadrant of the retina has shown that changes to the retinal anatomy are not exclusively neurodegenerative and therefore supports hypothesis 1. To ensure future studies are powered sufficiently and evidence can be gathered for the global differences seen, the power calculations included in chapter 7 should be used as an important guide for participant recruitment numbers. Much as changes to the RNFL and macular are deemed to be useful correlates for atrophy in the CNS, my findings could be indicative of vascular changes which occur to similarly sized vessels within the brain. The data collected can further be utilised to full effect, with additional analysis completed on vascular parameters such as tortuosity. This

would allow for a more comprehensive understanding of how the blood vessels change as a consequence to MS.

In an attempt to place the vascular changes found into the context of neurodegenerative changes which occur at baseline and over the course of the disease, my study provides important replication of the results from other research using OCT in MS. The evidence shown of reduced RNFL thickness and macular volume in patients with MS addresses and confirms hypothesis 2. Baseline data was more conclusive than longitudinal data, most likely because the changes expected over an approximately 2-year period are too small to be reliably measured with the number of participants in this study. However, the trend seen in linear regression modelling shows results which are similar to those found in the literature and suggests that neurodegenerative changes occur gradually over time. If possible, future studies should organise for participants to have follow-up scans no less than 6 years from baseline as this would allow for measurable differences in RNFL thickness to occur, given the rate-of-change predicted by linear regression modelling.

Finally, hypothesis 3 was addressed when analysing longitudinal UWF-SLO data. Unlike OCT, evidence of a longitudinal effect on vessel thickness was not found, which may either mean that the changes occurring over the period of this study were too small to be measured by the currently available devices, or that changes to the retinal vasculature do not occur longitudinally but over a short period of time early in the disease course. Discovering which of these is true should be a motivation for future investigations; if changes to the vasculature only occur early in the disease course, they could be used as a screening tool for MS before the onset of debilitating symptoms. Secondly, if these changes occur prior to changes to the RNFL and macular, then it would support the premise that inflammation strikes before neurodegeneration, helping us a gain a deeper insight into the disease and how it may be treated. Hypothesis 3 could be better examined in prospective studies by utilising an effective measure of disease severity, such as EDSS or MSFC, as *length of disease* has been shown throughout this study to be an ineffective measure of disease activity.

In conclusion, scanning the retina with different imaging modalities has shown promise to become an effective clinical tool for revealing information about MS, specifically pertaining to neurodegeneration in OCT and microvascular changes in UWF-SLO. The methods presented in this thesis may help expand the understanding of the initial disease mechanisms in MS, but also the development of future screening methods which identify patients with MS early in their disease course.

Bibliography

1. MS International Federation. What is MS? *MS International Federation.* [Online] Multiple Sclerosis International Federation, Nov 10, 2016. [Cited: June 29, 2017.] www.msif.org.

2. *Incidence and prevalence of multiple sclerosis in Europe: a systematic review.* Kingwell E, Marriott JJ, Jetté N, Pringsheim T, Makhani N, Morrow SA, Fisk JD, Evans C, Béland SG, Kulaga S, Dykeman J. 1, s.l. : BMC neurology, Dec 2013, BMC Neurology, Vol. 13, p. 128.

3. Wilkins, Alastair. *Progressive Multiple Sclerosis.* s.l. : Springer, 2017, pp. 1-7.

4. Kiernan J, Rajakumar R. *Barr's The human nervous system : an anatomical viewpoint.* Ninth. s.l. : Lippincott Williams & Wilkins, 2013.

5. McAlpine D, Compston A. *McAlpine's Multiple Sclerosis.* 4. s.l. : Elsevier Health Sciences., 2005.

6. *Multiple Sclerosis.* Compston A, Coles A. s.l. : Lancet, Oct 2008, The Lancet, Vol. 372.

7. *Blood-brain barrier disruption in multiple sclerosis.* Minagar A, Alexander JS. 6, Dec 2003, Multiple Sclerosis Journal, Vol. 9, pp. 540-549.

8. *Why does remyelination fail in multiple sclerosis?* RJ, Franklin. 9, s.l. : Nature Reviews Neuroscience, Sep 2002, Nature, Vol. 3, pp. 705-714.

9. *Multiple Sclerosis: Geoepidemiology, genetics and the environment.* Milo R, Kahana E. 5, Mar 2010, Autoimmunity Reviews, Vol. 9, pp. 387-394.

10. *Incidence and prevalence of multiple sclerosis in the UK 1990–2010: a descriptive study in the General Practice Research Database.* Mackenzie IS, Morant SV, Bloomfield GA, MacDonald TM, O'riordan J. 1, Jan 2014, J Neurol Neurosurg Psychiatry, Vol. 85, pp. 76-84.

11. *A new prevalence study of multiple sclerosis in Orkney, Shetland and Aberdeen city.* Visser EM, Wilde K, Wilson JF, Yong KK, Counsell CE. 7, Jul 2012, J Neurol Neurosurg Psychiatry, Vol. 83, pp. 719-724.

12. *Recommended diagnostic criteria for multiple sclerosis: guidelines from the International Panel on the diagnosis of multiple sclerosis.* McDonald WI, Compston A, Edan G, Goodkin D, Hartung HP, Lublin FD, McFarland HF, Paty DW, Polman CH, Reingold SC, Sandberg-Wollheim M. 1, Jul 2001, Annals of Neurology: Official

Journal of the American Neurological Association and the Child Neurology Society, Vol. 50, pp. 121-7.

13. *Diagnostic criteria for multiple sclerosis: 2010 revisions to the McDonald criteria.* Polman CH, Reingold SC, Banwell B, Clanet M, Cohen JA, Filippi M, Fujihara K, Havrdova E, Hutchinson M, Kappos L, Lublin FD. 2, Febuary 2011, Annals of Neurology, Vol. 69, pp. 292-302.

14. *Disease-modifying treatments for multiple sclerosis – a review of approved medications.* Torkildsen Ø, Myhr KM, Bø L. s.l. : Wiley, Jan 2016, European journal of neurology, Vol. 23, pp. 18-27.

15. *Fingolimod-associated macular edema: incidence, detection, and management.* Jain N, Bhatti MT. 9, s.l. : Neurology, Feb 28, 2012, Neurology, Vol. 78, pp. 672-680.

16. *The window of therapeutic opportunity in multiple sclerosis.* Coles AJ, Cox A, Le Page E, Jones J, Trip SA, Deans J, Seaman S, Miller DH, Hale G, Waldmann H, Compston DA. 1, Jan 2006, Journal of Neurology, Vol. 253, pp. 98-108.

17. *Optical coherence tomography: a window into the mechanisms of multiple sclerosis.* Frohman EM, Fujimoto JG, Frohman TC, Calabresi PA, Cutter G, Balcer LJ. 12, Dec 2008, Nature Reviews Neurology, Vol. 4, pp. 664-75.

18. *Depression in multiple sclerosis: A long-term longitudinal study.* Koch MW, Patten S, Berzins S, Zhornitsky S, Greenfield J, Wall W, Metz LM. 1, Jan 2015, Multiple Sclerosis Journal, Vol. 21, pp. 76-82.

19. *Rating neurologic impairment in multiple sclerosis: An expanded disability status scale (EDSS).* JF, Kurtzke. 11, Nov 1983, Neurology, Vol. 33, pp. 1444-52.

20. *Systematic literature review and validity evaluation of the Expanded Disability Status Scale (EDSS) and the Multiple Sclerosis Functional Composite (MSFC) in patients with multiple sclerosis.* Meyer-Moock S, Feng YS, Maeurer M, Dippel FW, Kohlmann T. 1, Dec 2014, BMC Neurology, Vol. 14, p. 58.

21. *The retina as a window to the brain—from eye research to CNS disorders.* London A, Benhar I, Schwartz M. 1, Jan 2013, Nature Reviews Neurology, Vol. 9, pp. 44-53.

22. *Retinal vascular image analysis as a potential screening tool for cerebrovascular disease: a rationale based on homology between cerebral and retinal microvasculatures.* Patton N, Aslam T, MacGillivray T, Pattie A, Deary IJ, Dhillon B. 4, s.l. : Journal of anatomy, Apr 2005, Vol. 206, pp. 319-48.

23. Forrester JV, Dick AD, McMenamin P, Lee W. *The Eye E-Book: Basic Sciences in Practice.* 5. s.l. : Elsevier Health Sciences UK, 2015.

24. *Retinal imaging as a source of biomarkers for diagnosis, characterization and prognosis of chronic illness or long-term conditions.* MacGillivray TJ, Trucco E, Cameron JR, Dhillon B, Houston JG, van Beek EJR. 1040, Jul 2014, The British Journal of Radiology, Vol. 87.

25. *A prospective cohort study of vitamin D in optic neuritis recovery.* Burton JM, Eliasziw M, Trufyn J, Tung C, Carter G, Costello F. 1, Jan 2017, Multiple Sclerosis Journal, Vol. 23, pp. 82-93.

26. *Clinical characteristics of autoimmune optic neuritis.* Kawachi, Izumi. Jan 2017, Clinical and Experimental Neuroimmunology, Vol. 8, pp. 8-16.

27. *Optical coherence tomography in multiple sclerosis: a systematic review and meta-analysis.* Petzold A, de Boer JF, Schippling S, Vermersch P, Kardon R, Green A, Calabresi PA, Polman C. 9, Sep 2010, The Lancet Neurology, Vol. 9, pp. 921-32.

28. *Optical coherence tomography and disease subtype in multiple sclerosis .* Pulicken M, Gordon-Lipkin E, Balcer LJ, Frohman E, Cutter G, Calabresi PA. 22, Nov 2007, Neurology, Vol. 69, pp. 2085-2092.

29. *Optical coherence tomography for retinal imaging in multiple sclerosis.* Zimmermann H, Oberwahrenbrock T, Brandt AU, Paul F, Dörr J. Dec 2014, Degenerative Neurological and Neuromuscular Disease, Vol. 4, p. 153:162.

30. *Macular Volume Determined by Optical Coherence Tomography as a Measure of Neuronal Loss in Multiple Sclerosis.* Burkholder BM, Osborne B, Loguidice MJ, Bisker E, Frohman TC, Conger A, Ratchford JN, Warner C, Markowitz CE, Jacobs DA, Galetta SL. 11, Nov 2009, Archives of neurology, Vol. 66, pp. 1366-1372.

31. *An investigation of the retinal nerve fibre layer in progressive multiple sclerosis using optical coherence tomography.* Henderson AP, Trip SA, Schlottmann PG, Altmann DR, Garway-Heath DF, Plant GT, Miller DH. 1, 2007, Brain, Vol. 131, pp. 277-287.

32. *The retinal nerve fiber layer, neuroretinal rim area, and visual evoked potentials in MS.* MacFadyen DJ, Drance SM, Douglas GR, Airaksinen PJ, Mawson DK, Paty DW. 9, Sep 1988, Neurology, Vol. 38, p. 1353.

33. *Timing of retinal neuronal and axonal loss in MS: a longitudinal OCT study.* Balk LJ, Cruz-Herranz A, Albrecht P, Arnow S, Gelfand JM, Tewarie P, Killestein J, Uitdehaag BM, Petzold A, Green AJ. 7, Jul 2016, Journal of neurology, Vol. 263, pp. 1323-31.

34. *Longitudinal study of vision and retinal nerve fiber layer thickness in multiple sclerosis.* Talman LS, Bisker ER, Sackel DJ, Long Jr DA, Galetta KM, Ratchford JN, Lile DJ, Farrell SK, Loguidice MJ, Remington G, Conger A. 6, Jun 2010, Annals of Neurology, Vol. 67, pp. 749-60.

35. *A preliminary longitudinal study of the retinal nerve fiber layer in progressive multiple sclerosis.* Henderson AP, Trip SA, Schlottmann PG, Altmann DR, Garway-Heath DF, Plant GT, Miller DH. 7, Jul 2010, Journal of neurology, Vol. 257, pp. 1083-91. 10.1007/s00415-010-5467-x.

36. *Retinal nerve fiber layer imaging with spectral-domain optical coherence tomography: a prospective analysis of age-related loss.* Leung CK, Yu M, Weinreb RN, Ye C, Liu S, Lai G, Lam DS. 4, Apr 2012, Ophthalmology, Vol. 119, pp. 731-7.

37. *Retinal thickness decreases with age: an OCT study.* Alamouti B, Funk J. 7, Jul 2003, British journal of ophthalmology, Vol. 87, pp. 899-901.

38. *Retinal periphlebitis is associated with multiple sclerosis severity.* Ortiz-Pérez S, Martínez-Lapiscina EH, Gabilondo I, Fraga-Pumar E, Martínez-Heras E, Saiz A, Sanchez-Dalmau B, Villoslada P. 10, Sep 2013, Neurology, Vol. 81, pp. 877-881.

39. *Differential Diagnosis of Retinal Vasculitis.* El-Asrar AM, Herbort CP, Tabbara KF. 4, Oct 2009, Middle East African Journal of Ophthalmology, Vol. 16, pp. 202-218.

40. *Detection of retinal blood vessel changes in multiple sclerosis with optical coherence tomography.* Bhaduri B, Nolan RM, Shelton RL, Pilutti LA, Motl RW, Moss HE, Pula JH, Boppart SA. 6, Jun 2016, Biomedical optics express, Vol. 7, pp. 2321-30.

41. *Validity of low-contrast letter acuity as a visual performance outcome measure for multiple sclerosis.* Balcer LJ, Raynowska J, Nolan R, Galetta SL, Kapoor R, Benedict R, Phillips G, LaRocca N, Hudson L, Rudick R, Multiple Sclerosis Outcome Assessments Consortium. 5, Apr 2017, Multiple Sclerosis Journal, Vol. 23, pp. 734-747.

42. *Longitudinal study of vision and retinal nerve fiber layer thickness in multiple sclerosis.* Talman LS, Bisker ER, Sackel DJ, Long Jr DA, Galetta KM, Ratchford JN, Lile DJ, Farrell SK, Loguidice MJ, Remington G, Conger A. 6, Jun 2010, Annals of Neurology, Vol. 67, pp. 749-760.

43. *Longitudinal study of visual function in patients with relapsing-remitting multiple sclerosis with and without a history of optic neuritis.* Gómez AG, García-Ben A, García AS, García-Basterra I, Parrado FP, García-Campos JM. Nov 2018, Neurología (English Edition).

44. *Association of Retinal and Macular Damage with Brain Atrophy in Multiple Sclerosis.* Dörr J, Wernecke KD, Bock M, Gaede G, Wuerfel JT, Pfueller CF, Bellmann-Strobl J, Freing A, Brandt AU, Friedemann P. 4, Apr 2011, PLOS one, Vol. 6, p. e18132.

45. *Anxiety and its determinants in patients undergoing Magnetic Resonance Imaging.* Katz RC, Wilson L, Frazer N. 2, Jun 1994, Journal of Behavior Therapy and Experimental Psychiatry, Vol. 25, pp. 131-134.

46. *Optical coherence tomography.* Huang D, Swanson EA, Lin CP, Schuman JS, Stinson WG, Chang W, Hee MR, Flotte T, Gregory K, Puliafito CA. 5035, s.l. : American Association for the Advancement of Science, Nov 1991, Science, Vol. 254, pp. 1178-81.

47. *Retinal Abnormalities in Early Alzheimer's Disease.* Berisha F, Feke GT, Trempe CL, McMeel JW, Schepens CL. 5, May 2007, Investigative Ophthalmology & Visual Science, Vol. 48, pp. 2285-2289.

48. *Diagnostic accuracy of retinal abnormalities in predicting disease activity in MS.* Sepulcre J, Murie-Fernandez M, Salinas-Alaman A, García-Layana A, Bejarano B, Villoslada P. 18, May 2007, Neurology, Vol. 68, pp. 1488-94.

49. *Optical coherence tomography.* Regar E, Schaar JA, Mont E, Virmani R, Serruys PW. 4, Oct 2003, Cardiovascular Radiation Medicine, Vol. 4, pp. 198-204.

50. Seth Goldstein MD, MPhil. Overview of Ultrasound Theory and Techniques. [ed.] Marcus D. Jarboe Stefan Scholz. *Diagnostic and Interventional Ultrasound in Pediatrics and Pediatric Surgery.* s.l. : Springer International Publishing, 2016.

51. Drexler, Wolfgang, Fujimoto, James G. *Optical Coherence Tomography.* 1. s.l. : Springer-Verlag, 2008.

52. *Clinical investigation of an infrared digital scanning laser ophthalmoscope.* Manivannan A, Kirkpatrick JN, Sharp PF, Forrester JV. 2, Feb 1994, British Journal of Ophthalmology, Vol. 78, pp. 84-90.

53. *Modern technologies for retinal scanning and imaging: an introduction for the biomedical engineer.* BI, Gramatikov. 1, Dec 2014, BioMedical Enginerring Online, Vol. 13, p. 52.

54. *Spectral Domain Optical Coherence Tomography and Glaucoma.* Chen TC, Zeng A, Sun W, Mujat M, de Boer JF. 4, 2008, International ophthalmology clinics, Vol. 48, p. 29.

55. *Optical coherence tomography in multiple sclerosis: a systematic review and meta-analysis.* Petzold A, de Boer JF, Schippling S, Vermersch P, Kardon R, Green A, Calabresi PA, Polman C. 9, Sep 2010, The Lancet Neurology, Vol. 9, pp. 921-32.

56. Brown MA, Semelka RC, Dale BM. *MRI : basic principles and applications.* 3. s.l. : John Wiley & Sons, 2015.

57. Heidelberg Engineering GmbH. Spectralis Hardware Operating Instructions. 2007.

58. *Macular Volume Determined by Optical Coherence Tomography as a Measure of Neuronal Loss in Multiple Sclerosis.* Burkholder BM, Osborne B, Loguidice MJ, Bisker E, Frohman TC, Conger A, Ratchford JN, Warner C, Markowitz CE, Jacobs DA, Galetta SL. 11, Nov 2009, Archives of neurology, Vol. 66, pp. 1366-1372.

59. *Adding Papillomacular Bundle Measurements to Standard Optical Coherence Tomography Does Not Increase Sensitivity to Detect Prior Optic Neuritis in Patients with Multiple Sclerosis.* Laible M, Jarius S, Mackensen F, Schmidt-Bacher A, Platten M, Haas J, Albrecht P, Wildemann B. 5, May 2016, PLOS one, Vol. 11, p. e0155322.

60. *Accuracy of the Heidelberg Spectralis in the alignment between near-infrared image and tomographic scan in a model eye: a multicenter study.* Barteselli G, Bartsch DU, Viola F, Mojana F, Pellegrini M, Hartmann KI, Benatti E, Leicht S, Ratiglia R, Staurenghi G, Weinreb RN. 3, Sep 2013, American journal of ophthalmology, Vol. 156, pp. 588-92.

61. *Aligning scan locations from consecutive spectral-domain optical coherence tomography examinations: a comparison among different strategies.* Giani A, Pellegrini M, Invernizzi A, Cigada M, Staurenghi G. 12, Nov 2012, Investigative ophthalmology & visual science, Vol. 53, pp. 7637-43.

62. Daytona product details. *Optos.* [Online] 2017. https://www.optos.com/en/products/daytona/.

63. *Wide-field Imaging of the Retina.* Witmer MT, Kiss S. 2, Mar 2013, Survey of Ophthalmology, Vol. 58, pp. 143-154.

64. *Quantifying Retinal Area in Ultra-Widefield Imaging Using a 3-Dimensional Printed Eye Model.* Nicholson L, Vazquez-Alfageme C, Clemo M, Luo Y, Hykin PG, Bainbridge JW, Sivaprasad S. 1, Jan 2018, Ophthalmology Retina, Vol. 2, pp. 65-71.

65. *Assessment of Accuracy and Precision of Quantification of Ultra-Widefield Images.* Sagong M, van Hemert J, de Koo LC, Barnett C, Sadda SR. 4, Apr 2015, Ophthalmology, Vol. 122, pp. 864-6.

66. *Ultra-Widefield Retina Imaging: Principles of Technology and Clinical Applications.* 준엽이, 공민사. 1, May 31, 2016, Journal of Retina, Vol. 1, pp. 1-10.

67. *Automated measurement of blood vessel features in ultra-wide retinal fundus images as biomarkers for cardiovascular disease.* Pelligrini, E & Trucco, Emanuele & Robertson, Gavin & Macgillivray, Thomas & Beek, Edwin & Peto, T & van Hemert, Jano & Belch, Jill & Struthers, AS & Sullivan, Frank & Littleford, Roberta & Lambert, Matthew & Houston, John. 2014. Biomed Opt Express.

68. *Blood vessel segmentation and width estimation in ultra-wide field scanning laser ophthalmoscopy.* Pellegrini E, Robertson G, Trucco E, MacGillivray TJ, Lupascu C, van Hemert J, Williams MC, Newby DE, van Beek EJ, Houston G. 12, Dec 2014, Biomedical Optics Express, Vol. 5, pp. 4329-37.

69. *Validation of a modified ETDRS chart for European-wide use in populations that use the Cyrillic, Latin or Greek alphabet.* Plainis S, Moschandreas J, Giannakopoulou T, Vitanova V, Nikolitsa P, Rozema JJ, Tassignon MJ, Tsilimbaris MK, Pallikaris IG. 1, Jan 2013, Journal of Optometry, Vol. 6, pp. 18-24.

70. *Retinal nerve fiber layer is associated with brain atrophy in multiple sclerosis.* Gordon-Lipkin E, Chodkowski B, Reich DS, Smith SA, Pulicken M, Balcer LJ, Frohman EM, Cutter G, Calabresi PA. 16, Oct 2007, Neurology, Vol. 69, pp. 1603-1609.

71. *Evaluating the effect of pupil dilation on spectral-domain optical coherence tomography measurements and their quality score.* Tanga L, Roberti G, Oddone F, Quaranta L, Ferrazza M, Berardo F, Manni G, Centofanti M. 1, Dec 2015, BMC Ophthalmology, Vol. 15, p. 175.

72. *Effect of image quality on tissue thickness measurements obtained with spectral-domain optical coherence tomography.* Balasubramanian M, Bowd C, Vizzeri G, Weinreb RN, Zangwill LM. 5, Mar 2009, Optics express, Vol. 17, p. 4019.

73. *Impact of B-Scan averaging on Spectralis optical coherence tomography image quality before and after cataract surgery.* Podkowinski D, Sharian Varnousfaderani E, Simader C, Bogunovic H, Philip AM, Gerendas BS, Schmidt-Erfurth U, Waldstein SM. 2017, Journal of Ophthalmology.

74. *Effectiveness of averaging strategies to reduce variance in retinal nerve fibre layer thickness measurements using spectral-domain optical coherence tomography.* Pemp B, Kardon RH, Kircher K, Pernicka E, Schmidt-Erfurth U, Reitner A. 7, Jul 2013, Graefe's Archive for Clinical and Experimental Ophthalmology, Vol. 251, pp. 1841-8.

75. *Reproducibility of retinal nerve fiber thickness measurements using the test-retest function of spectral OCT/SLO in normal and glaucomatous eyes.* Lee SH, Kim

SH, Kim TW, Park KH, Kim DM. 9, Dec 2010, Journal of glaucoma, Vol. 19, pp. 637-42.

76. *Automated segmentation errors when using optical coherence tomography to measure retinal nerve fiber layer thickness in glaucoma.* Mansberger SL, Menda SA, Fortune BA, Gardiner SK, Demirel S. Feb 2017, American journal of ophthalmology, Vol. 174, pp. 1-8.

77. *Spline-based refinement of vessel contours in fundus retinal images for width estimation.* Cavinato A, Ballerini L, Trucco E, Grisan E. Apr 2013, In2013 IEEE 10th International Symposium on Biomedical Imaging, pp. 872-875.

78. *Accurate estimation of retinal vessel width using bagged decision trees and an extended multiresolution Hermite model.* Lupaşcu CA, Tegolo D, Trucco E. 8, Dec 2013, Medical image analysis, Vol. 17, pp. 1164-80.

79. *Assessment of Accuracy and Precision of Quantification of Ultra-Widefield Images.* Sagong M, van Hemert J, de Koo LC, Barnett C, Sadda SR. 4, s.l. : Ophthalmology, Apr 2015, Vol. 122, pp. 864-6.

80. *Normality Tests for Statistical Analysis: A Guide for Non-Statisticians.* Ghasemi A, Zahediasl S. 2, 2012, International journal of endocrinology metabolism, Vol. 10, pp. 486-489.

81. *Lateral thinking – Interocular symmetry and asymmetry in neurovascular patterning, in health and disease.* Cameron JR, Megaw RD, Tatham AJ, McGrory S, MacGillivray TJ, Doubal FN, Wardlaw JM, Trucco E, Chandran S, Dhillon B. 59, July 2017, Progress in Retinal and Eye Research, Vol. 1, pp. 131-157.

82. *Relation of Visual Function to Retinal Nerve Fiber Layer Thickness in Multiple Sclerosis.* Fisher JB, Jacobs DA, Markowitz CE, Galetta SL, Volpe NJ, Nano-Schiavi ML, Baier ML, Frohman EM, Winslow H, Frohman TC, Calabresi PA. 2, Feb 2006, Ophthalmology, Vol. 113, pp. 324-332.

83. *Cooks Distance and Mahanabolis Distance Outlier Detection Methods to identify Review Spam.* SPA, Jyoti G. Biradar. 6, s.l. : ijecs [Internet], Jun 2017, Vol. 6.

84. *Fingolimod treatment in multiple sclerosis leads to increased macular volume.* Nolan R, Gelfand JM, Green AJ. 2, Jan 2013, Neurology, Vol. 80, pp. 139-144.

85. *Effect Of Fingolimod On Macular Volume And Retinal Nerve Fiber Layer Thickness: A One Year Longitudinal Study.* Repovic P, Lee DW, Hamilton S, May E, Bowen J. 10, Apr 2014, Neurology, Vol. 82, pp. 1526X-632X.

86. *How sensitive to clinical change are ETDRS logMAR visual acuity measurements?* Rosser DA, Cousens SN, Murdoch IE, Fitzke FW, Laidlaw DA. 8, s.l. : Investigative ophthalmology & visual science, Aug 2003, Vol. 44, pp. 3278-81.

87. *Foveal and parafoveal retinal thickness in healthy pregnant women in their last trimester.* Demir M, Oba E, Can E, Odabasi M, Tiryaki S, Ozdal E, Sensoz H. s.l. : Clinical ophthalmology , 2011, Vol. 5, p. 1397.

88. *Retinal Damage in Multiple Sclerosis Disease Subtypes Measured by High-Resolution Optical Coherence Tomography.* Oberwahrenbrock T, Schippling S, Ringelstein M, Kaufhold F, Zimmermann H, Keser N, Young KL, Harmel J, Hartung HP, Martin R, Paul F. s.l. : Multiple sclerosis international, 2012.

89. *Retinal nerve fiber layer thickness in multiple sclerosis subtypes.* Zamzam DA, Gaafar AA, Ismail AT, Elbassiouny A, Tork MA, Hamdy H. 3, Jul 2015, The Egyptian journal of neurology, psychiatry and neurosurgery, Vol. 52, p. 216.

90. *Retinal layer segmentation in multiple sclerosis: a systematic review and meta-analysis.* Petzold A, Balcer LJ, Calabresi PA, Costello F, Frohman TC, Frohman EM, Martinez-Lapiscina EH, Green AJ, Kardon R, Outteryck O, Paul F. 10, Oct 2017, The Lancet Neurolog, Vol. 16, pp. 797-812.

91. *The Temporal Retinal Nerve Fiber Layer Thickness Is the Most Important Optical Coherence Tomography Estimate in Multiple Sclerosis.* Birkeldh U, Manouchehrinia A, Hietala MA, Hillert J, Olsson T, Piehl F, Kockum IS, Brundin L, Zahavi O, Wahlberg-Ramsay M, Brautaset R. 8, Dec 2017, Frontiers in neurology, Vol. 13, p. 675.

92. *Optical Coherence Tomography Retinal Nerve Fiber Analysis: A Measure of Axon Loss in Multiple Sclerosis.* Antonio-Santos A, Eggenberger ER, Costello MF, Balcer L. 2016, Immunol. Infect. Dis, Vol. 4, pp. 13-19.

93. *Evaluating the Use of Optical Coherence Tomography in Optic Neuritis.* F, Costello. 2011, Multiple Sclerosis International.

94. *No evidence of disease activity is associated with reduced rate of axonal retinal atrophy in MS.* Pisa M, Guerrieri S, Di Maggio G, Medaglini S, Moiola L, Martinelli V, Comi G, Leocani L. 24, Dec 2017, Neurology, Vol. 89, pp. 2469-75.

95. *Optical coherence tomography angiography of optic nerve head and parafovea in multiple sclerosis.* Wang X, Jia Y, Spain R, Potsaid B, Liu JJ, Baumann B, Hornegger J, Fujimoto JG, Wu Q, Huang D. 10, Oct 2014, British Journal of Ophthalmology, Vol. 98, pp. 1368-73.

96. *Patient perception of bodily functions in multiple sclerosis: gait and visual function are the most valuable.* Heesen C, Böhm J, Reich C, Kasper J, Goebel M, Gold SM. 7, Aug 2008, Multiple Sclerosis, Vol. 14, pp. 988-991.

97. Azegrouz H, inventor and Optos PLC, assignee. *Laser scanning system and method. US 15/013,545* United States patent application US , Jan 15, 2019.

98. *Retinal and Optic Disc Alterations in Alzheimer's Disease: the Eye as a Potential Central Nervous System Window.* Bambo MP, Garcia-Martin E, Larrosa JM, Polo V, Gutiérrez-Ruiz F. 223, 2016, Journal of Alzheimer's Disease and Parkinsonism, Vol. 6, pp. 2161-0460.

99. *Retinal changes in patients with major depressive disorder–A controlled optical coherence tomography study.* Schönfeldt-Lecuona C, Schmidt A, Kregel T, Kassubek J, Dreyhaupt J, Freudenmann RW, Connemann BJ, Pinkhardt EH, Gahr M. Feb 2018, Journal of Affective Disorders, Vol. 1, pp. 665-71.

100. Expanded Disability Status Scale (EDSS). *MS Trust.* [Online] 2019. https://www.mstrust.org.uk/a-z/expanded-disability-status-scale-edss.

101. Carlson NR, Braun J. *Foundations of physiological psychology.* 2. Boston : Allyn and Bacon, 1995.